Available online at www.sciencedirect.com
SCIENCE DIRECT®
PHYSICS REPORTS
ELSEVIER
Physics Reports 377 (2003) 281–387
www.elsevier.com/locate/physrep

Ab initio theories of electric transport in solid systems with reduced dimensions

Peter Weinberger

Center for Computational Materials Science, Technical University Vienna, Getreidemarkt 9/134, A-1060 Vienna, Austria

Accepted 25 November 2002
editor: D.L. Mills

Abstract

Ab initio theories of electric transport in solid systems with reduced dimensions, i.e., systems that at best are characterized by two-dimensional translational invariance, are reviewed in terms of a fully relativistic description of the Kubo–Greenwood equation. As the use of this equation requires concepts such as collinearity and non-collinearity in order to properly define resistivities or resistances corresponding to particular magnetic configurations, respective consequences of the (local) density functional theory are recalled in quite a detailed manner. Furthermore, since theoretical descriptions of solid systems with reduced dimensions require quantum mechanical methods different from bulk systems (three-dimensional periodicity), the so-called Screened Korringa–Kohn–Rostoker (SKKR-) method for layered systems is introduced together with a matching coherent potential approximation (inhomogeneous CPA).

The applications shown are mainly meant to illustrate various aspects of electric transport in solid systems with reduced dimensions and comprise not only current-in-plane (CIP) experiments, but also current perpendicular to the planes of atoms geometries, consequences of tunneling, and finite nanostructures at or on metallic substrates.

In order to give a more complete view of available ab initio methods also a non-relativistic approach based on the Tight Binding Linear Combination of muffin tin orbitals (TB-LMTO-) method and the so-called Kubo–Landauer equation in terms of transmission and reflection matrices is presented.

A compilation of references with respect to ab-initio type approaches not explicitly discussed in here finally concludes the discussion of electric properties in solid systems with reduced dimensions.
© 2003 Elsevier Science B.V. All rights reserved.

PACS: 75.30.Gw; 75.70.Ak; 75.70.Cn

E-mail address: pw@cms.tuwien.ac.at (P. Weinberger).

0370-1573/03/$ - see front matter © 2003 Elsevier Science B.V. All rights reserved.
doi:10.1016/S0370-1573(02)00600-2

Contents

1. Introduction

Electric conduction in solid matter raised interests in its theoretical description since many years. In the context of this review there is an extensive list of exciting papers dealing with this aspect such as Refs. [1–10], some of which became very famous, others—unfortunately—are too little known, the latter definitely applies to Ref. [8]. In particular the interplay between microscopic, mesoscopic and macroscopic levels of description made this field right from the beginning so interesting from the theoretical standpoint of view, see, e.g., Ref. [11]. Although since even the early days of quantum mechanics metallic conductivity posed fundamental questions and found some answers in the following decades, it was essentially the reduction of dimensionality in solid systems that gave the whole field an enormous boost. The discovery of the giant magnetoresistance effect (1988), see also Ref. [12], turned out to trigger off a small industrial revolution considering the present and future applications in the recording and computer industry. Clearly enough this new physical property that is confined to systems with at best two-dimensional translational invariance (layered systems) required new types of theoretical descriptions, e.g., approaches, capable of dealing with semi-infinite systems. Luckily enough by then density functional theory [13–15] was already well-established and has to be considered now as *the* backbone of all ab initio type descriptions of electric transport in solid systems per se.

1.1. Icons and iconography

Current perpendicular to the planes of atoms (CPP) experiments seem to be very easy to understand: iconified pictures of charged particles moving from one reservoir (lead, partial system of given chemical potential) through matter to another reservoir are readily sketched. By shifting the chemical potential in one of the leads relative to the other one, a voltage drop is usually symbolized on the spot. Such (macroscopic) icons are of course of little help, if not completely counterproductive, if a microscopical (quantum mechanical) description of CPP is the scientific aim. In the case of current-in-plane (CIP) experiments an iconification of the travelling of electrons in solid systems with reduced dimensions is perhaps less easy achieved, although occasionally pictures of an ensemble of individual atomic planes—the electrons bounce back and forward within such planes and eventually move to the next plane—are still in use. Clearly enough all these macroscopical perceptions are futile once detailed answers to questions like “and how big is the parallel resistance in a particular system” are posed.

1.2. Quantum mechanical levels of description

Presently three conceptually quite different schemes of describing electric transport in terms of ab initio like methods are available, namely the *linearized Boltzmann equation*, a *Landauer-type approach*, see in particular Ref. [11], and applications of the *Kubo–Greenwood equation*. The use of the linearized Boltzmann equation is restricted to quantum mechanical schemes that are based on three-dimensional periodicity, i.e., on schemes providing a well-defined Fermi surface. Clearly enough supercell calculations are then in most cases the computational consequence. Landauer-type descriptions became rather popular in connection with the problem of tunneling of electrons through non-conducting matter; conceptually they are confined to CPP-like transport. The Kubo–Greenwood equation proved to be applicable not only for bulk-like problems, but also in the case of CIP and CPP. For this reason this review is mainly concerned about the Kubo–Greenwood equation and its use, although there will also be sections dealing with the so-called Kubo-Landauer equation and related applications.

1.3. Guide through sections

As already indicated all ab initio type calculations are based on density functional theory. It is therefore necessary to discuss basic consequences of the local spin density functional (LSDF) in particular in the context of collinearity and non-collinearity, magnetic configurations, and to review aspects of casting Kohn–Sham Hamiltonians into a Green's function concept. Furthermore, since Green's functions are the key-quantity not only in the Kubo–Greenwood, but also in the Kubo-Landauer equation and related approaches, the presently most flexible method for calculating Green's functions within the LSDF, namely the Screened Korringa–Kohn–Rostoker method (SKKR) needs to be shortly reviewed.

Perhaps it will be remembered that right from the beginning the giant magnetoresistance (GMR) and the interlayer exchange coupling (IEC) were considered to be just two sides of one and the same coin, i.e., to be caused by the very same type of microscopical effects. In order to question this, but also since the IEC (and the magnetic anisotropy energy in magnetic multilayers) is a perfect example for a consequent use of the concept of magnetic configurations this quantity is introduced even before the Kubo–Greenwood equation is mentioned. A proper discussion of the boundary conditions for the Kubo–Greenwood equation in solid systems with reduced dimensions will lead almost automatically to various applications and concepts either within CIP or CPP geometry. The correlation of a generalized IEC concept with the GMR is then questioned again in facing the problem of exchange bias effects in the GMR in spin valve systems.

Although presently all applications of the GMR are materialized in terms of layered systems, a future further reduction of the dimensionality of solid systems—a reduction to (spatially local) magnetic nanostructures—definitely will lead to another boost in recording devices. Therefore, also ab initio type descriptions of the electric properties of such structures need to be sketched.

All the above approaches and examples will refer to a *fully relativistic* level of description. As an illustration of a *non-relativistic* approach the TB-LMTO (tight binding linear combination of orbitals) method is then used to introduce the Kubo–Landauer equation and the transmission matrix formulation. Finally a list and classification in terms of applied methods using alternative approaches is provided. It should be noted that for matters of easy access this list only quotes from

Physical Review Letters, the Physical Review and the Journal of Applied Physics. Together with the references given in the other sections this list is basically meant to provide a quick guide to the present state of ab initio like calculations of electric properties in solid systems with reduced dimensions.

2. Kohn–Sham Hamiltonians and resolvents

2.1. Collinearity and non-collinearity

2.1.1. "Spinors"

Suppose one-particle (electron) wave functions are products of the following kind:

$$\Psi(\mathbf{r},\sigma)=\psi(\mathbf{r})\phi(\sigma);\quad \sigma\equiv m_s=\pm\tfrac{1}{2}\ , \tag{1}$$

$$\phi\left(\frac{1}{2}\right)=\begin{pmatrix}1\\0\end{pmatrix},\quad \phi\left(-\frac{1}{2}\right)=\begin{pmatrix}0\\1\end{pmatrix}\ , \tag{2}$$

where obviously the $\phi(\sigma)$, $\sigma=\pm\frac{1}{2}$, are not functions, but unit vectors in a two-dimensional vector space, usually termed "spin space":

$$(\phi(\sigma)\cdot\phi(\sigma'))=\delta_{\sigma\sigma'}\ . \tag{3}$$

In principle the transformation properties of $\Psi(\mathbf{r},\sigma)$ are conceptually very easy, since

$$R\in O(3)\text{: } R\Psi(\mathbf{r},\sigma)=\psi(R^{-1}\mathbf{r})\phi(\sigma)\equiv\phi(\sigma)\psi(R^{-1}\mathbf{r})=\phi(\sigma)D(R)\psi(\mathbf{r})\ , \tag{4}$$

where $D(R)$ is a representation of $R\in O(3)$ and

$$U(R)\in SU(2)\text{: } U(R)[\psi(\mathbf{r})\phi(\sigma)]=\psi(\mathbf{r})[U(R)\phi(\sigma)]\ . \tag{5}$$

Recalling now the definition of the vector of Pauli spin matrices,

$$\boldsymbol{\sigma}=(\sigma_x,\sigma_y,\sigma_z),\quad \sigma_x=\begin{pmatrix}0&1\\1&0\end{pmatrix},\quad \sigma_y=\begin{pmatrix}0&-i\\i&0\end{pmatrix},\quad \sigma_z=\begin{pmatrix}1&0\\0&-1\end{pmatrix}\ , \tag{6}$$

the non-relativistic (*Kohn–Sham*-) Hamiltonian is usually defined within the local density functional, see also Appendix A, as

$$\mathscr{H}(\mathbf{r})=I_2\left(-\tfrac{1}{2}\nabla^2+V(\mathbf{r})\right)+\sigma_z B(\mathbf{r})\ , \tag{7}$$

where I_n is a $n\times n$ unit matrix and $V(\mathbf{r})$ is the (effective) potential. One obvious meaning of the second term on the rhs of Eq. (7) is that the (effective) magnetization $\mathbf{B}(\mathbf{r})$ points along an arbitrary assumed $\hat{\mathbf{z}}$-direction, say $\mathbf{n}\in\mathscr{R}_3$, i.e., is of the form

$$\mathbf{B}(\mathbf{r})=B(\mathbf{r})\mathbf{n},\quad \mathbf{n}=(0,0,1)\ . \tag{8}$$

The general form of the scalar product between $\boldsymbol{\sigma}$ and $\mathbf{B}(\mathbf{r})$ is of course given by

$$(\boldsymbol{\sigma}\cdot\mathbf{B}(\mathbf{r}))=B(\mathbf{r})(\boldsymbol{\sigma}\cdot\boldsymbol{\xi})=B(\mathbf{r})(\sigma_x\xi_x+\sigma_y\xi_y+\sigma_z\xi_z)\ , \tag{9}$$

with $\boldsymbol{\xi}\in\mathscr{R}_3$ being a vector of unit length in an arbitrary direction.

Quite clearly by keeping in mind Eqs. (4), (5), a transformation of Eq. (7) of the following kind:

$$U(R)\mathscr{H}(\mathbf{r})U^{-1}(R) = I_2\left(-\tfrac{1}{2}\nabla^2 + V(\mathbf{r})\right) + U(R)\sigma_z B_z(\mathbf{r})U^{-1}(R)\ ,$$

$$U(R) \in SU(2)\ , \tag{10}$$

really means that *only* the second term on the rhs of Eq. (10) is transformed as

$$U(R)\sigma_z B(\mathbf{r})U^{-1}(R) = B(\mathbf{r})U(R)(\boldsymbol{\sigma}\cdot\mathbf{n})U^{-1}(R) = B(\mathbf{r})(\boldsymbol{\sigma}'\cdot\mathbf{n}) \tag{11}$$

where

$$\boldsymbol{\sigma}' = (\sigma_x', \sigma_y', \sigma_z') = U(R)\boldsymbol{\sigma}U^{-1}(R)\ . \tag{12}$$

Reviewing Eq. (11) again, it is obvious that the scalar product on the rhs of this equation can be written also as

$$(\boldsymbol{\sigma}'\cdot\mathbf{n}) = (\boldsymbol{\sigma}\cdot\boldsymbol{\xi})\ , \tag{13}$$

where—as should be noted in particular—

$$\boldsymbol{\xi} = D^{(3)}(R)\mathbf{n}\ . \tag{14}$$

$D^{(3)}(R)$ is a rotation in $\mathscr{R}_3$ such that the condition in Eq. (14) is met. Since obviously a transformation in spin-space corresponds to a similarity transformation for the Pauli spin matrices, such a transformation can be viewed also as an "induced" transformation for the orientation of $\mathbf{B}(\mathbf{r})$.

If $\mathscr{N}_0 = \{\mathbf{n}_i | \mathbf{n}_i = (0,0,1), \forall i\}$ denotes a set of unit vectors in $\hat{\mathbf{z}}$-direction centered in the sites $i = 1,2,\ldots N$, and the set $\mathscr{N} = \{\boldsymbol{\xi}_i\}$ specifies the actual orientations in these sites, an arbitrary pair of orientations, $\boldsymbol{\xi}_i$ and $\boldsymbol{\xi}_j$, is said to be "parallel" to $\mathscr{N}_0$, if

$$\boldsymbol{\xi}_i = D^{(3)}(E)\mathbf{n}_i; \quad \boldsymbol{\xi}_j = D^{(3)}(E)\mathbf{n}_j\ , \tag{15}$$

"*antiparallel*" to $\mathscr{N}_0$, if

$$\boldsymbol{\xi}_i = D^{(3)}(E)\mathbf{n}_i; \quad \boldsymbol{\xi}_j = D^{(3)}(i)\mathbf{n}_j\ , \tag{16}$$

and "*collinear*" to $\mathscr{N}_0$, if

$$\boldsymbol{\xi}_i = D^{(3)}(E)\mathbf{n}_i; \quad \boldsymbol{\xi}_j = D^{(3)}(R)\mathbf{n}_j; \quad R = E \text{ or } i\ , \tag{17}$$

where

$$D^{(3)}(E) = I_3, \quad D^{(3)}(i) = -I_3\ . \tag{18}$$

It should be recalled that $D^{(3)}(E)$ is *induced* by a transformation in spin space with

$$U(R) \equiv \begin{pmatrix} 1 & 0 \\ 0 & 1 \end{pmatrix} \to D^{(3)}(E)\ , \tag{19}$$

and $D^{(3)}(i)$ for example by

$$U(R) \equiv \sigma_y = \begin{pmatrix} 0 & -i \\ i & 0 \end{pmatrix} \rightarrow D^{(3)}(i) \ . \tag{20}$$

The last equation can easily be checked using the properties of the Pauli spin matrices, namely

$$U(R)U(R)^{-1} = \begin{pmatrix} 1 & 0 \\ 0 & 1 \end{pmatrix} = \sigma_y^2, \ \ \sigma_y\sigma_z\sigma_y = -\sigma_z \ , \tag{21}$$

from which immediately follows that also

$$U(R) \equiv \sigma_x = \begin{pmatrix} 0 & 1 \\ 1 & 0 \end{pmatrix} \rightarrow D^{(3)}(i) \ . \tag{22}$$

If, therefore in Eq. (17) R is *induced* by an arbitrary rotation in spin space, $U(R) \neq I_2, \sigma_x, \sigma_y$, then this pair of orientations is colloquially called "*non-collinear*".

It should be noted that the use of $D^{(3)}(E)$ or the choice of $\mathbf{n}$ in Eq. (17) does not imply a loss of generality, since the same description applies also to a pair of orientations

$$\boldsymbol{\xi}_i = D^{(3)}(S)D^{(3)}(E)\mathbf{n}_i, \ \ \boldsymbol{\xi}_j = D^{(3)}(S)D^{(3)}(R)\mathbf{n}_j \ , \tag{23}$$

with $D^{(3)}(S)$ being *induced* by some rotation $U(S) \in SU(2)$. As in Eq. (10) the first term on the rhs, namely

$$I_2 \left(-\tfrac{1}{2}\nabla^2 + V(\mathbf{r})\right)$$

remains unchanged for any arbitrary $U(R) \in SU(2)$ the definition of collinearity, see Eq. (17), is *not* restricted by the possible presence of a point group symmetry.

2.1.2. "Bispinors"

By using a relativistic description within the local density functional the Hamiltonian is given by

$$\mathscr{H}(\mathbf{r}) = c\boldsymbol{\alpha} \cdot \mathbf{p} + \beta mc^2 + I_4 V(\mathbf{r}) + \beta\Sigma_z B(\mathbf{r}) \ , \tag{24}$$

where $\boldsymbol{\alpha} = (\alpha_1, \alpha_2, \alpha_3)$,

$$\alpha_i = \begin{pmatrix} 0 & \sigma_i \\ \sigma_i & 0 \end{pmatrix}, \quad \beta = \begin{pmatrix} I_2 & \\ & -I_2 \end{pmatrix}, \quad \Sigma_i = \begin{pmatrix} \sigma_i & 0 \\ 0 & \sigma_i \end{pmatrix} \ . \tag{25}$$

The transformation properties of $\mathscr{H}(\mathbf{r})$ are now slightly more complicated. Consider a rotation R, then invariance by R implies that

$$S(R)\mathscr{H}(R^{-1}\mathbf{r})S^{-1}(R) = \mathscr{H}(\mathbf{r}) \ , \tag{26}$$

where $S(R)$ is a 4×4 matrix transforming the Dirac matrices α_i, β, and Σ_i

$$S(R) = \begin{pmatrix} U(R) & 0 \\ 0 & \det[\pm]U(R) \end{pmatrix} \ , \tag{27}$$

$U(R)$ is a (unimodular) 2×2 matrix and

$$\det[\pm] = \det[D^{(3)}(R)] \tag{28}$$

with $D^{(3)}(R)$ being the corresponding three-dimensional rotation matrix. Using now the invariance condition in (26) explicitly, one can see immediately that the condition

$$S(R)[I_4 V(R^{-1}\mathbf{r})]S^{-1}(R) = I_4 V(R^{-1}\mathbf{r}) = I_4 V(\mathbf{r}) \tag{29}$$

yields the usual *rotational invariance* condition for the potential, while the terms

$$S(R)[c\boldsymbol{\alpha}\cdot\mathbf{p}]S^{-1}(R), \quad S(R)[\beta\boldsymbol{\Sigma}\cdot\mathbf{B}(R^{-1}\mathbf{r})]S^{-1}(R)\ , \tag{30}$$

have to be examined with more care. Considering the scalar product in here explicitly term-wise, this reduces to the following *common condition* for *both* expressions in (29),

$$U(R)\boldsymbol{\sigma}U^{-1}(R) = \boldsymbol{\sigma}\ . \tag{31}$$

As in the previous "*spinor*"-case the obvious meaning of Eq. (24) is that the "magnetization" $\mathbf{B}(\mathbf{r})$ points along an arbitrary assumed $\hat{\mathbf{z}}$-direction, i.e., is of the form

$$\mathbf{B}(\mathbf{r}) = B(\mathbf{r})\mathbf{n}, \quad \mathbf{n} = (0,0,1)\ . \tag{32}$$

However, by comparing, now the transformation properties in the "*spinor*"- and the "*bispinor*"-*case*, one easily can see that in the "*bispinor*"-*case* for a proper definition of *collinearity* an *induced* rotation for the orientation of $\mathbf{B}(r)$, such as defined in Eqs. (13) and (14) *is restricted* by a possibly present rotational invariance condition for
(1) the (effective) potential $V(\mathbf{r})$,

$$V(R^{-1}\mathbf{r}) = V(\mathbf{r})\ , \tag{33}$$

(2) the (effective) magnetization $B(\mathbf{r})$,

$$B(R^{-1}\mathbf{r}) = B(\mathbf{r})\ , \tag{34}$$

and
(3) the invariance condition for the kinetic energy operator $c\boldsymbol{\alpha}\cdot\mathbf{p}$, whereby, because of the term $\beta\Sigma_z B(\mathbf{r})$, the sign of $\boldsymbol{\sigma}$ has to be preserved. Expressed in colloquial terms this simply means that "spin–orbit-coupling" also enters the definition of collinearity.

2.2. Translational properties

In the "*spinor*"-case translational invariance,

$$\mathscr{H}(\mathbf{r}+\mathbf{t}) = I_2\left(-\frac{1}{2}\nabla^2 + V(\mathbf{r}+\mathbf{t})\right) + \sigma_z B_z(\mathbf{r}+\mathbf{t}) = \mathscr{H}(\mathbf{r}), \quad t\in\mathscr{L}^{(n)}\ , \tag{35}$$

where $\mathscr{L}^{(n)}$ is a n-dimensional lattice, implies—as easily can be checked—that

$$\boldsymbol{\xi}_i = \boldsymbol{\xi}_0, \quad \forall i\in I(\mathscr{L}^{(n)}), \quad n\leqslant 3\ , \tag{36}$$

where $I(\mathscr{L}^{(n)})$ denotes the set of indices corresponding to $\mathscr{L}^{(n)}$ and $\boldsymbol{\xi}_0$ is some arbitrarily chosen orientation of $\mathbf{B}(\mathbf{r})$ such as for example $\hat{\mathbf{z}}$. Eq. (36) also applies in the "*bispinor*"-case, since for a translation the matrix $S(R)$ in Eq. (26) has to be the unit matrix.

The set T of elements $[E|t_i]$, $t_i \in \mathscr{L}^{(n)}$, where E denotes an identity rotation, and group closure is ensured such that

$$[E|t_i][E|t_j] = [E|t_i + t_j] \in T \ , \tag{37}$$

$$[E|t_i]([E|t_j][E|t_k]) = ([E|t_i][E|t_j])[E|t_k] \ , \tag{38}$$

$$[E|t_i][E|-t_i] = [E|-t_i][E|t_i] = [E|0] \ , \tag{39}$$

$$[E|t_i]^{|T|} = [E|0] \in T \ , \tag{40}$$

with $[E|0]$ being the identity element, is usually referred to as the $\mathscr{L}^{(n)}$ corresponding translational group of order $|T|$:

$$[E|t_i]\mathscr{H}(\mathbf{r}) = \mathscr{H}([E|t_i]^{-1}\mathbf{r}) = \mathscr{H}(\mathbf{r} - \mathbf{t}_i) = \mathscr{H}(\mathbf{r}) \ . \tag{41}$$

As is well-known only application of this translational group leads then to cyclic boundary conditions for the eigenfunctions of $\mathscr{H}(\mathbf{r})$, i.e., to Blochfunctions. Since $|T|$ has to be always finite,

$$|T| = \prod_{i=1}^{n} |T_i| \ , \tag{42}$$

it can be interpreted in physical terms as either the Lohschmidt number ($\mathscr{L}^{(3)}$; bulk, infinite system), the number of atoms in a given atomic plane of a layered structure ($\mathscr{L}^{(2)}$; semi-infinite system), the number of atoms in an atomic linear chain ($\mathscr{L}^{(1)}$), or the number of atoms in a magnetic domain. In the latter case this number is still quite large, sufficient, however, to observe a uniform direction of the magnetization within such a domain.

It should be noted that Eq. (34) can easily be extended to complex lattices. According to the discussions above non-collinearity can formally only be introduced by either reducing the dimensions of the lattice or, in special cases, considering complex lattices.

2.3. Magnetic configurations

Based on the previous section it is now very easy to define collinear magnetic structures in layered systems. Suppose that for a two-dimensional translational invariant system (layered system; one atom per unit cell for matters of simplicity) a particular configuration

$$\mathscr{C}_i = \{\ldots, n_{k-1}, n_k, n_{k+1}, \ldots\} \ , \tag{43}$$

where k numbers atomic layers, is defined by a set of collinear unit vectors n_k that characterize the orientations of the magnetization in all atomic layers considered, then configuration

$$\mathscr{C}_j = \{\ldots, n_{k-1}, -n_k, n_{k+1}, \ldots\} \tag{44}$$

refers to an arrangement in which with respect to $\mathscr{C}_i$ the orientation of the magnetization is reversed in the kth atomic layer. Taking also non-collinear configurations into account implies that $\mathscr{C}_j$ can be reached in a continuous manner by means of a rotation $U(\Theta)$ of n_k, $0 \leqslant \Theta \leqslant 2\pi$, around an axis perpendicular to n_k, i.e., by considering configurations of the form

$$\mathscr{C}_i(\Theta) = \{\ldots, n_{k-1}, U(\Theta)n_k, n_{k+1}, \ldots\} \ . \tag{45}$$

This implies that although within one atomic layer because of translational symmetry collinearity has to apply, with respect to each other the various layers can be orientated non-collinearly. Restricting, however, theoretical investigations to collinear configurations demands that in all atomic layers the corresponding orientations of the magnetization are either parallel or antiparallel to a given direction. This is indeed important to recall since even in the simplest case of a ferromagnetic configuration (all orientations are parallel) the prechosen direction of reference can be in-plane or perpendicular to the planes of atoms. According to Eq. (42) a ferromagnetic configurations can be formulated as

$$\mathscr{C}_0 = \{n_k | n_k = n_0, \forall k\} \ , \tag{46}$$

where n_0 is a prechosen direction such as e.g. within the planes of atoms.

2.4. Resolvents and Greens functions

The resolvent of a hermitean operator (Hamilton operator) is defined as follows

$$G(z) = (z - H)^{-1}, \quad z = \varepsilon + \mathrm{i}\delta \ , \tag{47}$$

where in the present case H is given in terms of a Kohn–Sham Hamiltonian, see Eqs. (17) and (24). Any representation of such a resolvent is called a Greens functions, e.g., also the following configuration space representation of $G(z)$,

$$\langle \mathbf{r}|G(z)|\mathbf{r}'\rangle = G(\mathbf{r}, \mathbf{r}'; z) \ . \tag{48}$$

The so-called side-limits of $G(z)$ are then defined by

$$\lim_{|\delta|\to 0} G(z) = \begin{cases} G^+(\varepsilon); & \delta > 0 \ , \\ G^-(\varepsilon); & \delta < 0 \end{cases} \tag{49}$$

and automatically lead to the property,

$$\mathrm{Im}\, G^+(\varepsilon) = \frac{1}{2\mathrm{i}}(G^+(\varepsilon) - G^-(\varepsilon)) \ , \tag{50}$$

or, e.g., by making use of the properties of Dirac delta functions,

$$\mathrm{Tr}[\mathrm{Im}\, G^{\pm}(\mathbf{r}, \mathbf{r}; \varepsilon)] = \mp\pi^{-1} \sum_k \delta(\varepsilon - \varepsilon_k) \ , \tag{51}$$

$$n(\varepsilon) = \mp \mathrm{Tr}[\mathrm{Im} G^{\pm}(\mathbf{r}, \mathbf{r}; \varepsilon)] \ , \tag{52}$$

where Tr denotes the trace in configuration space and $n(\varepsilon)$ is the density of states (of a Hamiltonian with discrete eigenvalue spectrum). A Dirac delta function can therefore be simply viewed as the Cauchy part of a first order pole in the resolvent $G(z)$.

2.5. Scaling transformations

Suppose the Hamilton operator H (e.g., the Kohn–Sham–Dirac operator) is given in terms of an unperturbed Hamiltonian H_0 and a perturbation operator V, then clearly H can immediately be written as

$$H = H_0 + V \equiv H_0 + V + W - W \equiv H_0' + V' \ , \tag{53}$$

where

$$H_0' = H_0 - W, \quad V' = V + W \ . \tag{54}$$

The resolvents of H and H_0 are defined in the following manner:

$$G(z) = (z - H)^{-1}, \quad G_0(z) = (z - H_0)^{-1} \ , \tag{55}$$

from which readily the resolvent of H_0' follows:

$$G_0'(z) = (z - H_0')^{-1} = (z - H_0 + W)^{-1} \ , \tag{56}$$

or written in terms of a Dyson equation,

$$G_0'(z) = G_0(z)[1 - WG_0'(z)] \ , \tag{57}$$

where $z = \varepsilon + \mathrm{i}\delta$, $\delta > 0$. From Eqs. (56) and (57) then follows directly that the Dyson equation for $G(z)$ can be written either in terms of $G_0(z)$ or $G_0'(z)$

$$G(z) = G_0(z)[1 + VG(z)] = G_0'(z)[1 + V'G(z)] \ . \tag{58}$$

It should be noted that this little quantum mechanical "trick" is the basis of "screening" in the KKR- and in the LMTO-method.

3. Multiple scattering theory

3.1. Green's functions and scattering path operators

Using "traditional" multiple-scattering theory [16,17], the Green's function can be written in a partial wave representation as

$$G(\mathbf{r}_i + \mathbf{R}_i, \mathbf{r}_i' + \mathbf{R}_j; \varepsilon) = \sum_{\Lambda\Lambda'} R_\Lambda^i(\mathbf{r}_i; \varepsilon)\tau_{\Lambda\Lambda'}^{ij}(\varepsilon)R_{\Lambda'}^j(\mathbf{r}_j') + \delta_{ij}\sum_L R_\Lambda^i(\mathbf{r}_{i,<}; \varepsilon)H_\Lambda^i(\mathbf{r}_{j,>}; \varepsilon) \ , \tag{59}$$

$$\Lambda = \begin{cases} \ell m & \text{non-relativistic,} \\ \kappa\mu & \text{relativistic,} \end{cases} \tag{60}$$

where the $\mathbf{R}_i$ denote positions of Coulomb singularities (positions of atoms) or of empty sites (centers of "empty spheres"), the $R^i_\Lambda(\mathbf{r};\varepsilon)$ and $H^i_\Lambda(\mathbf{r};\varepsilon)$ are properly normalized regular and irregular scattering solutions of the radial Schrödinger or Dirac equation corresponding to the energy ε and the potential $V_i(R_i)$. The so-called Green's function matrix

$$\mathbf{G}(\varepsilon) = \{G^{ij}(\varepsilon)\}, \quad G^{ij}(\varepsilon) = \{G^{ij}_{\Lambda\Lambda'}(\varepsilon)\} \tag{61}$$

is then given by

$$\mathbf{G}(\varepsilon) = \mathbf{G}^0(\varepsilon) + \mathbf{G}^0(\varepsilon)\boldsymbol{\tau}(\epsilon)\mathbf{G}^0(\varepsilon) = \mathbf{t}(\varepsilon)^{-1}\boldsymbol{\tau}(\epsilon)\mathbf{t}(\varepsilon)^{-1} - \mathbf{t}(\varepsilon)^{-1} \ , \tag{62}$$

namely given in terms of single-site t matrices,

$$\mathbf{t}(\varepsilon) = \{\mathbf{t}^i(\varepsilon)\delta_{ij}\}, \quad \mathbf{t}^i(\varepsilon) = \{t^i_\Lambda(\varepsilon)\delta_{ij}\} \ , \tag{63}$$

the so-called "structure constants",

$$\mathbf{G}^0(\varepsilon) = \{\mathbf{G}^{0,ij}(\varepsilon)\}, \quad \{\mathbf{G}^{0,ij}(\varepsilon)\} = \{G^{0,ij}_{\Lambda\Lambda'}(\varepsilon)\} \ , \tag{64}$$

and the scattering-path operator,

$$\boldsymbol{\tau}(\varepsilon) = [\mathbf{t}(\varepsilon)^{-1} - \mathbf{G}^0(\varepsilon)]^{-1} \ , \tag{65}$$

$$\boldsymbol{\tau}(\varepsilon) = \{\boldsymbol{\tau}^{ij}(\varepsilon)\}, \quad \{\boldsymbol{\tau}^{ij}(\varepsilon)\} = \{\tau^{ij}_{\Lambda\Lambda'}(\varepsilon)\} \ . \tag{66}$$

It should be noted that in the above equations a "supermatrix" notation was introduced, which will be very handy in the next section and simply implies matrix structures of the type

$$\mathbf{t}(\varepsilon) = \begin{pmatrix} \ddots & 0 & 0 & 0 & 0 \\ 0 & \mathbf{t}^i(\varepsilon) & 0 & 0 & 0 \\ 0 & 0 & \mathbf{t}^j(\varepsilon) & 0 & 0 \\ 0 & 0 & 0 & \mathbf{t}^k(\varepsilon) & 0 \\ 0 & 0 & 0 & 0 & \ddots \end{pmatrix} , \tag{67}$$

$$\mathbf{t}(\varepsilon) = \begin{pmatrix} \boldsymbol{\tau}^{i,i}(\varepsilon) & \boldsymbol{\tau}^{i,i+1}(\varepsilon) & \boldsymbol{\tau}^{i,i+2}(\varepsilon) & \cdots & \cdots \\ \boldsymbol{\tau}^{j-1,j}(\varepsilon) & \boldsymbol{\tau}^{j,j}(\varepsilon) & \boldsymbol{\tau}^{j,j+1}(\varepsilon) & \boldsymbol{\tau}^{j,j+2}(\varepsilon) & \cdots \\ \boldsymbol{\tau}^{k-2,k}(\varepsilon) & \boldsymbol{\tau}^{k-1,k}(\varepsilon) & \boldsymbol{\tau}^{k,k}(\varepsilon) & \boldsymbol{\tau}^{k,k+1}(\varepsilon) & \boldsymbol{\tau}^{k,k+2}(\varepsilon) \\ \vdots & \vdots & \vdots & \boldsymbol{\tau}^{k+1,k+1}(\varepsilon) & \cdots \\ \vdots & \vdots & \vdots & \vdots & \ddots \end{pmatrix} , \tag{68}$$

where according to Eqs. (63) and (65) each matrix element is itself an angular momentum representation.

3.2. Muffin-tin-geometries

Let us assume that the potentials and the exchange fields in the Kohn–Sham Hamiltonian for a system with only two-dimensional translational symmetry are superpositions of non-overlapping functions,

$$V(\mathbf{r}) = \sum_i V(\mathbf{r}_i + \mathbf{R}_{i,\parallel} + R_{i,z}\mathbf{z}) = \sum_i V_i(R_{i,z}) \ , \tag{69}$$

$$B(\mathbf{r}) = \sum_i B(\mathbf{r}_i + \mathbf{R}_{i,\parallel} + R_{i,z}\mathbf{z}) = \sum_i B_i(R_{i,z}) \ , \tag{70}$$

$$\mathbf{R}_i = (\mathbf{R}_{i,\parallel}, R_{i,z}), \quad \mathbf{R}_{i,\parallel} \in \mathscr{L}^{(2)} \ . \tag{71}$$

Furthermore, let assume that they are of "muffin-tin"-type, i.e.,

$$V_i(R_{i,z}) = V(\mathbf{r}_i + \mathbf{R}_{i,\parallel} + R_{i,z}\mathbf{z}) \equiv \begin{cases} V_i(|\mathbf{r}_i|; R_{i,z}), & |\mathbf{r}_i| \leqslant b_i(R_{i,z}) \ , \\ V_0 & \text{otherwise} \ , \end{cases} \tag{72}$$

$$B_i(R_{i,z}) = B(\mathbf{r}_i + \mathbf{R}_{i,\parallel} + R_{i,z}\mathbf{z}) \equiv \begin{cases} B_i(|\mathbf{r}_i|; R_{i,z}), & |\mathbf{r}_i| \leqslant b_i(R_{i,z}) \ , \\ B_0 & \text{otherwise} \end{cases} \ , \tag{73}$$

where the $b_i(R_{i,z})$ are the so-called "muffin-tin"-radii, V_0 and B_0 are the "muffin-tin"-constants, *and* that the perturbation W in Eq. (53) is also a superposition of individual (non-overlapping) potentials,

$$W(\mathbf{r}) = \sum_i W(\mathbf{r}_i + \mathbf{R}_{i,\parallel} + R_{i,z}\mathbf{z}) = \sum_i W_i(R_{i,z}) \ , \tag{74}$$

with

$$W_i(R_{i,z}) = \begin{cases} W_r, & |\mathbf{r}_i| \leqslant b_i(R_{i,z}) \ , \\ V_0 & \text{otherwise} \ , \end{cases} \qquad \forall i \in I(\mathscr{L}^{(2)}), \forall R_{i,z} \ , \tag{75}$$

where W_r is a suitable constant, and the index r stands for 'reference system'.

3.3. "Screening transformations"

Eq. (62) can easily be reformulated with respect to a new reference system r. If the single-site t matrices corresponding to W_r are denoted by $\mathbf{t}^r(\varepsilon)$, the respective Green's function matrix, $\mathbf{G}^r(\varepsilon) = \{G^{r,ij}(\varepsilon)\}$, $G^{r,ij}(\varepsilon) = \{G^{r,ij}_{LL'}(\varepsilon)\}$, see in particular also Eqs. (57) and (58), is given by

$$\mathbf{G}^r(\varepsilon) = \mathbf{G}^0(\varepsilon)[\mathbf{I} - \mathbf{t}^r(\varepsilon)\mathbf{G}^0(\varepsilon)]^{-1} \ , \tag{76}$$

where $\mathbf{I}$ denotes a unit matrix. By introducing the following difference:

$$\mathbf{t}_\Delta(\varepsilon) = \mathbf{t}(\varepsilon) - \mathbf{t}^r(\varepsilon) \ , \tag{77}$$

one obtains for $\mathbf{G}(\varepsilon)$:

$$\mathbf{G}(\varepsilon) = \mathbf{G}^r(\varepsilon)[\mathbf{I} - \mathbf{t}_\Delta(\varepsilon)\mathbf{G}^r(\varepsilon)]^{-1} \ . \tag{78}$$

Defining finally the following scattering-path operator:

$$\boldsymbol{\tau}_{\Delta}(\varepsilon) = [\mathbf{t}_{\Delta}(\varepsilon)^{-1} - \mathbf{G}^{r}(\varepsilon)]^{-1} \ , \tag{79}$$

$\mathbf{G}(\varepsilon)$ can also be expressed as

$$\mathbf{G}(\varepsilon) = \mathbf{G}^{r}(\varepsilon) + \mathbf{G}^{r}(\varepsilon)\boldsymbol{\tau}_{\Delta}(\varepsilon)\mathbf{G}^{r}(\varepsilon) = \mathbf{t}_{\Delta}(\varepsilon)^{-1}\boldsymbol{\tau}_{\Delta}(\varepsilon)\mathbf{t}_{\Delta}(\varepsilon)^{-1} - \mathbf{t}_{\Delta}(\varepsilon)^{-1} \ . \tag{80}$$

Therefore, once $\mathbf{t}^{r}(\varepsilon)$ and $\mathbf{G}^{r}(\varepsilon)$ are known, Eqs. (78)–(80) represent an equivalent set of equations to Eqs. (62)–(65). Combining Eq. (62) with Eq. (80) the below relation can easily be read off,

$$\boldsymbol{\tau}(\epsilon) = \mathbf{t}(\varepsilon)[\mathbf{t}_{\Delta}(\varepsilon)^{-1}\boldsymbol{\tau}_{\Delta}(\varepsilon)\mathbf{t}_{\Delta}(\varepsilon)^{-1} + (\mathbf{t}(\varepsilon)^{-1} - \mathbf{t}_{\Delta}(\varepsilon)^{-1})]\mathbf{t}(\varepsilon) \ . \tag{81}$$

3.4. Screened structure constants

By choosing a suitable W_r Eq. (75) can be solved such that

$$G^{r,ij}(\varepsilon) \equiv G^{r,ij}(\varepsilon) \sim 0 \quad \text{for } \forall|\mathbf{R}_i - \mathbf{R}_j| \geqslant d \ , \tag{82}$$

where the distance d has to be viewed as the radius of a sphere that comprises only a few types of "neighboring" sites such as e.g. first- and second-nearest neighbors.

Suppose now that in all atomic layers one and the same two-dimensional translational symmetry applies, with $\mathscr{L}^{(2)}$ referring to a simple two-dimensional lattice, and—in order to simplify the notation—position vectors are simply denoted by $\mathbf{R}_{pi}$,

$$\mathbf{R}_{pi} = \mathbf{C}_p + \mathbf{R}_{i,\|}; \quad \mathbf{R}_{i,\|} \in \mathscr{L}^{(2)}, \quad \mathbf{C}_p = R_{i,z}\mathbf{z} \ , \tag{83}$$

where $\mathbf{C}_p$ is sometimes referred to as the "spanning vector" of a particular layer p. According to Eq. (82) for the lattice Fourier transformed screened structure constants,

$$G^{r,pq}(\mathbf{k}_{\|};\varepsilon) = \sum_{\mathbf{R}_{\|}\in\mathscr{L}} \exp[\mathrm{i}\mathbf{k}_{\|}\cdot\mathbf{R}_{\|}]G^{r}(\mathbf{C}_p + \mathbf{R}_{\|}, \mathbf{C}_q;\varepsilon); \quad p,q = 1,\ldots,n \ , \tag{84}$$

therefore the following assumption can be made:

$$G^{r,pq}(\mathbf{k}_{\|};\varepsilon) = 0 \quad \text{if } |p-q| > N \ , \tag{85}$$

where N is a suitably chosen parameter. Consider now the following tridiagonal supermatrix:

$$\begin{pmatrix} \underline{A}_{11} & \underline{A}_{12} & 0 & 0 & 0 \\ \underline{A}_{21} & \underline{A}_{22} & \underline{A}_{23} & 0 & 0 \\ 0 & \underline{A}_{32} & \underline{A}_{33} & \underline{A}_{34} & 0 \\ 0 & 0 & \underline{A}_{43} & \underline{A}_{44} & \underline{A}_{45} \\ \vdots & & & & \ddots \end{pmatrix} \ , \tag{86}$$

i.e., a matrix where each matrix element $\underline{A}_{ij}$ is a square matrix.

A non-vanishing block of dimension N of elements $G^{r,pq}(\mathbf{k}_\parallel;\varepsilon)$, $|p-q| \leqslant N$, can therefore be viewed as one particular element of such a tridiagonal matrix. Labelling the rows and columns of this tridiagonal matrix by P and Q ("principal layers") the supermatrix of the screened structure constants, $\mathbf{G}^r(\mathbf{k}_\parallel;\varepsilon) = \{G^{r,pq}(\mathbf{k}_\parallel;\varepsilon)\}$, can be viewed also as a tridiagonal matrix in "principal layers",

$$\mathbf{G}^r(\mathbf{k}_\parallel;\varepsilon) = \{\underline{G}^{r,PQ}(\mathbf{k}_\parallel;\varepsilon)\} \ . \tag{87}$$

Furthermore, if a parent three-dimensional lattice [18] can be assumed, i.e., if all interlayer distances are equal (no layer relaxation), then obviously the elements of this tridiagonal matrix are of the following form:

$$\underline{G}^{r,PQ}(\mathbf{k}_\parallel;\varepsilon) = \begin{cases} \underline{G}^{r,00}(\mathbf{k}_\parallel;\varepsilon), & P = Q \ , \\ \underline{G}^{r,01}(\mathbf{k}_\parallel;\varepsilon), & P = Q-1 \ , \\ \underline{G}^{r,10}(\mathbf{k}_\parallel;\varepsilon), & P = Q+1 \ , \\ 0, & \text{otherwise} \ , \end{cases} \tag{88}$$

where the index zero refers to an arbitrarily chosen origin of $\mathscr{L}^{(2)}$. It should be noted that in the case of layer relaxations in principle all $\underline{G}^{r,PQ}(\mathbf{k}_\parallel;\varepsilon)$ are different, although $\mathbf{G}^r(\mathbf{k}_\parallel;\varepsilon)$ is still formally tridiagonal.

The $\mathbf{k}_\parallel$th projection of $\boldsymbol{\tau}_\Delta(\varepsilon)$, see Eq. (79), is then given by

$$\boldsymbol{\tau}_\Delta(\mathbf{k}_\parallel;\varepsilon) = [\mathbf{t}_\Delta(\varepsilon)^{-1} - \mathbf{G}^r(\mathbf{k}_\parallel;\varepsilon)]^{-1} \ , \tag{89}$$

where

$$\mathbf{t}_\Delta(\varepsilon) = \{\underline{t}^P_\Delta(\varepsilon)\delta_{PQ}\}, \quad \underline{t}^P_\Delta(\varepsilon) = \{t^p_\Delta(\varepsilon)\delta_{pq}\} \ , \tag{90}$$

$$\boldsymbol{\tau}_\Delta(\mathbf{k}_\parallel;\varepsilon) = \{\underline{\tau}^{PQ}_\Delta(\mathbf{k}_\parallel;\varepsilon)\}, \quad \underline{\tau}^{PQ}_\Delta(\varepsilon) = \{\tau^{pq}_\Delta(\varepsilon)\} \ . \tag{91}$$

Quite clearly, since $\mathbf{t}_\Delta(\varepsilon)$ formally is a diagonal supermatrix, the inverse of $\boldsymbol{\tau}_\Delta(\mathbf{k}_\parallel;\varepsilon)$ is of tridiagonal form.

3.5. Partitioning of configuration space

Usually for a system with a surface or with interfaces three regions of different physical properties can be distinguished, namely a *left semi-infinite system* (L), a *right semi-infinite system* (R) and an *intermediate region* (I). These regions correspond to the following numbering scheme for principal layers:

$$\begin{aligned} &\mathrm{L} : -\infty < P \leqslant 0 \ , \\ &\mathrm{I} : 1 \leqslant P \leqslant n \ , \\ &\mathrm{R} : \mathrm{n}+1 \leqslant P < \infty \ , \end{aligned} \tag{92}$$

which in turn implies, that $[\boldsymbol{\tau}_{\Delta}(\mathbf{k}_{\parallel};\varepsilon)]^{-1}$ can be partitioned as follows:

$$[\boldsymbol{\tau}_{\Delta}(\mathbf{k}_{\parallel};\varepsilon)]^{-1} = \begin{pmatrix} [\boldsymbol{\tau}_{\Delta}(\mathbf{k}_{\parallel};\varepsilon)]^{-1}_{\mathrm{L,L}} & [\boldsymbol{\tau}_{\Delta}(\mathbf{k}_{\parallel};\varepsilon)]^{-1}_{\mathrm{L,I}} & \mathbf{0} \\ [\boldsymbol{\tau}_{\Delta}(\mathbf{k}_{\parallel};\varepsilon)]^{-1}_{\mathrm{I,L}} & [\boldsymbol{\tau}_{\Delta}(\mathbf{k}_{\parallel};\varepsilon)]^{-1}_{\mathrm{I,I}} & [\boldsymbol{\tau}_{\Delta}(\mathbf{k}_{\parallel};\varepsilon)]^{-1}_{\mathrm{I,R}} \\ \mathbf{0} & [\boldsymbol{\tau}_{\Delta}(\mathbf{k}_{\parallel};\varepsilon)]^{-1}_{\mathrm{R,I}} & [\boldsymbol{\tau}_{\Delta}(\mathbf{k}_{\parallel};\varepsilon)]^{-1}_{\mathrm{R,R}} \end{pmatrix} . \tag{93}$$

In order to evaluate $\boldsymbol{\tau}(\mathbf{k}_{\parallel};\varepsilon)_{\mathrm{I,I}}$ use can be made of the so-called surface scattering path operators, which in turn refer to the so-called "missing elements" in the above tridiagonal matrix,

$$\underline{\Delta}_{\mathrm{L}}(\mathbf{k}_{\parallel};\varepsilon) = [\underline{t}^{\mathrm{L}}_{\Delta}(\varepsilon)^{-1} - \underline{G}^{r,00}(\mathbf{k}_{\parallel};\varepsilon) - \underline{G}^{r,10}(\mathbf{k}_{\parallel};\varepsilon)\underline{\Delta}_{\mathrm{L}}(\mathbf{k}_{\parallel};\varepsilon)\underline{G}^{r,01}(\mathbf{k}_{\parallel};\varepsilon)]^{-1} , \tag{94}$$

$$\underline{\Delta}_{\mathrm{R}}(\mathbf{k}_{\parallel};\varepsilon) = [\underline{t}^{\mathrm{R}}_{\Delta}(\varepsilon)^{-1} - \underline{G}^{r,00}(\mathbf{k}_{\parallel};\varepsilon) - \underline{G}^{r,01}(\mathbf{k}_{\parallel};\varepsilon)\underline{\Delta}_{\mathrm{R}}(\mathbf{k}_{\parallel};\varepsilon)\underline{G}^{r,10}(\mathbf{k}_{\parallel};\varepsilon)]^{-1} . \tag{95}$$

It should be noted that in Eqs. (94)–(95) and in the following equation a parent three-dimensional lattice is assumed. In terms of these two quantities, which have to be calculated selfconsistently, the PQth element of the scattering path operator in the interface region is then given by

$$\begin{aligned}[[\boldsymbol{\tau}_{\Delta}(\mathbf{k}_{\parallel};\varepsilon)]^{-1}_{\mathrm{I,I}}]^{PQ} = {} & (\underline{t}^{P}_{\Delta}(\varepsilon)^{-1} - \underline{G}^{r,00}(\mathbf{k}_{\parallel};\varepsilon))\delta_{PQ} - \underline{G}^{r,01}(\mathbf{k}_{\parallel};\varepsilon)\delta_{P,Q-1} - \underline{G}^{r,10}(\mathbf{k}_{\parallel};\varepsilon)\delta_{P,Q+1} \\ & - \underline{G}^{r,01}(\mathbf{k}_{\parallel};\varepsilon)\underline{\Delta}^{r}_{\mathrm{L}}(\mathbf{k}_{\parallel};\varepsilon)\underline{G}^{r,01}(\mathbf{k}_{\parallel};\varepsilon)\delta_{P,1}\delta_{Q,1} \\ & - \underline{G}^{r,10}(\mathbf{k}_{\parallel};\varepsilon)\underline{\Delta}^{r}_{\mathrm{R}}(\mathbf{k}_{\parallel};\varepsilon)\underline{G}^{r,10}(\mathbf{k}_{\parallel};\varepsilon)\delta_{P,\mathrm{n}}\delta_{Q,\mathrm{n}} .\end{aligned} \tag{96}$$

Finally, with respect to two given sites, $\mathbf{R}_n = \mathbf{R}_{n,\parallel} + \mathbf{C}_p$ and $\mathbf{R}_n = \mathbf{R}_{n,\parallel} + \mathbf{C}_q$, respectively, $\mathbf{R}_{n,\parallel}, \mathbf{R}_{m,\parallel} \in \mathscr{L}^{(2)}$, the so-called site representation of $\boldsymbol{\tau}_{\Delta}(\mathbf{k}_{\parallel};\varepsilon)$ in the interface region can be obtained by means of the following surface Brillouin zone integral:

$$\tau^{nm}_{\Delta}(\varepsilon) = \frac{1}{\Omega_{\mathrm{SBZ}}} \int \exp[-\mathrm{i}\mathbf{k}_{\parallel}\cdot(\mathbf{R}_{n,\parallel} - \mathbf{R}_{m,\parallel})]\tau^{pq}_{\Delta}(\mathbf{k}_{\parallel};\varepsilon)\,\mathrm{d}\mathbf{k}_{\parallel} , \tag{97}$$

where Ω_{SBZ} is the unit area of the two-dimensional Surface Brillouin Zone (SBZ). Since the "unscreened" scattering path operator $\tau^{nm}(\varepsilon)$ is always related to $\tau^{nm}_{\Delta}(\varepsilon)$ via Eq. (81), in the following sections simply $\tau^{nm}(\varepsilon)$ is used.

3.6. Rotation of frames

Now we shall go back to the Kohn–Sham–Dirac Hamiltonian in Eq. (24) and the section that introduced the concept of magnetic configurations. Let $R \in \mathrm{O}(3)$ be a rotation, which transforms the orientation of the effective magnetization $\boldsymbol{\xi}^{pi}$ of site i in the pth layer into the direction $\hat{\mathbf{z}}$. Furthermore, let $t^{pi}(\varepsilon)$ refer to the single-site t-matrix if $\boldsymbol{\xi}^{pi}$ is parallel to $\hat{\mathbf{z}}$, while $t^{pi}_{R}(\varepsilon)$ refers to the t-matrix if $\boldsymbol{\xi}^{pi}$ points along the direction $R^{-1}\hat{\mathbf{z}}$. Because the effective potential and the effective exchange field are spherical symmetric, see Eqs. (72) and (73), these two single-site t-matrices are related to each other by the following similarity transformation,

$$t^{pi}_{R}(\varepsilon) = D(R)t^{pi}(\varepsilon)D(R)^{\dagger} , \tag{98}$$

where $D(R)$ contains blockwise the irreducible projective representations [20] of R. Clearly enough two-dimensional translational invariance then implies that

$$t_R^{pi}(\varepsilon) = t_R^{p0}(\varepsilon), \quad \forall i \in I(\mathscr{L}^{(2)}) \ , \tag{99}$$

where $i = 0$ refers to the origin of $\mathscr{L}^{(2)}$.

Special care has to be taken in performing the occurring Brillouin zone integrals needed to evaluate the elements of the scattering path operator, see Eq. (97), since in the presence of a magnetic field these integrals can no longer be restricted to an irreducible wedge of the corresponding Surface Brillouin Zone. Let G be the point group of the underlying two-dimensional lattice, such as for example C_{4v} in the case of an fcc(0 0 1) surface, and suppose $D(S)$ contains blockwise the irreducible projective representations [20] of $S \in G$. If IBZ_1 denotes an irreducible wedge of the SBZ, then any other wedge IBZ_S of the SBZ is defined by

$$\mathrm{IBZ}_S = \{S\mathbf{k}_\parallel \mid \mathbf{k}_\parallel \in \mathrm{IBZ}_1\}; \quad S \in G \ , \tag{100}$$

such that

$$\mathrm{SBZ} = \sum_{S \in G} \mathrm{IBZ}_S \ . \tag{101}$$

It easily can be shown that

$$\tau^{pq}(S^{-1}\mathbf{k}_\parallel; \varepsilon) = D(S)^+ \tau_S^{pq}(\mathbf{k}_\parallel; \varepsilon) D(S) \ , \tag{102}$$

where—as should be noted—p, q are layer indices and $\tau_S^{pq}(\mathbf{k}_\parallel; \varepsilon)$ refers to the corresponding similarity transformed t-matrix $t_S^{p0}(\varepsilon)$, as defined in Eq. (99). The SBZ-integral, Eq. (97), can therefore be expressed as

$$\tau^{pq}(\varepsilon) = \sum_{S \in G} D(S)^+ \left[\frac{1}{\Omega_{\mathrm{IBZ}_1}} \int_{\mathrm{IBZ}_1} \tau_S^{pq}(\mathbf{k}_\parallel; \varepsilon) \, \mathrm{d}\mathbf{k}_\parallel \right] D(S) \ , \tag{103}$$

where Ω_{IBZ_1} denotes the surface area of IBZ_1. Eq. (103) implies (i) that the structure constants need only be evaluated for a chosen set of $\mathbf{k}_\parallel \in \mathrm{IBZ}_1$ and (ii) that for any pair $S, R \in G$ for which $t_S^{p0}(\varepsilon) = t_R^{p0}(\varepsilon)$ the integrals in Eq. (103) are identical.

3.7. Atomic sphere approximation

Frequently in practical calculations the so-called atomic sphere approximation (ASA) is used in which the unit volume Ω^p corresponding to the origin of the two-dimensional lattice characterizing atomic layer p is replaced by a sphere of equal volume,

$$\frac{4\pi}{3}(R_{\mathrm{WS}}^p)^3 = \Omega^p \ . \tag{104}$$

The radius of this sphere—the Wigner–Seitz radius—is then used to (a) calculate respective single site t-matrices and (b) to determine the normalization integrals of scattering solutions needed to

evaluate densities of states, Bloch spectral functions, or magnetic moments, see in particular the discussion in [17], i.e., R^p_{WS} replaces uniformly the muffin-tin radii.

3.8. The coherent potential approximation for inhomogeneously disordered solid systems

For a given intermediate region of n layers the so-called coherent scattering path operator $\tau_c(z)$ is defined as

$$\tau_c^{pi,qj}(z) = \Omega_{\mathrm{SBZ}}^{-1} \int \exp[-\mathrm{i}\mathbf{k}_\parallel \cdot (\mathbf{R}_{i,\parallel} - \mathbf{R}_{j,\parallel})] \tau_c^{pq}(\mathbf{k}_\parallel, z)\, \mathrm{d}\mathbf{k}_\parallel \ , \tag{105}$$

which implies that in each layer p for the coherent single-site t-matrices the following translational invariance applies:

$$t_c^{pi}(z) = t_c^p(z); \quad \forall i \in I(\mathscr{L}^{(2)}) \ . \tag{106}$$

In Eq. (106) it is supposed that in all atomic layers one and the same two-dimensional translational symmetry applies, where $\mathscr{L}^{(2)}$ refers to a simple two-dimensional lattice, and that position vectors are simply denoted by $\mathbf{R}_{pi}$,

$$\mathbf{R}_{pi} = \mathbf{C}_p + \mathbf{R}_{i,\parallel}; \quad \mathbf{R}_{i,\parallel} \in \mathscr{L}^{(2)}, \quad \mathbf{C}_p = R_{i,z}\mathbf{z} \ . \tag{107}$$

In the following only (super-) matrices, labelled by layers shall be used:

$$\mathbf{t}_c(z) = \begin{pmatrix} t_c^{11}(z) & 0 & \cdots & \cdots & 0 \\ \vdots & \ddots & \cdots & \cdots & 0 \\ \vdots & 0 & t_c^{pp}(z) & 0 & \vdots \\ \vdots & \cdots & \cdots & \ddots & \cdots \\ 0 & \cdots & \cdots & 0 & t_c^{nn}(z) \end{pmatrix} , \tag{108}$$

$$\boldsymbol{\tau}_c(z) = \begin{pmatrix} & \vdots & & \vdots & \\ \cdots & \tau_c^{pp}(z) & \cdots & \tau_c^{pq}(z) & \cdots \\ & \vdots & & \vdots & \\ \cdots & \tau_c^{qp}(z) & \cdots & \tau_c^{qq}(z) & \cdots \\ & \vdots & & \vdots & \end{pmatrix} , \tag{109}$$

with $t_c^{pp}(z) \equiv t_c^p(z)$ and $p, q = 1, \ldots, n$.

Quite clearly a particular element of $\tau_c(z)$,

$$\tau_c^{pq}(z) = \tau_c^{pi,qi}(z) = \tau_c^{p0,q0}(z) = \Omega_{\mathrm{SBZ}}^{-1} \int \tau_c^{pq}(\mathbf{k}_\parallel, z)\, \mathrm{d}\mathbf{k}_\parallel \ , \tag{110}$$

refers to the unit cells ($i=0$) at the origin of $\mathscr{L}^{(2)}$ in layers p and q. Suppose now the concentration for constituents A and B in layer p is denoted by c_p^α ($p=1,\ldots,n$),

$$\sum_{\alpha=A,B} c_p^\alpha = 1 \ , \tag{111}$$

and one specifies the occupation in the unit cell at the origin of $\mathscr{L}^{(2)}$ of a particular layer p in terms of the following matrix $\mathbf{m}_{p\alpha}(z)$

$$\mathbf{m}_{p\alpha}(z) = \begin{pmatrix} 0 & & \cdots & & \\ & \ddots & & & \\ 0 & \cdots & m_\alpha^p(z) & \cdots & 0 \\ & & & \ddots & \\ & & \cdots & & 0 \end{pmatrix} \ , \tag{112}$$

$$m_\alpha^p(z) = t_c^p(z)^{-1} - t_\alpha^p(z)^{-1}, \quad \alpha = A,B \ , \tag{113}$$

where $t_\alpha^p(z)$ is the single-site t-matrix for constituent α in layer p. The corresponding layer-diagonal element of the so-called impurity matrix is then given by

$$D_\alpha^{pp}(z) \equiv D_\alpha^{p0,\,p0}(z) = [1 - m_\alpha^p(z)\tau_c^{p0,\,p0}(z)]^{-1} \ , \tag{114}$$

and specifies a single impurity of type α in the translational invariant "host" formed by layer p. The coherent scattering path operator for the intermediate region (multilayer) $\tau_c(z)$, is therefore obtained from the following inhomogeneous CPA condition [19]:

$$\tau_c^{pp}(z) = \sum_{\alpha=A,B} c_p^\alpha \langle \tau^{pp}(z) \rangle_{p,\alpha} \ , \tag{115}$$

$$\langle \tau^{pp}(z) \rangle_{p,\alpha} = \tau_\alpha^{pp}(z) = D_\alpha^{pp}(z)\tau_c^{pp}(z) \ , \tag{116}$$

$$p = 1,\ldots,n \ , \tag{117}$$

i.e., from a condition that implies solving *simultaneously* a layer-diagonal CPA condition for layers $p=1,\ldots,n$. Once this condition is met then translational invariance in each layer under consideration is achieved,

$$\langle \tau^{pp}(z) \rangle_{p,\alpha} \equiv \langle \tau^{p0,\,p0}(z) \rangle_{p0,\alpha} = \langle \tau^{pi,\,pi}(z) \rangle_{pi,\alpha} \ , \tag{118}$$

$$\forall i \in I(\mathscr{L}^{(2)}), \quad \alpha = \mathrm{A,B}, \quad p = 1,\ldots,n \ . \tag{119}$$

Similarly, by specifying the occupation in two different sites, see e.g. [17,19], the following restricted averages are obtained,

$$p \neq q\text{: } \langle \tau^{pi,qj}(z) \rangle_{pi\alpha,qj\beta} = D_\alpha^{pp}(z)\tau_c^{pi,qj}(z)D_\beta^{qq}(z)^t, \quad \forall i,j \in I(\mathscr{L}^{(2)}) \ , \tag{120}$$

$$p = q\text{: } = \langle \tau^{pi,\,pj}(z) \rangle_{pi\alpha,\,pj\beta} = D_\alpha^{pp}(z)\tau_c^{pi,\,pj}(z)D_\beta^{pp}(z)^t, \quad \forall (i \neq j) \in I(\mathscr{L}^{(2)}) \ , \tag{121}$$

where $\langle \tau_c^{pi,qj}(z) \rangle_{pi\alpha,qj\beta}$ has the meaning that site (subcell) pi is occupied by species α and site (subcell) qj by species β and the symbol t indicates a transposed matrix.

3.9. The embedded cluster method

Let us assume a finite set of impurities interacts within a given finite range of a semi-infinite host such as is the case of finite nanostructures on or in the surface of a (metallic) substrate ("host"). By choosing a certain set $\mathbb{C} = \{\mathbf{R}_m\}$ of (lattice) sites ("cluster") occupied by these impurities but also by perturbed host atoms, such that outside $\mathbb{C}$ the potentials can be considered to be identical with those of the unperturbed host, then $\mathbb{C}$ can be treated as a perturbation of the host. Suppose the lattice Fourier transformed scattering path operator of the two-dimensional translationally invariant layered host is denoted by $\boldsymbol{\tau}_h(\mathbf{k}_\parallel, E) = \{\tau_h^{pq}(\mathbf{k}_\parallel, E)\}$, see also Eqs. (85), (97) and (103),

$$\tau_h^{mn}(E) = \frac{1}{\Omega_{\mathrm{SBZ}}} \int_{\mathrm{SBZ}} \mathrm{e}^{-\mathrm{i}\mathbf{k}_\parallel \cdot (\mathbf{R}_{i,\parallel} - \mathbf{R}_{j,\parallel})} \tau_h^{pq}(\mathbf{k}_\parallel, E)\, \mathrm{d}^2 k_\parallel \ , \tag{122}$$

$$\mathbf{R}_m = \mathbf{R}_{i,\parallel} + \mathbf{C}_p, \quad \mathbf{R}_n = \mathbf{R}_{j,\parallel} + \mathbf{C}_q, \quad \mathbf{R}_{i,\parallel}, \mathbf{R}_{j,\parallel} \in \mathscr{L}^{(2)} \ , \tag{123}$$

where p and q refer to layers and $\mathbf{k}_\parallel \in \mathrm{SBZ}$. By replacing the t-matrices of the unperturbed host, $\mathbf{t}_h(E)$, with those of the cluster-atoms, $\mathbf{t}_{\mathbb{C}}(E)$, leads to the following Dyson like equation,

$$\boldsymbol{\tau}_{\mathbb{C}}(E) = \boldsymbol{\tau}_h(E)[1 - (\mathbf{t}_h^{-1}(E) - \mathbf{t}_{\mathbb{C}}^{-1}(E))\boldsymbol{\tau}_h(E)]^{-1} \ , \tag{124}$$

where $\boldsymbol{\tau}_{\mathbb{C}}(E)$ is the SPO-matrix corresponding to all sites in cluster $\mathbb{C}$, from which in turn all corresponding local quantities, i.e., charge and magnetization densities, spin- and orbital moments, as well as the total energy can be calculated. Note, that Eq. (124) takes into account all scattering events, both, inside and outside the cluster [21].

4. Interlayer exchange energy and the magnetic anisotropy energy

4.1. Interlayer exchange energy (IEC)

At a first glance it would seem that by simply taking the total energy difference between two relevant magnetic configurations such as for example the ferromagnetic ("parallel") and the antiferromagnetic ("antiparallel") ones, the IEC can readily be obtained. Unfortunately this implies to take the difference between two very large numbers, i.e., one has to be sure that not only both total energies are well converged with respect to the Brillouin zone integration used but also with respect to a sufficient number of decimal places since the IEC usually is only of the order of a few meV or even less. Independent from the actual "band structure" method applied this *caveat* makes the use of total energies numerically not quite advisable. Furthermore, electronic structure methods based on three-dimensional translational periodicity ("supercell approaches") can be quite misleading for essentially two reasons: (1) in reality, i.e., in experiments, usually only trilayer systems consisting of 2 magnetic slabs and a spacer are measured and not a periodic array of trilayers, and

(2) by changing for example the thickness of the spacer the Fermi energy changes causing in turn incompatibilities with respect to the magnetic slabs. For these reasons essentially only approaches based on two-dimensional periodicity ("surface Green's function approaches for layered systems") guarantee a physically correct description of a system consisting of a substrate and a magnetic trilayer with a free surface, in particular since only Green's function approaches are suitable for taking into account effects of alloying and interdiffusion at interfaces in terms of the coherent potential approximation.

In most applications up to now the magnetic force theorem [22] was applied by considering the grand-potentials of the two magnetic configurations under investigation

$$\Delta E_b = E_b(\mathscr{C}) - E_b(\mathscr{C}_0) \ , \tag{125}$$

evaluating, however, only one magnetic configuration ($\mathscr{C}_0$, one of them) selfconsistently. If c_α^p denotes the respective concentrations of the constituents A and B in layer p then in terms of the (inhomogeneous) CPA for layered systems, see the previous section, ΔE_b is given by

$$\Delta E_b = \sum_{p=1}^{N} \sum_{\alpha=A,B} c_\alpha^p \Delta E_\alpha^p, \quad \sum_{\alpha=A,B} c_\alpha^p = 1 \ , \tag{126}$$

where the

$$\Delta E_\alpha^p = \int_{\varepsilon_b}^{\varepsilon_F} (n_\alpha^p(\mathscr{C},\varepsilon) - n_\alpha^p(\mathscr{C}_0,\varepsilon))(\varepsilon - \varepsilon_F)\,\mathrm{d}\varepsilon \ , \tag{127}$$

refer to component- and layer-resolved contributions to the grand-potential at T=0. In Eq. (127) the $n_\alpha^p(\mathscr{C},\varepsilon)$ are component and layer projected DOS's corresponding to magnetic configuration $\mathscr{C}$, ε_b denotes the bottom of the valence band and ε_F is the Fermi energy of the (nonmagnetic) substrate serving as electron reservoir. Only in the case that Eqs. (126)–(127) are used for bulk systems (three-dimensional translational invariance) the Fermi energy becomes configuration dependent. If the substrate (two-dimensional invariance) is magnetic then ε_F simply refers to the chosen magnetic configuration in the substrate, e.g., in-plane or perpendicular to the surface, and remains constant upon deposition of other materials. The energy integral in Eq. (127) is usually performed in the upper half of the complex plane using a contour starting at ε_b and ending at ε_F.

Note that because of the definition given in Eq. (125) this implies the following energetic order of magnetic configurations

$$\Delta E_b = \begin{cases} > 0; & \to \mathscr{C}; \text{preferred configuration} \\ < 0; & \to \mathscr{C}_0; \text{preferred configuration} \end{cases} \tag{128}$$

The numerical advantage of using grand-potentials is that (1) they can be calculated very accurately and (2) only differences of reasonably small numbers have to be taken. The error made by evaluating just one magnetic configuration selfconsistently is usually of the order of 3–5%, see [23].

The example displayed in Fig. 1 shows *inter alia* that $\mathscr{C}$ in Eq. (125) not necessarily is restricted to *the* "antiferromagnetic" configuration. In this example [23]—the interlayer exchange coupling in

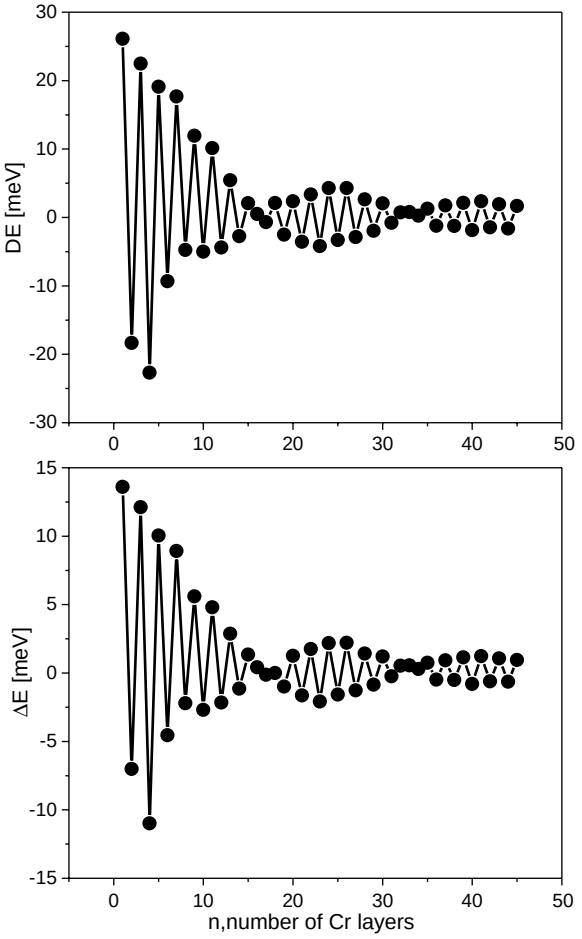

Fig. 1. Antiferromagnetic (top) and perpendicular (bottom) interlayer exchange coupling energy in bcc-Fe(1 0 0)/$Fe_6Cr_nFe_6$/Vac. From Ref. [23].

a particular Fe/Cr/Fe trilayer—one can see quite impressively not only two kinds of periods, namely a short and a long period, but also the "phase slip" famous for this system.

4.2. Magnetic anisotropy energy (E_a)

Let $\mathscr{C}$ and $\mathscr{C}_0$ refer to a uniform in-plane and a uniform perpendicular to the planes of atoms orientation of the magnetization, respectively. The magnetic anisotropy energy E_a is then given as a sum of two contributions, the so-called band energy part (ΔE_b) defined by Eq. (125), and the magnetic dipole–dipole interaction (ΔE_{dd}), frequently also called shape anisotropy,

$$E_a = \Delta E_b + \Delta E_{dd} \ , \tag{129}$$

$$\Delta E_{dd} = E_{dd}(\mathscr{C}) - E_{dd}(\mathscr{C}_0) \ . \tag{130}$$

The (classical) magnetostatic dipole–dipole interaction energy for a given magnetic configuration $\mathscr{C}$ appearing in this context is defined (in atomic Rydberg units) by

$$E_{dd}(\mathscr{C}) = \frac{1}{c^2} \sum_{i,j;i\neq j} \left\{ \frac{\mathbf{m}_i \mathbf{m}_j}{|\mathbf{R}_i - \mathbf{R}_j|^3} - 3\, \frac{[\mathbf{m}_i \cdot (\mathbf{R}_i - \mathbf{R}_j)][\mathbf{m}_j \cdot (\mathbf{R}_i - \mathbf{R}_j)]}{|\mathbf{R}_i - \mathbf{R}_j|^5} \right\} , \tag{131}$$

where the magnetic moments $\mathbf{m}_i$ corresponding to $\mathscr{C}$ are located at sites $\mathbf{R}_i$ and c is the speed of light. In the presence of two-dimensional translational symmetry ($\mathbf{R}_i = \mathbf{R}_{i,\parallel} + \mathbf{R}_{i,z}, \mathbf{R}_{i,\parallel} \in \mathscr{L}^{(2)}$) Eq. (131) can be evaluated [16] very efficiently using Ewald's summation technique.

4.3. Disordered systems

In terms of the inhomogeneous CPA for layerwise, binary substitutionally disordered systems the magnetic moments arising from the constituents have to be weighted with their respective concentrations such that to each site in a given layer p a uniform magnetic moment applies,

$$\langle \mathbf{m}_p \rangle = \sum_{\alpha} c_p^{\alpha} \mathbf{m}_p^{\alpha} , \tag{132}$$

where $\langle\rangle$ denotes an average over statistical configurations [16] and $\mathbf{m}_p^{\alpha}$ refers to the magnetic moment of component α in layer p. It should be noted that by using the above averaged magnetic moments in Eq. (131), one in fact neglects vertex corrections of the kind $\langle \mathbf{m}_i \mathbf{m}_j \rangle - \langle \mathbf{m}_i \rangle \langle \mathbf{m}_j \rangle$, $i \neq j$.

5. The Kubo–Greenwood equation

Suppose the diagonal elements of the electrical conductivity tensor of a disordered system, namely $\sigma_{\mu\mu}$, is calculated using the Kubo–Greenwood formula [2,5,6]:

$$\sigma_{\mu\mu} = \frac{\pi\hbar}{N_0 \Omega_{at}} \left\langle \sum_{m,n} J^{\mu}_{mn} J^{\mu}_{nm} \delta(\varepsilon_F - \varepsilon_m) \delta(\varepsilon_F - \varepsilon_n) \right\rangle . \tag{133}$$

In this equation $\mu \in \{x, y, z\}$, N_0 is the number of atoms, J^{μ} is a representation of the μ-th component of the current operator,

$$J_{\mu} = \{J^{\mu}_{nm}\}; \quad J^{\mu}_{nm} = \langle n | J_{\mu} | m \rangle , \tag{134}$$

ε_F is the Fermi energy, $|m\rangle$ an eigenstate of a particular configuration of the random system under consideration, Ω_{at} the atomic volume, and $\langle \cdots \rangle$ denotes an average over configurations. Eq. (133) can be reformulated in terms of the imaginary part of the (one-particle) Green's function $G(z), z = \varepsilon + \mathrm{i}\delta$, see Eq. (51),

$$\sigma_{\mu\mu} = \frac{\hbar}{\pi N_0 \Omega_{at}} \operatorname{Tr} \langle J_{\mu} \operatorname{Im} G^{+}(\varepsilon_F) J_{\mu} \operatorname{Im} G^{+}(\varepsilon_F) \rangle , \tag{135}$$

or, by using "up-" and "down-" side limits, see Eq. (50), this equation can be rewritten [19,24] as

$$\sigma_{\mu\mu} = \tfrac{1}{4} \{ \tilde{\sigma}_{\mu\mu}(\varepsilon^+, \varepsilon^+) + \tilde{\sigma}_{\mu\mu}(\varepsilon^-, \varepsilon^-) - \tilde{\sigma}_{\mu\mu}(\varepsilon^+, \varepsilon^-) - \tilde{\sigma}_{\mu\mu}(\varepsilon^-, \varepsilon^+) \} , \tag{136}$$

where $\varepsilon^{+} = \varepsilon_F + \mathrm{i}\delta$, $\varepsilon^{-} = \varepsilon_F - \mathrm{i}\delta$; $\delta \to 0$, and

$$\tilde{\sigma}_{\mu\mu}(\varepsilon_1, \varepsilon_2) = -\frac{\hbar}{\pi N_0 \Omega_{at}} \operatorname{tr}\langle J_\mu G(\varepsilon_1) J_\mu G(\varepsilon_2)\rangle; \quad \varepsilon_i = \varepsilon^{\pm}; \quad i = 1,2 \ . \tag{137}$$

The actual form of the off-diagonal elements of the conductivity tensor is slightly more complicated, see, e.g., Refs. [6,8,25], however, for the present purpose they are of little interest.

5.1. Current matrices

Let $J_\mu^{i\alpha}(\varepsilon_1, \varepsilon_2)$ denote the angular momentum representation of the μth component of the current operator according to component $\alpha = A, B$ in a particular site i. Using a non-relativistic formulation for the current operator, namely $\mathbf{J} = (e\hbar/im)\boldsymbol{\nabla}$, the elements of $J_\mu^{i\alpha}(\varepsilon_1, \varepsilon_2)$ are given by [19]

$$J^{i\alpha}_{\mu,\Lambda\Lambda'}(\varepsilon_1, \varepsilon_2) = \frac{e}{m}\frac{\hbar}{i}\int_{\mathrm{WS}} Z^{i\alpha}_{\Lambda}(\mathbf{r}_i, \varepsilon_1)^{\dagger} \frac{\partial}{\partial r_{i,\mu}} Z^{i\alpha}_{\Lambda'}(\mathbf{r}_i, \varepsilon_2)\, \mathrm{d}^3 r_i, \quad \Lambda = (\ell m) \ , \tag{138}$$

while within a relativistic formulation for the current operator, namely $\mathbf{J} = ec\,\boldsymbol{\alpha}$, one gets

$$J^{i\alpha}_{\mu,\Lambda\Lambda'}(\varepsilon_1, \varepsilon_2) = ec \int_{\mathrm{WS}} Z^{i\alpha}_{\Lambda}(\mathbf{r}_i, \varepsilon_1)^{\dagger} \alpha_\mu Z^{i\alpha}_{\Lambda'}(\mathbf{r}_i, \varepsilon_2)\, \mathrm{d}^3 r_i, \quad \Lambda = (\kappa\mu) \ . \tag{139}$$

In Eqs. (138) and (139) the functions $Z^{i\alpha}_{\Lambda}(\mathbf{r}_i, z)$ are the usual (regular) scattering solutions [16,17] introduced earlier in Eq. (59).

5.2. Conductivity in real space for a finite number of scatterers

If no translational symmetry at all is present then in principle one has to sum over all sites in the system including leads, contacts, etc., i.e., a typical contribution to the conductivity is given by [19,26]

$$\tilde{\sigma}_{\mu\mu}(\mathscr{C}; \varepsilon_1, \varepsilon_2) = \sum_{i,j=1}^{N_0} \tilde{\sigma}^{ij}_{\mu\mu}(\mathscr{C}; \varepsilon_1, \varepsilon_2) \ , \tag{140}$$

$$\tilde{\sigma}^{ij}_{\mu\mu}(\mathscr{C}; \varepsilon_1, \varepsilon_2) = (w/N_0) \operatorname{tr}\langle J^i_\mu(\varepsilon_2, \varepsilon_1) \tau^{ij}(\varepsilon_1) J^j_\mu(\varepsilon_1, \varepsilon_2) \tau^{ji}(\varepsilon_2)\rangle \ , \tag{141}$$

where $w = -(4m^2/\hbar^3 \pi \Omega_{\mathrm{at}})$, N_0 is the total number of scattering sites in the system, i.e., is of the order of 10^{23} and the $\tau^{ij}(\varepsilon)$ refer to the scattering path operator defined in the previous section. As such a procedure is numerically not accessible one can define the following quantity

$$\tilde{\sigma}_{\mu\mu}(\mathscr{C}; \varepsilon_1, \varepsilon_2; n) = \sum_{i,j=1}^{n} \tilde{\sigma}^{ij}_{\mu\mu}(\mathscr{C}; \varepsilon_1, \varepsilon_2) \ , \tag{142}$$

with n being the number of sites in a chosen region ("cluster"). This implies, however, that the convergence properties of $\tilde{\sigma}_{\mu\mu}(\varepsilon_1, \varepsilon_2; n)$ with respect to n have to be investigated. It should be noted that in order to specify the magnetic configuration $\mathscr{C}$ the orientations of the magnetization in all sites of the chosen region has to be given.

Clearly enough the most useful test cases for the reliability of a "real space" approach are those where the answer is known, namely for pure (bulk) metals or binary bulk substitutional alloys.

If $i = 0$ refers to the (chosen) site at the origin of a cluster and $\mathbf{R}_{oj}$ denotes the distance vector to the jth neighboring site, then Eq. (142) can be also written as

$$\tilde{\sigma}_{\mu\mu}(\mathscr{C};\varepsilon_1,\varepsilon_2;r) = \sum_{|\mathbf{R}_{oj}|\leqslant r} \tilde{\sigma}^{0j}_{\mu\mu}(\mathscr{C};\varepsilon_1,\varepsilon_2) \ . \tag{143}$$

In the case of a planar cluster, r, the "size of the cluster", is the radius of a circle within all sites are encountered for; in a similar sense, in the case of a three-dimensional cluster, r refers to the radius of a sphere. In the case of a bulk system (infinite system) the corresponding contribution to the conductivity is then given by

$$\tilde{\sigma}_{\mu\mu}(\mathscr{C};\varepsilon_1,\varepsilon_2) = \lim_{r\to\infty} \tilde{\sigma}_{\mu\mu}(\mathscr{C};\varepsilon_1,\varepsilon_2;r) \ . \tag{144}$$

It should be noted that the Coherent Potential Approximation (CPA) can only be used in a "real space" approach when attempting to describe the properties of bulk systems or in describing finite clusters embedded properly in a statistically disordered substrate such as e.g. magnetic nanostructures on alloy surfaces.

5.3. Two-dimensional translational symmetry

Assuming that (one and the same) two-dimensional invariance applies in all layers under consideration, for a particular magnetic configuration $\mathscr{C}$, see also Eq. (43), a typical contribution $\tilde{\sigma}_{\mu\mu}(\mathscr{C};\varepsilon_1,\varepsilon_2)$ reduces to a double sum over all atomic layers (n) [19] considered in the intermediate region, see Eq. (92),

$$\tilde{\sigma}_{\mu\mu}(\mathscr{C};\varepsilon_1,\varepsilon_2;n) = \sum_{p,q=1}^{n} \tilde{\sigma}^{pq}_{\mu\mu}(\mathscr{C};\varepsilon_1,\varepsilon_2;n) \ , \tag{145}$$

$$\tilde{\sigma}^{pq}_{\mu\mu}(\mathscr{C};\varepsilon_1,\varepsilon_2;n) = w \left\{ \sum_{j\in I(L^{(2)})} \mathrm{tr}\langle J^{p0}_{\mu}(\varepsilon_2,\varepsilon_1)\tau^{p0,qj}(\varepsilon_1)J^{qj}_{\mu}(\varepsilon_1,\varepsilon_2)\tau^{qj,p0}(\varepsilon_2)\rangle \right\} \ , \tag{146}$$

where $p0$ specifies the origin of the two-dimensional lattice $L^{(2)}$ in the pth layer and $I(L^{(2)})$ simply refers to the set of indices corresponding to $L^{(2)}$. The lattice sum in Eq. (146) can then be evaluated in terms of a two-dimensional lattice Fourier transformation [19]. This implies [18], however, as already said, that in all atomic layers (including the substrate layers) *one and the same* two-dimensional translational invariance applies.

5.3.1. Vertex corrections for the average of the product of two single-particle Green's functions

In the case of interdiffused interfaces and spacers, or substitutionally disordered alloys serving as leads, configurational averages have to be performed. Consider a typical contribution in Eq. (146). In principle the average over the occurring products can be formulated as a product of

averages

$$\langle J_\mu^{p0}(\varepsilon_2,\varepsilon_1)\tau^{p0,qj}(\varepsilon_1)J_\mu^{qj}(\varepsilon_1,\varepsilon_2)\tau^{qj,p0}(\varepsilon_2)\rangle$$
$$= \langle J_\mu^{p0}(\varepsilon_2,\varepsilon_1)\tau^{p0,qj}(\varepsilon_1)\rangle(1-\Omega)\langle J_\mu^{qj}(\varepsilon_1,\varepsilon_2)\tau^{qj,p0}(\varepsilon_2)\rangle \ . \tag{147}$$

Omitting the so-called vertex corrections Ω, i.e., in using $\Omega = 0$, one gets

$$\langle J_\mu^{p0}(\varepsilon_2,\varepsilon_1)\tau^{p0,qj}(\varepsilon_1)J_\mu^{qj}(\varepsilon_1,\varepsilon_2)\tau^{qj,p0}(\varepsilon_2)\rangle$$
$$= J_\mu^{p0}(\varepsilon_2,\varepsilon_1)\langle\tau^{p0,qj}(\varepsilon_1)\rangle J_\mu^{qj}(\varepsilon_1,\varepsilon_2)\langle\tau^{qj,p0}(\varepsilon_2)\rangle \ , \tag{148}$$

since because of (two-dimensional) translational invariance

$$\langle J_\mu^{p0}(\varepsilon_2,\varepsilon_1)\rangle = J_\mu^{p0}(\varepsilon_2,\varepsilon_1) \ . \tag{149}$$

In order to average expressions of the type $\langle\tau^{pi,qj}(\varepsilon)\rangle$ usually the Coherent Potential Approximation (CPA) introduced earlier, see Eqs. (105)–(121), is used. One then obtains [19] for the layer-diagonal terms

$$\tilde\sigma_{\mu\mu}^{pp}(\varepsilon_1,\varepsilon_2) = w\sum_{\alpha=A,B} c_p^\alpha\{tr[\tilde J_\mu^{p\alpha}(\varepsilon_2,\varepsilon_1)\tau_c^{pp}(\varepsilon_1)J_\mu^{p\alpha}(\varepsilon_1,\varepsilon_2)\tau_c^{pp}(\varepsilon_2)]$$
$$- \sum_{\beta=A,B} c_p^\beta tr[\tilde J_\mu^{p\alpha}(\varepsilon_2,\varepsilon_1)\tau_c^{pp}(\varepsilon_1)\tilde J_\mu^{p\beta}(\varepsilon_1,\varepsilon_2)\tau_c^{pp}(\varepsilon_2)]\} \tag{150}$$

and the layer-off-diagonal terms as

$$\tilde\sigma_{\mu\mu}^{pq}(\varepsilon_1,\varepsilon_2)$$
$$= (w/n\Omega_{\mathrm{SBZ}})\sum_{\alpha,\beta=A,B} c_p^\alpha c_q^\beta tr\left[\int \tilde J_\mu^{p\alpha}(\varepsilon_2,\varepsilon_1)\tau_c^{pq}(\mathbf{k},\varepsilon_1)\tilde J_\mu^{q\beta}(\varepsilon_1,\varepsilon_2)\tau_c^{qp}(\mathbf{k},\varepsilon_2)\,\mathrm{d}^2k\right] \ , \tag{151}$$

$$\tilde J_\mu^{p\alpha}(\varepsilon_2,\varepsilon_1) = D_\alpha^{pp}(\varepsilon_2)^t J_\mu^{p\alpha}(\varepsilon_2,\varepsilon_1)D_\alpha^{pp}(\varepsilon_1) \ , \tag{152}$$

where the matrices $D_\alpha^{pp}(\varepsilon_1)$ are defined in Eq. (114) and the symbol t indicates a transposed matrix. Note that in Eq. (151) use has been made of a two-dimensional lattice Fourier transformation: Ω_{SBZ} is the unit area ("volume") in the surface Brillouin zone.

5.3.2. Boundary conditions

Although the summation within the layers is now exact, convergence properties with respect to n, the number of layers, have to be considered. In viewing n as a parameter the conductivity tensor elements for a layered system are then given by

$$\sigma_{\mu\mu}(\mathscr{C};n) = \frac{1}{n}\sum_{p,q=1}^{n}\sigma_{\mu\mu}^{pq}(\mathscr{C};n) \ , \tag{153}$$

$$\sigma_{\mu\mu}^{pq}(\mathscr{C};n) = \frac{1}{4}\sum_{i,j=1}^{2}(-1)^{i+j}\tilde\sigma_{\mu\mu}^{pq}(\mathscr{C};\varepsilon_i,\varepsilon_j;n) \ . \tag{154}$$

Boundary conditions with respect to n shall be discussed separately for the geometries corresponding to a current-in-plane (CIP) and a current perpendicular to the planes (CPP) of atoms. These boundary conditions are very much related to a quite general problem in dealing with physical properties of solid systems of reduced dimensions.

5.4. The question of the characteristic volume

Already from the two cases discussed above it is clear that only in the so-called bulk case (three-dimensional periodicity) there exists a well-defined characteristic volume V per which intrinsic properties have to be expressed:

$$V = \begin{cases} V_0 & \text{“}\textit{unit volume}\text{” }\textit{for bulk}: \\ & V_0 \text{ volume of unit cell} \\ nLA_0 & \text{“}\textit{unit volume}\text{” }\textit{for multilayers}: \\ & A_0 \text{ unit area, } L \text{ interlayer distance, } n \text{ number of layers} \\ nV_0 & \text{“}\textit{unit volume}\text{” }\textit{for nanostructures}: \\ & n \text{ number of sites, } V_0 \text{ atomic volume} \end{cases} . \tag{155}$$

In the case of multilayers (two-dimensional translational invariance) or clusters (real space) the characteristic volume is simple that volume per which the physical property under consideration becomes a constant, i.e., depends no longer on the inclusion of additional sites or planes of atoms. It should be noted that only in the case of three-dimensional periodicity (infinite) systems the characteristic volume for transport coincides with the volume of the unit cell. Clearly enough, for all other cases n, the number of sites or atomic planes, has to become sufficiently large such that the electric properties under consideration can be considered as an “intrinsic quantity”. The question of the “characteristic volume” is not just of academic kind: it is essential to specify in multilayers or heterostructures “per what” electric properties are measured.

5.4.1. The “fiction” of bulk values

Usually not very much thought is given to the concept of “bulk” values for the conductivity or the resistivity of a particular system. One has to realize, however, that any kind of measurement is always performed from the “outside”, i.e., that any electric measurement is with respect to a solid with a surface. Experimental investigations therefore very often vary the thickness of a given system and record e.g. the resistivity as a function of this thickness, see for example Ref. [27]. The extrapolation of the thus obtained data points to infinite thickness is then referred to as *the* “bulk value”. Obviously such extrapolations rely on models and/or fitting parameters and give rise to fitting errors. It is useful to recall occasionally that “hard fact bulk values” refer to an asymptotic case, namely to a fictitious experimental situation! In other words: the above posed question of the characteristic volume applies even when bulk-like systems are thought to be measured or theoretically described.

6. Current-in-plane (CIP)

For computational reasons it is necessary, but also advantageous to perform the side limits, see Eqs. (49) and (136), at the latest possible stage and evaluate the elements of the conductivity tensor for finite imaginary values δ of a complex Fermi energy $\mathscr{E}_F = \varepsilon_F + \mathrm{i}\delta$. In the case of a current-in-plane geometry the resistivity for a layered system with surface normal along the z-axis, is then simply given [28] by

$$\rho_{xx}(n;\mathbf{c};\mathscr{C}) = \lim_{\delta\to 0}\rho_{xx}(n;\mathbf{c};\mathscr{C};\delta), \quad \rho_{xx}(n;\mathbf{c};\mathscr{C};\delta) = 1/\sigma_{xx}(n;\mathbf{c};\mathscr{C};\delta)\ , \tag{156}$$

where as should be recalled n is the total number of atomic layers considered and in general $\mathbf{c}$ refers to the layer-wise concentrations of species A and B in an inhomogeneous binary alloy. The giant magnetoresistance ratio (GMR) is defined in the so-called "pessimistic view" by

$$\mathrm{GMR} = \frac{\rho_{xx}(n;\mathbf{c};\mathscr{C}) - \rho_{xx}(n;\mathbf{c};\mathscr{C}_0)}{\rho_{xx}(n;\mathbf{c};\mathscr{C})}\ , \tag{157}$$

and in the "optimistic view" by

$$\mathrm{GMR} = \frac{\rho_{xx}(n;\mathbf{c};\mathscr{C}) - \rho_{xx}(n;\mathbf{c};\mathscr{C}_0)}{\rho_{xx}(n;\mathbf{c};\mathscr{C}_0)}\ , \tag{158}$$

where $\mathscr{C}_0$ refers to the chosen reference (ferromagnetic) configuration and $\mathscr{C}$ to a given (antiferromagnetic) configuration, see also the section on magnetic configurations. In here mostly the "pessimistic definition" will be used, since then the GMR is bounded by one, i.e., can reach only a maximum of 100%.

Very often the exact value of the GMR is not so much of interest (e.g., because of experimental ambiguities caused by sample preparation) and one can simply use also the following "estimate"

$$\mathrm{GMR}(\delta) = \frac{\rho_{xx}(n;\mathbf{c};\mathscr{C};\delta) - \rho_{xx}(n;\mathbf{c};\mathscr{C}_0;\delta)}{\rho_{xx}(n;\mathbf{c};\mathscr{C};\delta)}\ , \tag{159}$$

since

$$\mathrm{GMR}(\delta) \leqslant \mathrm{GMR}\ . \tag{160}$$

As easily can be seen from Eq. (156) the resistivity depends on $n, \mathbf{c}$ and $\mathscr{C}$, i.e., on the number of atomic layers taken into account (boundary conditions), on the actual composition in each atomic layer and on the magnetic configuration. The latter is in particular important if anisotropic effects occur or more than one antiferromagnetic configuration has to be considered.

6.1. Boundary conditions

The effect of boundary conditions can be seen directly from a three-dimensional view of the $\sigma^{ij}_{xx}(\mathscr{C};n;\delta)$ as displayed in Fig. 2 for a Co/Cu/Co spin valve consisting of 36 atomic layers, or, in terms of layer-diagonal conductivities $\sigma^{i}_{xx}(\mathscr{C};n;\delta)$,

$$\sigma^{i}_{xx}(\mathscr{C};n;\delta) = \sum_{j=1}^{n}\sigma^{ij}_{xx}(\mathscr{C};n;\delta)\ , \tag{161}$$

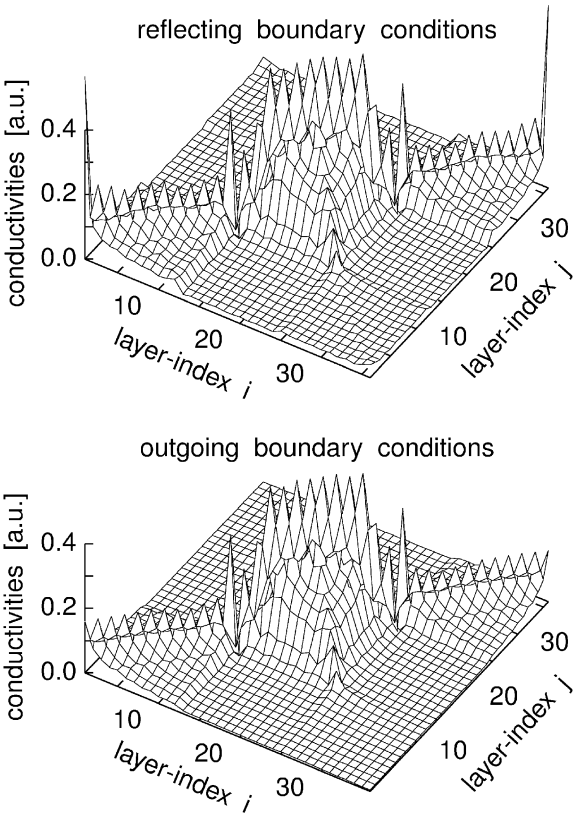

Fig. 2. Layer-resolved contributions to the conductivity, $\delta = 2$ mry, of a model spin valve structure with reflecting (vacuum/$Co_{12}Cu_{12}Co_{12}$/Vac; top) and outgoing (Co(1 0 0)/$Co_{12}Cu_{12}Co_{12}$/Co(1 0 0; bottom)) boundary conditions. From Ref. [28].

as shown in Fig. 3, considering different boundary conditions. Particular attention should be paid to the endpoints in these figures, since there in the case of reflecting boundary conditions sizeable peaks show up. From these two figures it is quite obvious that it is very important to describe exactly the system under consideration before attempting to compare to experimental values or make predictions. A reflecting boundary condition always occurs at the surface of a solid system; an outgoing boundary condition is necessary to describe a semi-infinite system, which in turn determines the Fermi energy and acts as an electron reservoir (metallic substrate).

6.2. Complex Fermi energies

However, before commenting further on the physical significance of these boundary conditions, the importance of the other—more computational—parameter, namely the imaginary part of the complex

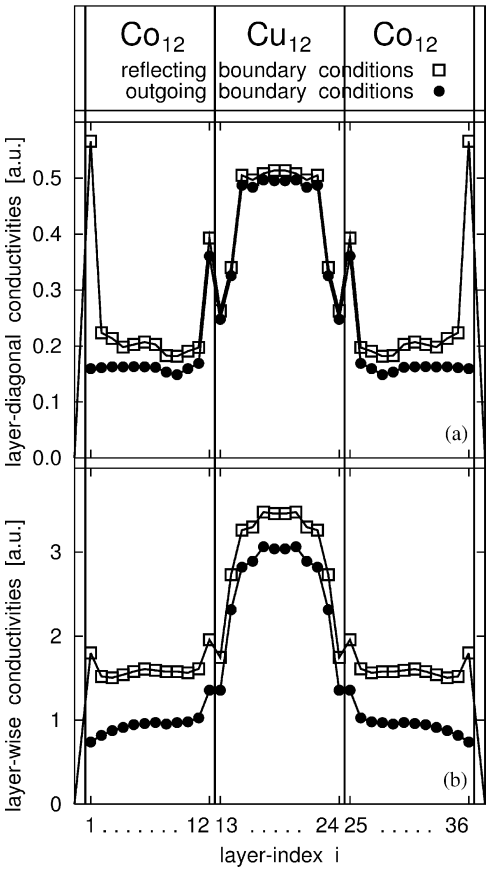

Fig. 3. Layer-diagonal conductivities σ_{xx}^{i}, see Eq. (161), $\delta = 2$ mry, of a model spin valve structure with reflecting (vacuum/$Co_{12}Cu_{12}Co_{12}$/Vac; open squares) and outgoing (Co(1 0 0)/$Co_{12}Cu_{12}Co_{12}$/Co(1 0 0; full circles)) boundary conditions. From Ref. [28].

Fermi energy, $\mathscr{E}_F$, has to be illustrated. In Fig. 4 the condition

$$\rho_{xx}(n;\mathscr{E}) = \lim_{\delta\to 0} \rho_{xx}(n;\mathscr{E};\delta) \ , \tag{162}$$

is performed for 36 layers of Fe embedded properly in bcc-Fe(1 0 0) by continuing $\rho_{xx}(n;\mathscr{E};\delta)$ numerically to the real axis. As can be seen $\rho_{xx}(n;\mathscr{E};\delta)$ can be fitted linearly quite accurately with respect to the imaginary part of the Fermi energy. The magnetic configuration in this particular case is ferromagnetic with the orientation of the magnetization pointing along the surface normal.

6.3. Bulk values

Suppose now one is interested in mimicking experimental measurements of "bulk" values by evaluating the resistivity as a function of n such as shown in Fig. 5 for permalloy (Fe_cNi_{1-c}) and

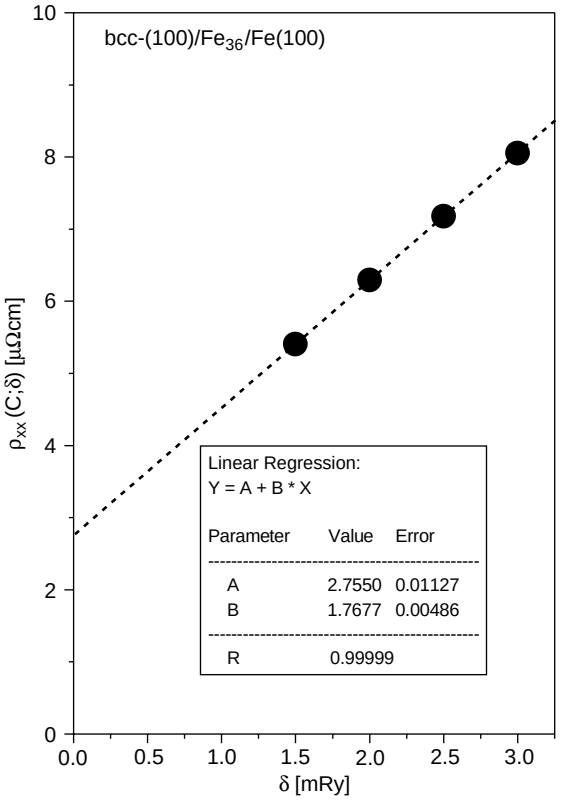

Fig. 4. Numerical continuation of $\rho_{xx}(\mathscr{C};\delta)$ for the system bcc-Fe(1 0 0)/Fe_{36}/Fe(1 0 0) to the real energy axis. The parameters for the linear fitting (dashed line) are shown in a box.

by performing the limiting procedure

$$\rho_{xx}(c;\mathscr{C}) = \lim_{n\to\infty} \rho_{xx}(n;c;\mathscr{C}) \ , \tag{163}$$

numerically. As can be seen in Fig. 6 the values ("residual resistivities") extrapolated to an infinite system fit quite well available experimental low temperature "bulk" values. In comparison with the experimental data in Fig. 7 (Fig. 1 of the section on Ni_cFe_{1-c} in Ref. [27]) even the onset of the Martensitic phase transformation from bcc to fcc can be read off. From Fig. 7 it is evident that by lowering the temperature the electrical resistivity becomes increasingly sensitive to the structural phase transition from bcc to fcc; at the temperature of liquid nitrogen ($-195°$C, the lowest isothermal curve displayed) in the Fe-rich bcc α-phase the resistivity reaches a maximum at about 15% of Ni and then slowly decreases up to 30% of Ni, whereas in the Ni-rich fcc γ-phase the resistivity starts to grow below 50% of Ni and seems to diverge near the critical concentration for the structural phase transition.

From the above performed limiting procedures one has to conclude that only

$$\rho_{xx}(\mathscr{C}) = \lim_{n\to\infty} \lim_{\delta\to 0} \rho_{xx}(n;\mathscr{C};\delta) \ , \tag{164}$$

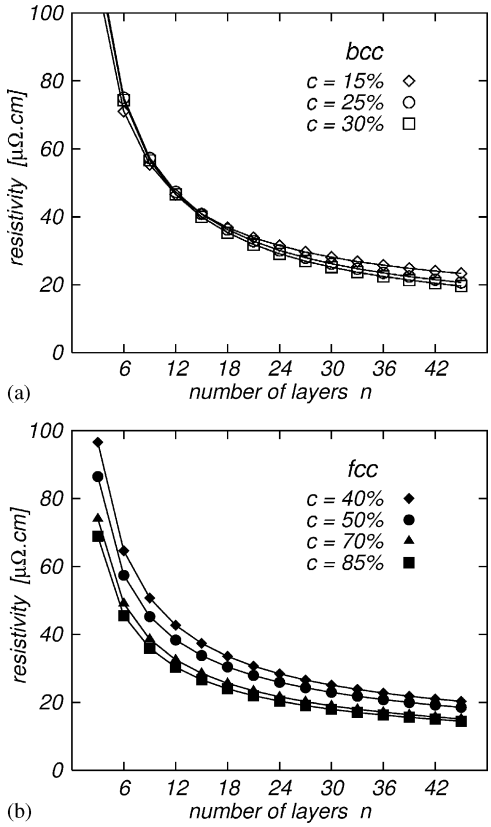

Fig. 5. Thickness dependence of the current-in-plane resistivity in bcc (a) and fcc (b) $Ni_cFe_{1-c}(1\,0\,0)/(Ni_cFe_{1-c})_n/Ni_cFe_{1-c}(1\,0\,0)$ alloys. The Ni concentration in % is indicated explicitly, n denotes the number of layers considered. From Ref. [29].

corresponds to an "intrinsic" property. Only by taking n to infinity (practically to a sufficiently large number) the influence of the boundary conditions such as the presence of a surface becomes irrelevant. The question of the characteristic volume posed earlier seems therefore to be more important than perhaps usually envisaged.

6.4. Interdiffusion at interfaces

In realistic systems, in particular in those used as GMR devices, frequently interdiffusion at the interfaces occurs. Interdiffusion implies that from the two kinds of materials (metals) joined up at an interface one diffuses into the other one and vice versa. Taking as an example a Co/Cu interface then—depending very much on the growth conditions—there will be finite concentrations of Co in interface near atomic layers of Cu and Cu diffuses into Co. A two layer interdiffusion means that the atomic layers $[Co_cCu_{1-c}]$ and $[Cu_cCo_{1-c}]$ are neighboring layers at the interface; all other atomic layers are "pure", i.e., are either Co or Cu.

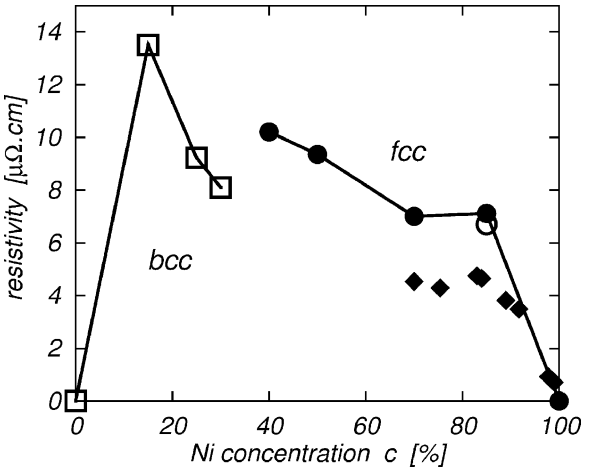

Fig. 6. Concentration dependence of the current-in-plane resistivity of "bulk" Ni_cFe_{1-c} alloys calculated as the infinite-thickness limit of $Ni_cFe_{1-c}(1\,0\,0)/(Ni_cFe_{1-c})_{n\to\infty}/Ni_cFe_{1-c}(1\,0\,0)$. The results for the bcc α-phase are shown as empty squares, for the fcc γ-phase as full circles, the open circle at $c = 85\%$ refers to a calculation with $\ell_{max} = 3$. Low temperature (4.2 K) experimental values are displayed by crosses, diamonds, pluses, and open triangles. From Ref. [29].

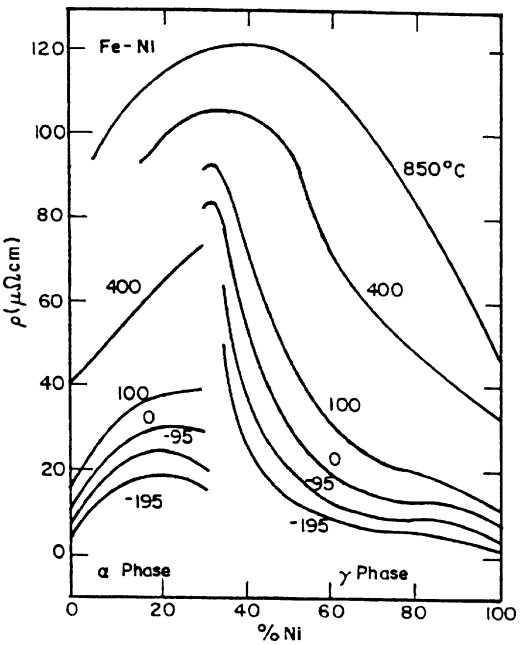

Fig. 7. Reproduction of Fig. 1 of the section on Ni_cFe_{1-c} in Ref. [27] showing temperature dependent resistivities in this system. Note the change in resistivities close to the structural phase transition at about 35% Ni as the temperature decreases.

Very often the actual concentration profiles of interdiffusion are not known and have to be assumed parametrically. The effect of interdiffusion on the resistivity and the GMR (outgoing boundary conditions) is shown in Fig. 9 for a Co/Cu/Co trilayer, the various concentration profiles assumed

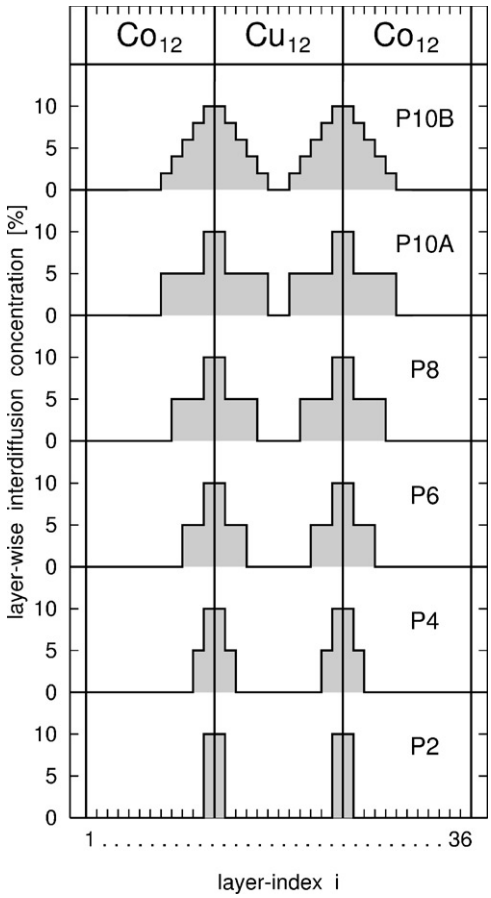

Fig. 8. Various concentration profiles considered in Co(1 0 0)/Co_{12}/Cu_{12}/Co_{12}/Co(1 0 0). From Ref. [28].

in these calculations are summarized in Fig. 8. As can be seen up to an interdiffusion concentration of about 15% the GMR is almost independent of the shape of the concentration profile. Much broader interdiffusion profiles and larger interdiffusion concentrations, however, can reduce the GMR substantially.

6.5. *Alloying in the spacer*

Not only interdiffusion at interfaces has drastic effects on the resistivities and in turn on the GMR, also (homogeneous) alloying in the spacer can produce wanted or unwanted effects. In Fig. 10 the spacer part in Co(1 0 0)/$Co_{12}Cu_{12}$ Co_{12}/Co(1 0 0) is alloyed homogeneously with various metals. From this figure it is evident that even in small concentrations certain admixtures such as for example Ti can whip out the GMR completely or reduce the effect drastically. Alloying the Cu spacer with Ag, on the other hand, increases slightly the GMR.

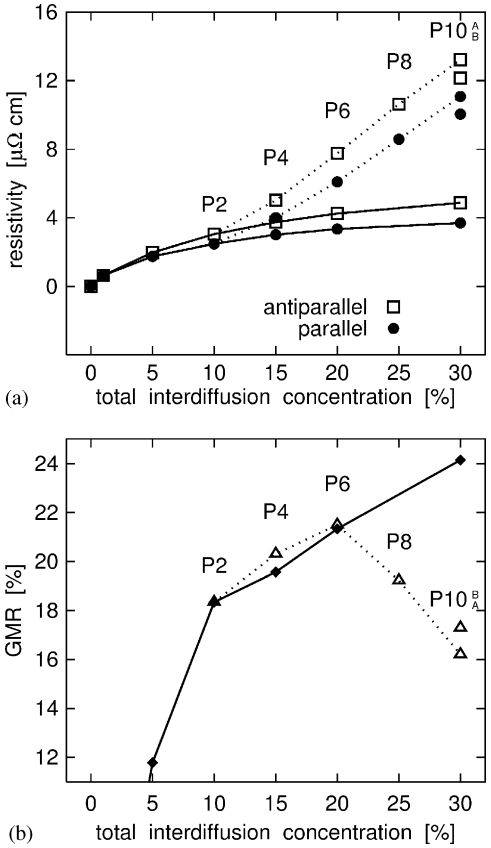

Fig. 9. (a) Resistivities, and (b) GMR as a function of interdiffusion amount and profile for the model spin-valve structure $Co_{12}Cu_{12}Co_{12}$. Resistivities for the antiparallel configuration are displayed by open squares, resistivities for the parallel configuration by full circles. The solid lines connect the values corresponding to P2 profiles (interdiffusion confined to the two monolayers adjacent to the interface), the dotted lines connect the various broader profiles P4–10 as illustrated in Fig. 8. From Ref. [28].

6.6. CIP-GMR in realistic spin valve systems

6.6.1. "Dips" in the GMR

By varying the thickness of the spacer material "dips" in the GMR can occur. This is for example the case in the experimental sample of Ref. [30]. Underlayer [55Å] | NiFe[10Å] | CoFe[xÅ] | Cu[yÅ] | CoFe[xÅ] | Ru[4Å] | CoFe[xÅ] | IrMn[70Å]| Overlayer [55Å] that was grown on 3000Å of SiO_2 and covered by a thick cap of Ta (overlayer). Theoretically this system was modelled [31] by considering the permalloy (NiFe) slab as substrate and replacing the artificial antiferromagnetic part consisting of IrMn layers and the overlayer by vacuum. In order to sort out the effect of the thickness of the Cu spacer, of the Ru spacer, and of the slabs of the hard magnets, four partial systems were considered (systems A–D, see Table 1) with system D reflecting closely the experimental sample.

As can be seen from Fig. 11 the pronounced "dip" observed experimentally at about 10Å is caused by a node in the oscillations of the IEC with respect to the Cu spacer thickness; a node that

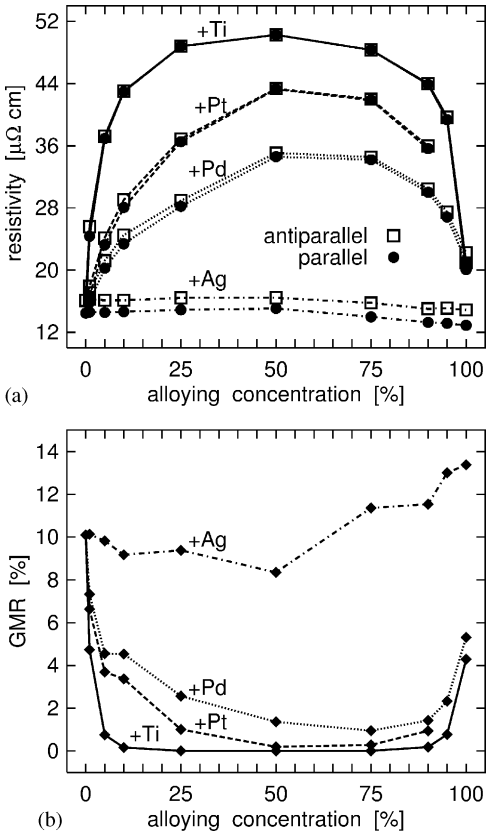

Fig. 10. (a) Resistivities, and (b) GMR for the model spin-valve structure with homogeneously alloying the Cu spacer layers $Co(1\,0\,0)/Co_{12}(Cu_{100-c}X_c)_{12}Co_{12}/Co(1\,0\,0)$ with $\delta = 2$ mRy and with outgoing boundary conditions. X = Ag (dash-dotted lines), Pd (dotted lines), Pt (dashed lines), or Ti (solid lines). Resistivities for the antiparallel configuration are displayed by open squares, resistivities for the parallel configuration by full circles. From Ref. [28].

occurs in both partial systems, A and B, i.e., a thin Ru cap (partial system B) does not change the position of the "dip" in the GMR, although the actual value of the GMR at this spacer thickness is modified.

6.6.2. *Oscillations with respect to the thickness of the magnetic slabs*

When varying the thickness of one of the magnetic slabs (partial system C, see Table 1) oscillations in the corresponding IEC and the GMR can be traced, see Fig. 12. Since the IEC remains negative (antiferromagnetic coupling) the dip in the GMR at 10Å of Cu still occurs but the GMR is again modified in size. In this particular case the oscillations in the IEC with respect to the thickness of the relevant Co slab are mapped remarkably well in the corresponding oscillations of the GMR. From theoretical IEC studies it is well-known that by varying the thickness of one (or both) of the magnetic slabs, and by varying the thickness of the cap, which is usually deposited in order to protect the surface, additional oscillations set in Fig. 12 confirms therefore the experience made before considering the IEC only.

Table 1
$Ni_{80}Fe_{20}/Co_{90}Fe_{10}/Cu/Co_{90}Fe_{10}Ru$ partial systems

System A		System B	
Thickness (ML)	fcc(1 1 1)	Thickness (ML)	fcc(1 1 1)
∞	$Ni_{80}Fe_{20}$	∞	$Ni_{80}Fe_{20}$
6	$Ni_{80}Fe_{20}$	6	$Ni_{80}Fe_{20}$
5	$Co_{90}Fe_{10}$	5	$Co_{90}Fe_{10}$
$2 \leqslant n \leqslant 12$	Cu	$2 \leqslant n \leqslant 12$	Cu
5	$Co_{90}Fe_{10}$	5	$Co_{90}Fe_{10}$
	Vacuum	2	Ru
			Vacuum
System C		System D	
Thickness (ML)	fcc(1 1 1)	Thickness (ML)	fcc(1 1 1)
∞	$Ni_{80}Fe_{20}$	∞	$Ni_{80}Fe_{20}$
6	$Ni_{80}Fe_{20}$	6	$Ni_{80}Fe_{20}$
5	$Co_{90}Fe_{10}$	5	$Co_{90}Fe_{10}$
5	Cu	5	Cu
$5 \leqslant m \leqslant 12$	$Co_{90}Fe_{10}$	5	$Co_{90}Fe_{10}$
	Vacuum	$1 \leqslant p \leqslant 8$	Ru
		5	$Co_{90}Fe_{10}$
			Vacuum

6.6.3. The question of the "correct" antiferromagnetic configuration

Considering finally the electric properties of partial system D, see Table 1, namely the one that resembles most closely the experimental situation, one has to realize that in the presence of three magnetic slabs the question of the appropriate antiferromagnetic configuration arises. In Table 2 possible magnetic configurations of this system are listed, including also a non-collinear one. In this table the angle Θ refers to a rotation around an axis perpendicular to the surface normal; $\Theta = 0$ specifies the case that in the respective atomic layer (row) the orientation of the magnetization is parallel to the surface normal, $\Theta = 180$ corresponds to an antiparallel alignment; n refers to the number of Cu spacer layers, p to the number of Ru spacer layers. In order to understand Table 2 correctly it is important to recall that both spacers, Cu and Ru, carry (very) small induced magnetic moments (less than $0.1\mu_B$ in the vicinity of an interface to Co), the directions of which have to be specified in a proper definition of magnetic configurations. These induced magnetic moments vanish eventually in the middle of sufficiently thick spacers.

In Fig. 13 the IEC for the collinear configurations in Table 2 is shown with respect to the thickness of the Ru spacer. From this figure it is evident that typical oscillations with respect to the Ru spacer thickness arise only considering configurations 1 and 2 in Table 2. However, as Fig. 14 shows, these two configurations are not always the energetically lowest antiferromagnetic configurations. In fact, the corresponding resistivities and magnetoresistances show quite different behavior when compared to each other, see Fig. 14. It needs indeed Fig. 14 to sort out what is

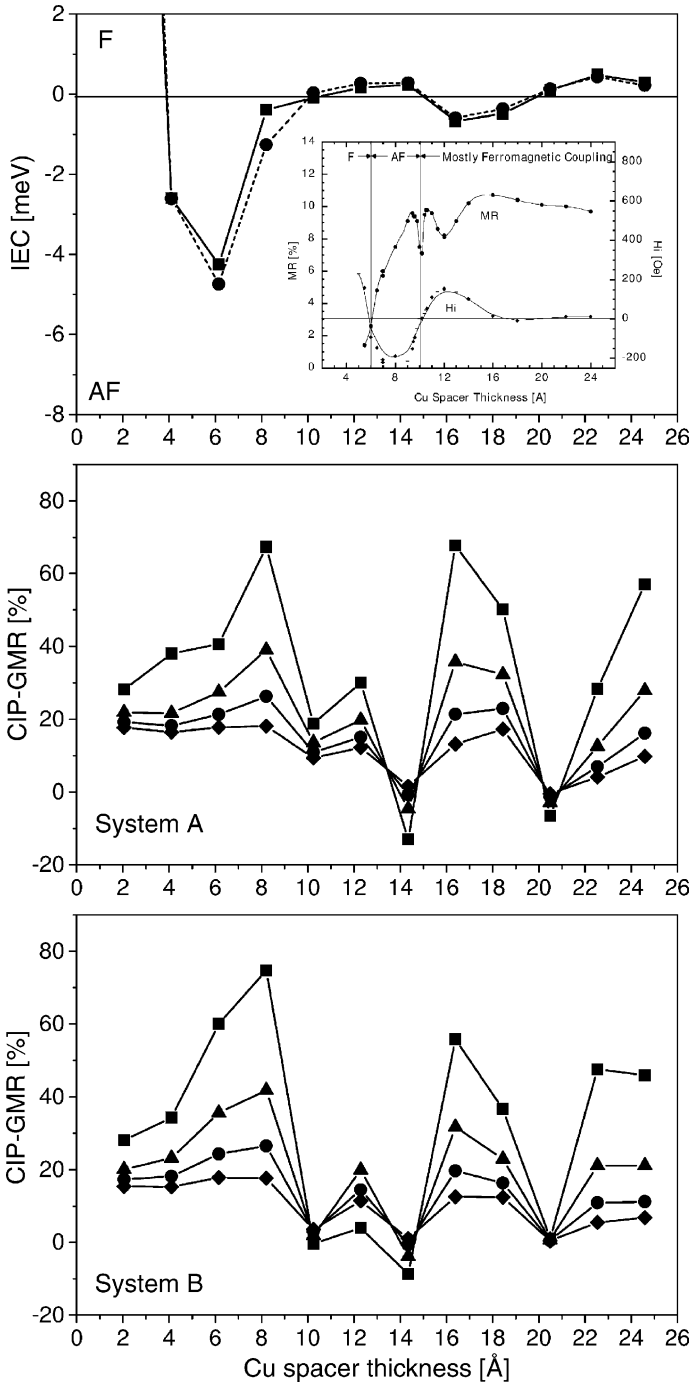

Fig. 11. IEC (top) for partial systems A (squares) and B (circles) in Table 1. In the GMR for system A (middle) and B (bottom) diamonds, triangles, circles and squares refer to an imaginary part δ of the Fermi energy of 0, 1, 2 and 3 mry. The inset shows the experimental results from Ref. [30]. Note that the thickness of the Cu spacer is given in [Å], 1 ML corresponds to about 2 Å. From Ref. [31].

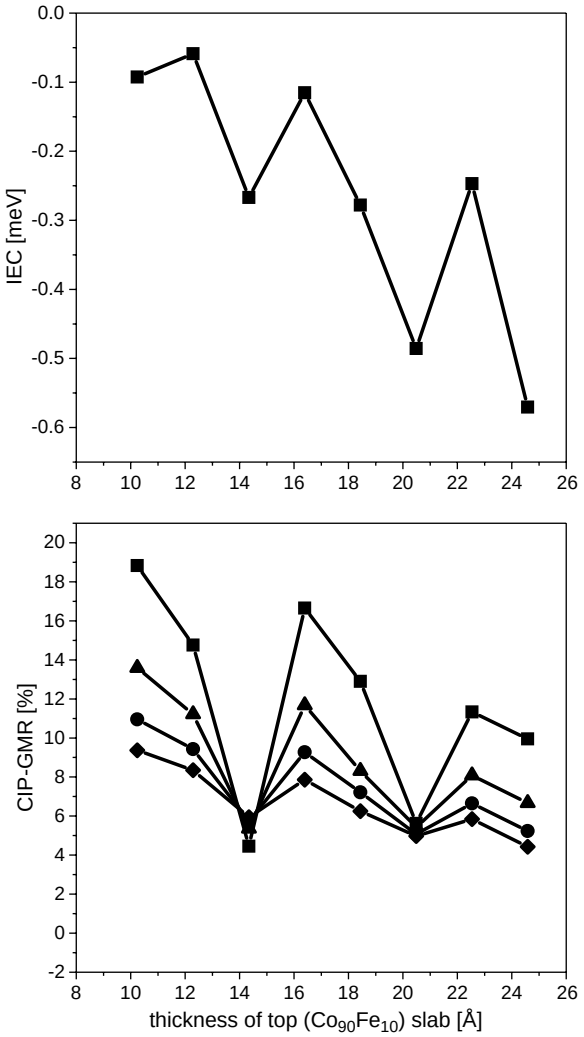

Fig. 12. IEC (top) and the GMR (bottom) of partial system C in Table 1, versus the thickness of the top $Co_{90}Fe_{10}$ magnetic slab. For the GMR squares, triangles, circles and diamonds refer to an imaginary part δ of the Fermi energy of 0, 1, 2 and 3 mry. Note that the thickness of the $Co_{90}Fe_{10}$ slab is given in [Å], 1 ML corresponds to about 2 Å. From Ref. [31].

the most likely antiferromagnetic configuration to be used in order to calculate the actual magnetoresistance.

At the experimental Ru spacer thickness of 4Å and a Cu spacer thickness of 10Å configuration 3 in Table 2 applies, the corresponding theoretical GMR of about 5%, displayed in Fig. 15, compares then quite favorably with the experimental one of about 7%, see the inset in Fig. 11. It should be noted from Fig. 15 that the GMR for the other magnetic configurations, namely configurations 0 and 1, which do not correspond to the lowest IEC, is quite a bit higher in value and varies differently in shape with the number of Ru spacer layers.

Table 2
Magnetic configurations investigated in partial system D. The labels 0 and 180 refer to orientations of the magnetization parallel and antiparallel to the surface normal

Layer	0	1	2	3	4	5
$Ni_{80}Fe_{20}$	0	0	0	0	0	0
$(Co_{90}Fe_{10})_5$	0	0	0	0	0	0
$(Cu)_i, i < n/2$	0	0	0	0	0	0
$(Cu)_i, i \geqslant n/2$	0	0	180	0	180	Θ
$(Co_{90}Fe_{10})_5$	0	180	180	180	180	Θ
$(Ru)_i, i < p/2$	0	180	180	180	180	Θ
$(Ru)_i, i \geqslant p/2$	0	0	0	180	180	0
$(Co_{90}Fe_{10})_5$	0	0	0	180	180	0
Vac	0	0	0	180	180	0

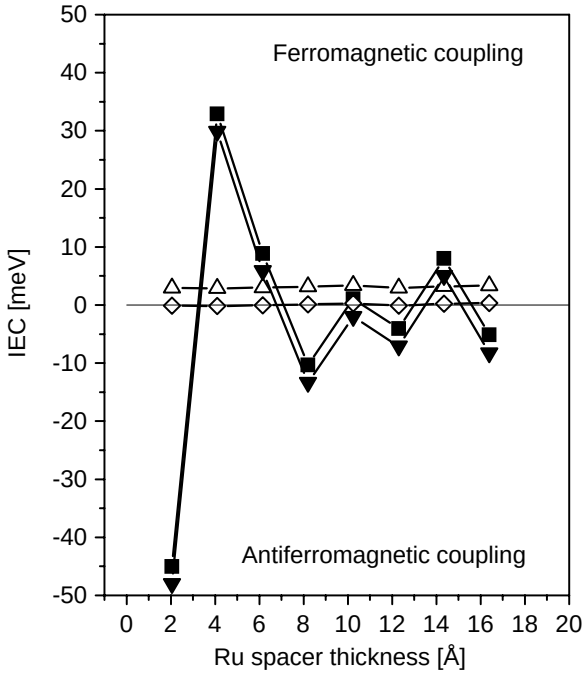

Fig. 13. IEC of partial system D, see Table 1, with respect to the thickness of the Ru spacer. Full squares and triangles refer to the IEC's corresponding to configurations 1 and 2 in Table 2, open triangles and diamonds to configurations 3 and 4. Note that the thickness of the Ru spacer is given in [Å], 1 ML corresponds to about 2 Å. From Ref. [31].

6.6.4. Rotational behavior of the GMR

In Fig. 16 the orientation of the magnetization is rotated (rotation angle Θ around an axis $\hat{\mathbf{n}}$ perpendicular to the surface normal) in finite steps from 0^0 (configuration 0; ferromagnetic

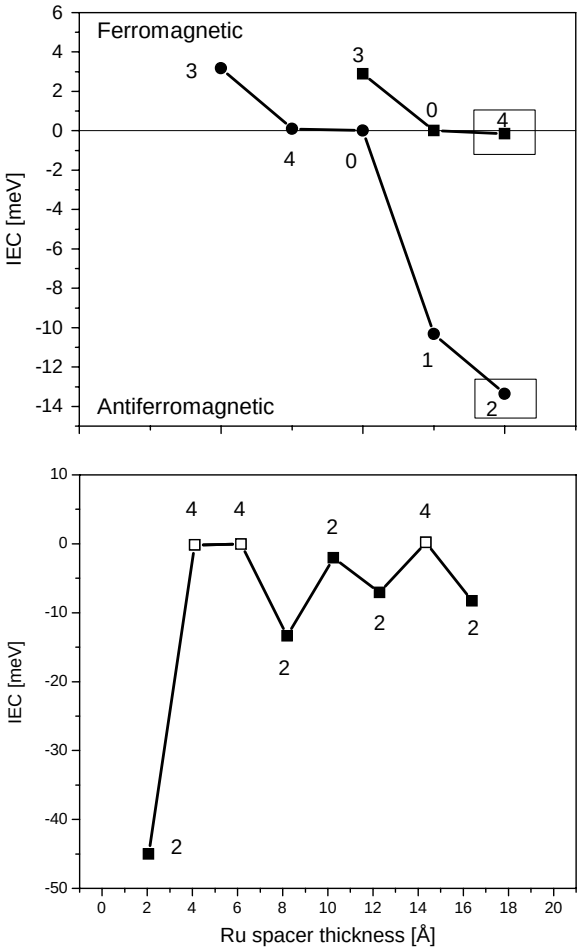

Fig. 14. Top: The lowest configuration dependent IEC's for 2 (squares) and 4 ML (circles) of Ru in partial system D, see Table 1. The (collinear) ground state configuration is marked by a box. Bottom: Oscillations of the IEC corresponding to configurations 2 and 4 (Table 2) with respect to the thickness of the Ru spacer. Note that the thickness of the Ru spacer is given in [Å], 1 ML corresponds to about 2 Å. The antiparallel configurations, see Table 2, are marked explicitly. From Ref. [31].

configuration) to 180° (configuration 2), see also configuration 5 in Table 2. It should be recalled that a function $f(\hat{\mathbf{n}}, \Theta)$ can be fitted in terms of the following expansion:

$$f(\hat{\mathbf{n}}, \Theta) = f(\hat{\mathbf{n}}, 0) + \sum_{m=1}^{\infty} a_m(\hat{\mathbf{n}})(1 - \cos^m \Theta) \ , \tag{165}$$

whereby usually two important cases can be distinguished, namely (1) $a_1(\hat{\mathbf{n}}) \gg a_2(\hat{\mathbf{n}})$ and (2) $|a_1(\hat{\mathbf{n}})| \sim |a_2(\hat{\mathbf{n}})|$.

In Fig. 16 the functional form of the IEC, the resistivities and the GMR of configuration 5 (Table 2) is depicted for two systems of type D, see also Table 1, namely for two and four ML of Ru, the parameters $a_1(\hat{\mathbf{n}})$ and $a_2(\hat{\mathbf{n}})$ for these two cases are listed in Table 3. While the IEC

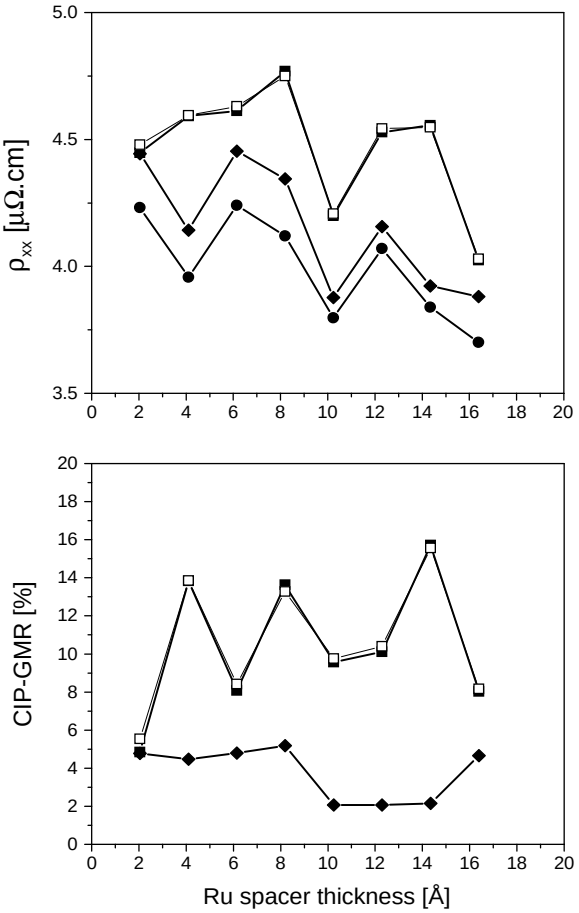

Fig. 15. Resistivities (top) and GMR (bottom) as a function of the thickness of the Ru spacer. Full circles, squares and diamonds refer to configurations 0, 1 and 3, open squares to configuration 2, see also Table 2. Note that the thickness is given in [Å], 1 ML corresponds to about 2 Å. From Ref. [31].

for both cases mostly shows a $(1 - \cos(\Theta))$ like behavior, the resistivity as well as the GMR do exhibit considerable deviations from this form: there is a well-pronounced shoulder at 90°. It should be noted that for matters of comparison in both cases (two and four ML of Ru) one and the same type of "switching" is shown although only for four ML of Ru configuration 2 is the (collinear) antiparallel ground state configuration. Fig. 16 proves that the actual "switching process" to be seen in the resistivities or in the GMR can be quite different from that in the IEC.

6.6.5. *Leads as yet another kind of boundary condition*

Finally the question of a comparison of calculated resistivities and the GMR values with corresponding experimental data in a well-characterized layered system has to be addressed, since the fact that in the limit of bulk systems the theoretical description seems to be quite appropriate not necessarily implies that this is also the case for spin valve type systems.

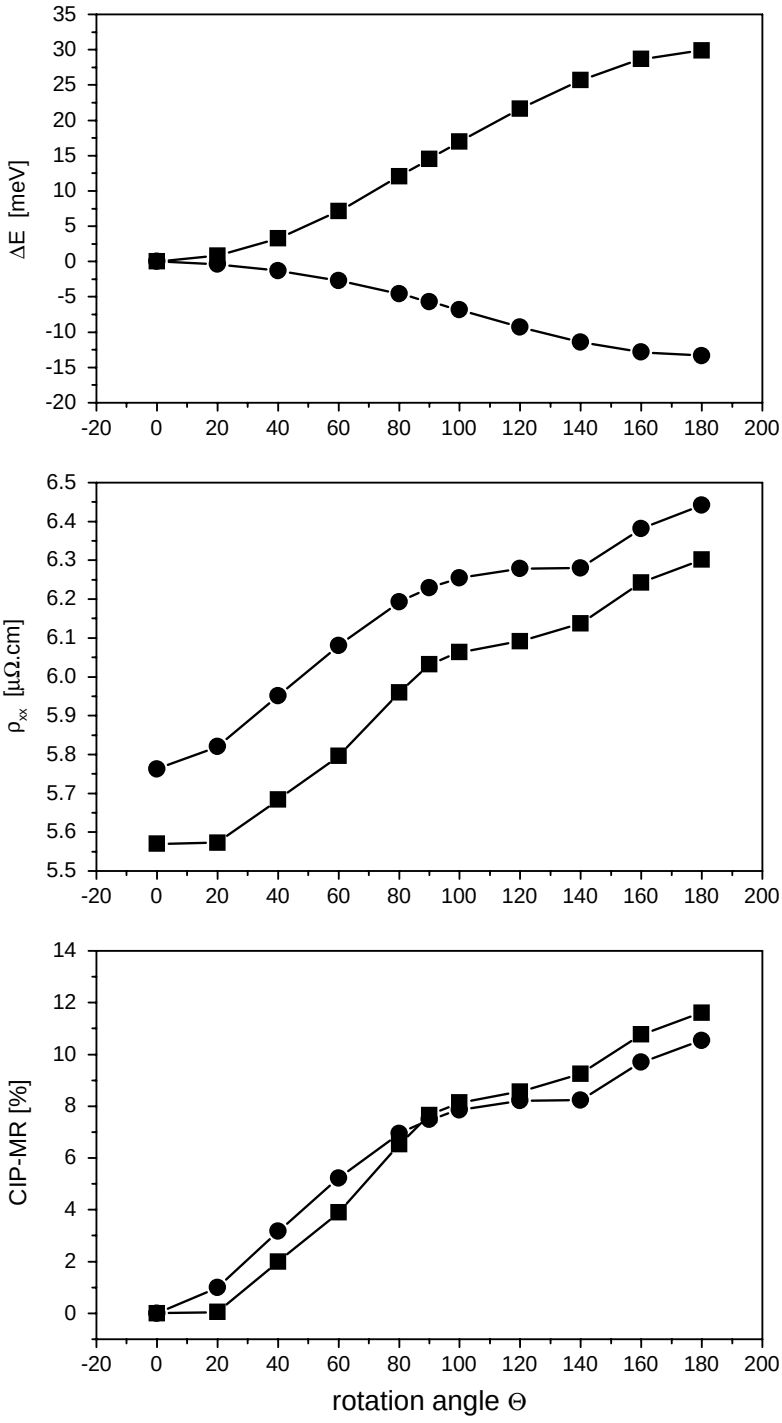

Fig. 16. IEC (top), resistivity (middle) and GMR (bottom) for 2 (squares) and 4 (circles) ML of Ru in system D as a function of the rotation angle Θ, see also Table 2. For the electric transport properties shown in here an imaginary part of the Fermi energy of 2 mry is used. From Ref. [31].

Table 3
Expansion coefficients related to magnetic configuration 2

Property	$m = 2$	$m = 2$	$m = 4$	$m = 4$
	a_1	a_2	a_1	a_2
IEC [meV]	14.932	−0.388	−6.681	0.998
ρ_{xx} [μΩ.cm]	0.366	−0.096	0.340	−0.127
CIP-MR [%]	5.80	−1.86	5.27	−2.22

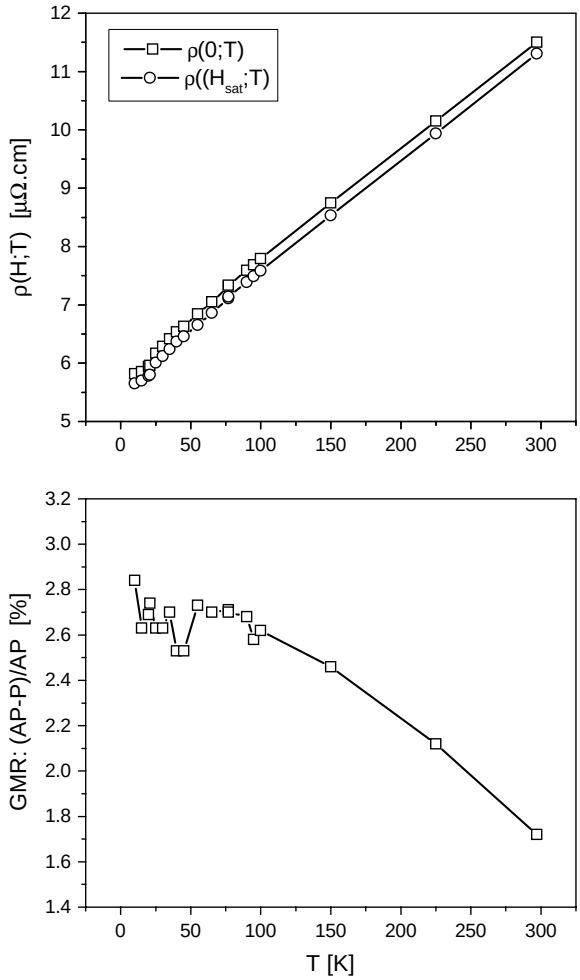

Fig. 17. Experimental field and temperature dependent resistivities (top) and temperature dependent giant magnetoresistance (bottom). From Ref. [32].

Table 4
The Fe/Au/Fe/Au spinvalve-investigated systems

System A	System B	System C
2 ML interdiffusion at	2 ML interdiffusion at	2 ML interdiffusion at
two Fe/Au interfaces	all Fe/Au interfaces	all Fe/Au interfaces
bcc-Fe(1 0 0)	bcc-Fe(1 0 0)	fcc-Au(1 0 0)
Fe_{11}	Fe_{11}	Au_5
$[Fe_cAu_{1-c}]$	$[Fe_cAu_{1-c}]$	$[Au_cFe_{1-c}]$
$[Au_cFe_{1-c}]$	$[Au_cFe_{1-c}]$	$[Fe_cAu_{1-c}]$
Au_5	Au_5	Fe_8
$[Au_cFe_{1-c}]$	$[Au_cFe_{1-c}]$	$[Fe_cAu_{1-c}]$
$[Fe_cAu_{1-c}]$	$[Au_cFe_{1-c}]$	$[Au_cFe_{1-c}]$
Fe_9	Fe_8	Au_5
Au_5	$[Fe_cAu_{1-c}]$	$[Au_cFe_{1-c}]$
vac	$[Au_cFe_{1-c}]$	$[Fe_cAu_{1-c}]$
	Au_4	Fe_{10}
	vac	vac

In Fig. 17 the experimentally recorded resistivities and the GMR for the system $Au_{20}Fe_{10}Au_7Fe_{28}$/GaAs(1 0 0) [32] are shown. Since in this system the left Au and the right Fe slab are quite thick and the GaAs substrate can be replaced by a vacuum barrier, the question arises which of the two slabs can be considered as the electron reservoir, i.e., can be assumed to be the semi-infinite system that determines the Fermi energy. Therefore both (theoretically) limiting cases were investigated [32], namely a bcc-Fe(1 0 0) substrate and a fcc-Au(1 0 0) substrate considering also interdiffusion at the Fe/Au interfaces, see in particular Table 4. The corresponding theoretical values for the various systems listed in this table are displayed in Fig. 18 versus the interdiffusion concentration. As can be seen systems A and B (Fe substrate) differ considerably from system C (Au substrate). Since in experiment the contacts were placed on the Au parts of the system, only system C reproduces the experimental situation realistically: the thick Au slab refers to the experimental leads. Comparing now the calculated resistivities with the measured ones, it turns out that the former are only by factor of about four smaller, whereas the GMR value agrees remarkably well with experiment. The overall agreement with the experimental data is therefore quite good, taking into account that in both cases absolute numbers are compared with and not values extrapolated to the limiting case of a bulk system. Furthermore, Fig. 18 confirms that in the experimental measurements indeed surprisingly clean interfaces were present.

Using layer-diagonal conductivities, see Eq. (161), the layer-resolved difference between the antiferromagnetic and the ferromagnetic configurations reveals that the GMR effect is mostly due to the Fe slabs, the biggest contribution to the total difference arising from the Fe/Au interfaces, see Fig. 19.

6.7. *References to fully relativistic ab initio CIP calculations*

In Table 5 references are given to those studies in which the fully relativistic, spin-polarized Kubo–Greenwood equation in the context of the screened Korringa-Kohn-Rostoker method was applied.

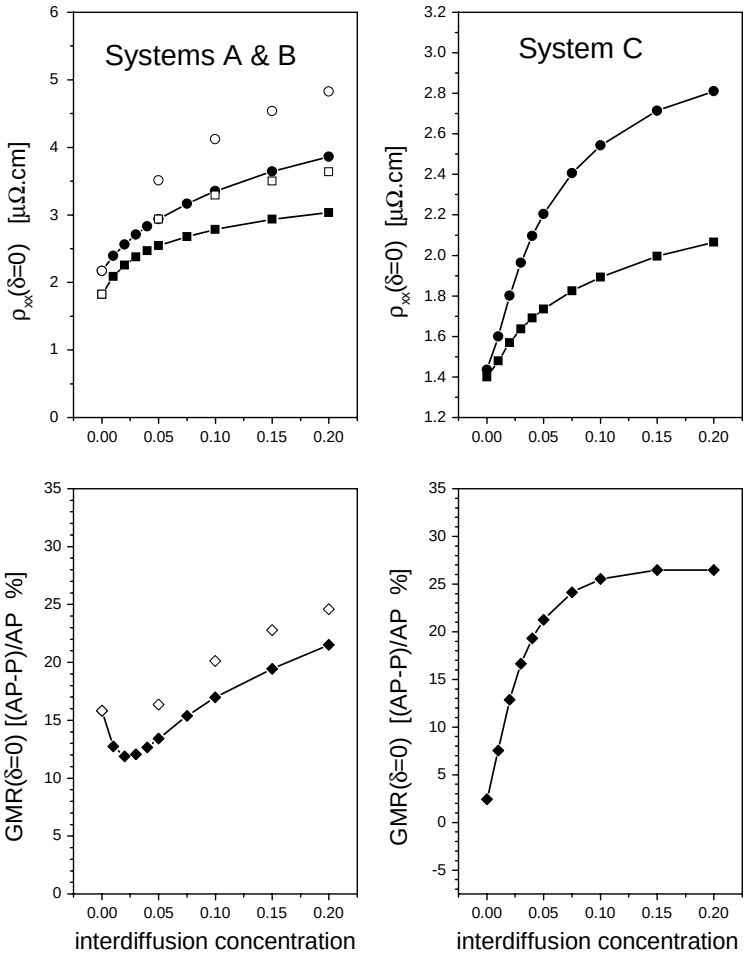

Fig. 18. CIP-resistivity and GMR in Fe/Au/Fe multilayers as continued to the real axis. Squares refer to the parallel alignment, circles to the antiparallel alignment. For systems A and C full symbols apply, for system B open symbols, see also Table 4. From Ref. [32].

Table 5
References to CIP calculations using the fully relativistic versions of SKKR-method and the Kubo–Greenwood equation

System	Reference
Cu/Ni repeats	[35]
Fe/Au/Fe	[32,34]
Co/Cu/Co	[28,33]
Fe/Cr/Fe	[23]
Ni_cFe_{1-c} spin valves	[29,31]
exchange bias	[49–51]

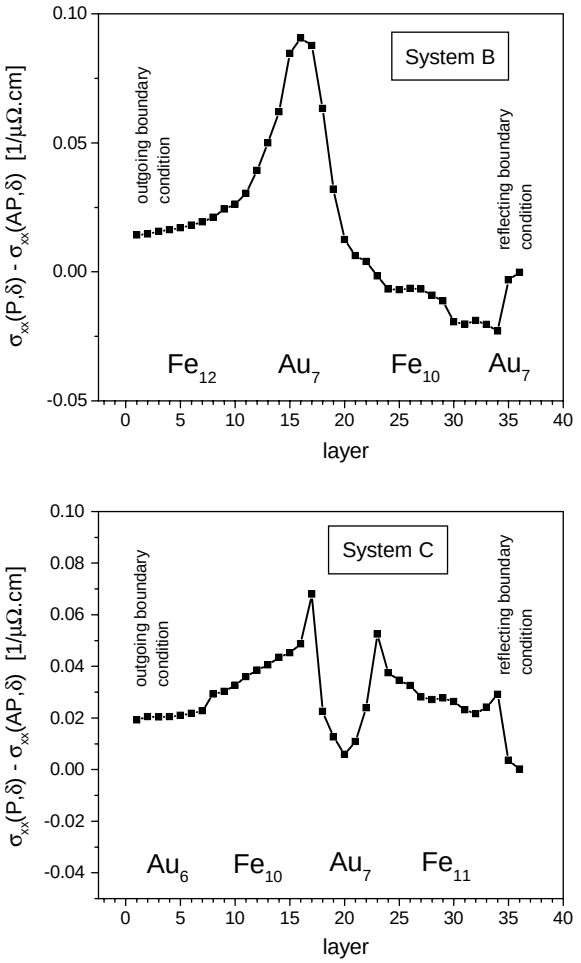

Fig. 19. Layer-resolved difference conductivities corresponding to an imaginary part of the Fermi energy of 2 mryd and an interdiffusion concentration of $c = 0.05$. From Ref. [32].

7. Current-perpendicular to the planes of atoms (CPP)

Suppose z and z' denote continuous coordinate variables perpendicular to the planes of atoms in a multilayer system (two-dimensional translationally invariant system). As the current is independent of z in the steady state one can write the resistivity in the current-perpendicular to the planes of atoms geometry (CPP) as [36–39]

$$\rho_{\mathrm{CPP}} = \frac{1}{L}\int \rho(z,z')\,\mathrm{d}z\,\mathrm{d}z' \ , \tag{166}$$

where $\rho(z,z')$ is the inverse of $\sigma(z,z')$ as defined by

$$\int \sigma(z,z'')\rho(z'',z')\,\mathrm{d}z'' = \delta(z-z') \ , \tag{167}$$

and L is the overall length of the structure for which the conductivity is calculated. The sheet resistance r and resistance R are then defined by the following relations:

$$r = AR = L\rho_{\mathrm{CPP}} = \int \rho(z,z')\,\mathrm{d}z\,\mathrm{d}z' \ , \tag{168}$$

where A is the unit area.

In the following the conductivity tensor $\sigma(z,z')$ as defined in Eq. (167) is mapped [40] (f :) onto the zz-components of the conductivity tensor for a layered system [19], $\sigma_{zz}^{ij}(n) \equiv \sigma_{ij}(n)$, $i,j = 1,n$, with i and j denoting planes of atoms,

$$f : \sigma(z,z') \to \sigma_{ij}(n) \ , \tag{169}$$

such that the algebraic structure established by Eq. (167) is conserved,

$$\sum_{k=1}^{n} \rho_{ik}(n)\sigma_{kj}(n) = \delta_{ij} \ . \tag{170}$$

Clearly enough the sheet resistance r in Eq. (168) then serves as measure (g :) for the mapping f,

$$g : r \to r(n), \quad r(n) = \sum_{i,j=1}^{n} \rho_{ij}(n) \ , \tag{171}$$

since according to the Cauchy convergence criterion the integral in Eq. (168) can be replaced by a sum, i.e., by $r(n)$, if and only if,

$$\left| r - \lim_{n\to\infty} r(n) \right| < \Delta, \quad n \in \mathbb{N}^+ \ , \tag{172}$$

or,

$$|r(n+m) - r(n)| < \Delta, \quad n,m \in \mathbb{N}^+ \ , \tag{173}$$

where Δ is an infinitesimal small number.

7.1. Complex Fermi energies

As already said, because of computational reasons (k-space integrations, surface Green's function, etc.) it is extremely useful to evaluate the elements of the $\sigma_{ij}(n)$ matrix using a small imaginary part δ to the Fermi energy. The sheet resistance for a given magnetic configuration $\mathscr{C}$ is then defined by

$$r(\mathscr{C};n) = \lim_{\delta\to 0} r(\mathscr{C};n;\delta) \ , \tag{174}$$

where

$$r(\mathscr{C};n;\delta) = \sum_{i,j=1}^{n} \rho_{ij}(\mathscr{C};n;\delta) \ , \tag{175}$$

and

$$\sum_{k=1}^{n} \rho_{ik}(\mathscr{C};n;\delta)\sigma_{kj}(\mathscr{C};n;\delta) = \delta_{ij} \ . \tag{176}$$

As the sheet resistance $r(\mathscr{C};n;\delta)$ depends on both the number of layers n and the imaginary part of the Fermi energy δ in following first the functional properties of $r(C;n;\delta)$ with respect to these two parameters are investigated [40].

7.2. Layer-dependence:

In principle, for a large enough n ($n \geqslant n_0$) and (because of) a given imaginary part δ of the complex Fermi energy $\varepsilon_F + \mathrm{i}\delta$, the sheet resistance $r(\mathscr{C};n;\delta)$ can be thought [40] to vary linearly with n,

$$k_1(\mathscr{C};\delta) = \frac{r(\mathscr{C};n+m;\delta) - r(\mathscr{C};n;\delta)}{m}; \quad m,n \in \mathbb{N}^+ \ , \tag{177}$$

i.e., the following relation can be assumed

$$r(\mathscr{C};n;\delta) = r_0(\mathscr{C};\delta) + nk_1(\mathscr{C};\delta) \ , \tag{178}$$

with $r_0(\mathscr{C};\delta)$ being the value of the linear form defined by Eq. (177) at $n = 0$. In a typical trilayer system of the type Fe(1 0 0)/$\mathrm{Fe}_p\mathrm{X}_s\mathrm{Fe}_p$/Fe(1 0 0), $n = 2p + s$, i.e., for a given value of s of spacer layers, the number of lead layers (Fe) serving as buffer to the semi-infinite system has to be sufficiently large in order to reach the linear regime defined by Eq. (178).

7.3. Dependence on the imaginary part of the Fermi energy

Investigating now for a given value of n the dependence of $r(\mathscr{C};n;\delta)$ with respect to δ one finds that $r(\mathscr{C};n,\delta)$ also varies linearly [40] in δ:

$$k_2(\mathscr{C};n) = \frac{1}{n}\frac{r(\mathscr{C};n;\delta_2) - r(\mathscr{C};n;\delta_1)}{\Delta}, \quad \Delta = \delta_2 - \delta_1 \ , \tag{179}$$

i.e.,

$$r(\mathscr{C};n;\delta) = r_0(\mathscr{C};n) + n\delta k_2(\mathscr{C};n) \ , \tag{180}$$

where as will become clear in a moment the constant $k_2(\mathscr{C};n)$ is chosen to be normalized per layer.

Combining finally Eq. (178) with Eq. (180), one gets [40]

$$r_0(\mathscr{C};\delta) = r_0(\mathscr{C};n) + n\Phi(\delta) \ , \tag{181}$$

where

$$\Phi(\delta) = \delta k_2(\mathscr{C};n) - k_1(\mathscr{C};\delta) \ . \tag{182}$$

By taking the limit of $\delta \to 0$ it is easy to see that demanding

$$r_0(\mathscr{C};n) = \lim_{\delta\to 0} r_0(\mathscr{C};\delta)\ , \tag{183}$$

in turn implies that

$$\lim_{\delta\to 0} k_1(\mathscr{C};\delta) = 0\ , \tag{184}$$

since $\delta k_2(\mathscr{C};n)$ trivially vanishes for $\delta \to 0$.

Although at the present stage Eqs. (179)–(184) appear to be just a formal trick, it will turn out in the section on the tunneling magnetoresistance that the slope with respect to the imaginary part of the Fermi energy can be used as a qualitative criterion for the occurrence of tunneling.

7.4. Resistivity and boundary condition at $n\to\infty$

From Eqs. (178) and (183) follows that for $n \geqslant n_0$, where n_0 is as sufficiently large number,

$$\lim_{\delta\to 0} r(\mathscr{C};n+m;\delta) = r_0(\mathscr{C};n) \equiv r_0(\mathscr{C}); \quad m,n \in \mathbb{N}^+\ , \tag{185}$$

which, however, is nothing but the Cauchy convergence criterion for the sheet resistance demanded in Eq. (173):

$$\lim_{\delta\to 0} [r(\mathscr{C};n+m;\delta) - r(\mathscr{C};n;\delta)] = 0; \quad m,n \in \mathbb{N}^+,\ n \geqslant n_0\ . \tag{186}$$

Quite clearly since $r_0(\mathscr{C})$ is a constant for a pure metal by performing the limit $n \to \infty$ this leads to a correct resistivity $\rho_{\mathrm{CPP}}(\mathscr{C})$,

$$\rho_{\mathrm{CPP}}(\mathscr{C}) = \lim_{n\to\infty}\left[\frac{r_0(\mathscr{C})}{L}\right] = \frac{r_0(\mathscr{C})}{d}\lim_{n\to\infty}\frac{1}{n} = 0\ , \tag{187}$$

where d is the interplanar distance.

For a substitutionally disordered alloy $r(\mathscr{C};n;\delta)$ has to vary with respect to n in the following manner, see also Eq. (178),

$$r(\mathscr{C};n;\delta) = r_0(\mathscr{C};\delta) + n(k_1(\mathscr{C};\delta) + \bar{k}_1(\mathscr{C};\delta)), \quad n \geqslant n_0\ , \tag{188}$$

where

$$\bar{k}_1(\mathscr{C}) = \lim_{\delta\to 0}\bar{k}_1(\mathscr{C};\delta)\ , \tag{189}$$

simply is the resistivity caused by disorder. In general $\rho_{\mathrm{CPP}}(\mathscr{C})$ is therefore given by

$$\rho_{\mathrm{CPP}}(\mathscr{C}) = \frac{1}{d}\lim_{\delta\to 0}\left\{\lim_{n\to\infty}\frac{r(\mathscr{C};n;\delta)}{n}\right\}\ . \tag{190}$$

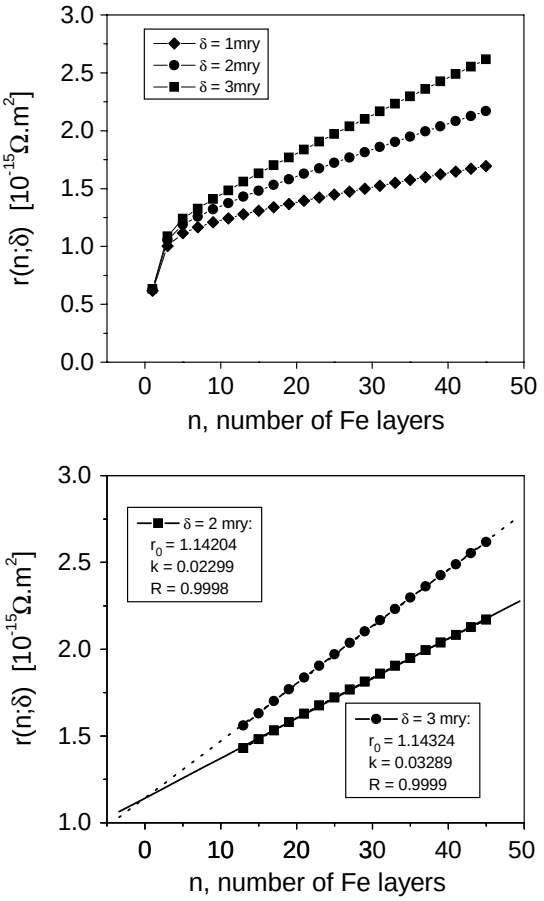

Fig. 20. Top: Variation of the sheet resistance $r(\mathscr{C};n;\delta)$ for ferromagnetic bcc Fe(1 0 0)/Fe$_n$/Fe with respect to n for three values of the imaginary part δ to the Fermi energy. Bottom: Numerical extrapolation (full line) of the linear regime of the sheet resistance $r(\mathscr{C};n;\delta)$ for ferromagnetic bcc Fe(1 0 0)/Fe$_n$/Fe. $r_0(\mathscr{C};\delta)$ and $k_1(\mathscr{C};\delta)$ refer to the value of $r(\mathscr{C};n;\delta)$ at $n=0$ and the slope, respectively, R is the quality of fitting. From Ref. [40].

7.5. CPP-magnetoresistance ratio

The magnetoresistance ratio of the relevant part of the heterostructure with n_0 lead and s spacer layers and is defined in the "pessimistic view" by

$$R = \frac{r(\mathscr{C};2n_0+s) - r(\mathscr{C}_0;2n_0+s)}{r(\mathscr{C};2n_0+s)}\ , \tag{191}$$

and can—as before in the CIP case—be approximated by

$$R(\delta) = \frac{r(\mathscr{C};2n_0+s;\delta) - r(\mathscr{C}_0;2n_0+s;\delta)}{r(\mathscr{C};2n_0+s;\delta)}\ , \tag{192}$$

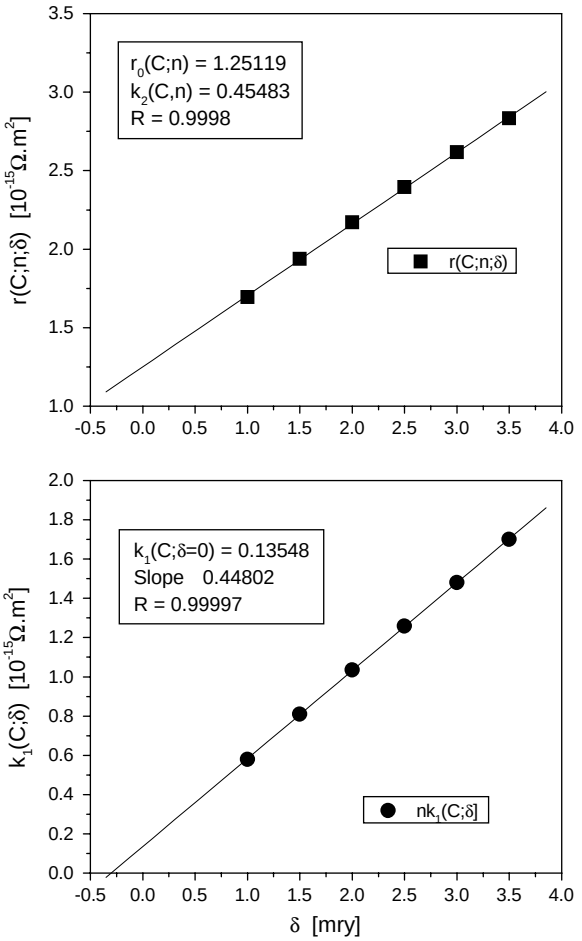

Fig. 21. Top: Variation of $r(\mathscr{C};n;\delta)$ for Fe(1 0 0)/Fe_{45}/Fe with respect to δ. The linear fit is shown as full line. Bottom: Variation of $k_1(\mathscr{C};\delta)$ with respect to δ for the same system. R refers to the quality of fitting. From Ref. [40].

where $\mathscr{C}_0$ and $\mathscr{C}$ refer to the reference (parallel, $\mathscr{P}$) and chosen (antiparallel, $\mathscr{AP}$) magnetic configuration, respectively. As already mentioned this definition is not unique, because the difference in the sheet resistances can also be related to the sheet resistance in the parallel configuration ("optimistic value").

7.6. Illustration of the fitting procedures

Fig. 20 refers to the case that n layers of Fe are embedded in bulk bcc-Fe(1 0 0). Shown are the sheet resistances $r(\mathscr{C};n;\delta)$ with respect to the number of embedded Fe layers, whereby $\mathscr{C}$ refers to the ferromagnetic configuration along (1 0 0). In Fig. 21 the properties with respect to δ are illustrated. One easily can see that for $\delta \to 0$ the slope of $r(\mathscr{C};n;\delta)$ with respect to δ goes to

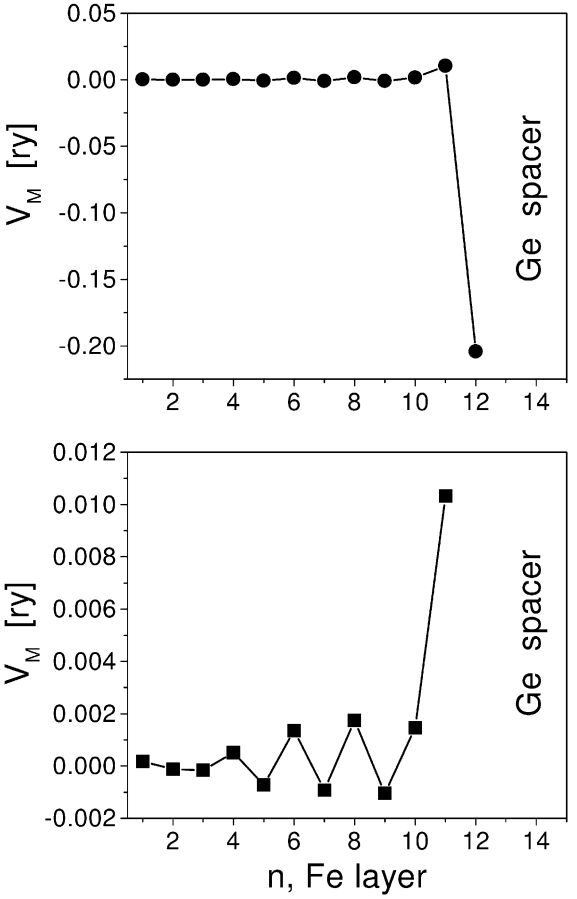

Fig. 22. Layer-resolved Madelung potentials for the Fe layers next to the Fe/Ge interface in bcc Fe(1 0 0)/$Fe_{12}Ge_9Fe_{12}$/Fe. The bottom figure shows the oscillations of the Madelung potentials into the interior of the Fe leads on an enlarged scale. From Ref. [40].

zero. The very small finite value of this slope at $\delta = 0$ defines the remaining numerical error. Both figures prove that in principle the sheet resistance of pure metals can be calculated sufficiently accurately.

7.7. Magnetic multilayers and heterostructures

7.7.1. The role of the leads

The actual reason of why convergence with respect to the lead layers in a particular heterostructure (see the above remarks on the "characteristic volume" or "Cauchy convergence criterion") has to be investigated is based on the fact that near an interface oscillations of the layer-resolved Madelung potentials are present, see Fig. 22. Once these oscillations become sufficiently small one has reached the regime of pure metal lead layers. This is illustrated in Fig. 23 for the system

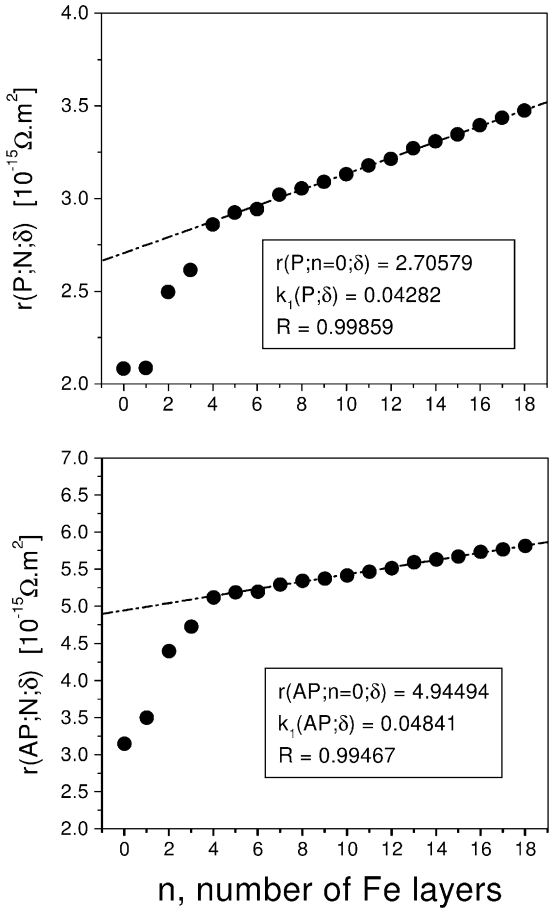

Fig. 23. Variation of the sheet resistance $r(\mathscr{C};n;\delta)$, $\delta = 2$ mry, for bcc Fe(1 0 0)/$Fe_nGe_sFe_n$/Fe, $\delta = 2$ mry, $s = 9$, with respect to n. The upper panel refers to the parallel configuration, the lower to the antiferromagnetic configuration. Dashed lines indicate the extrapolation of the linear regime to $n = 0$. From Ref. [40].

bcc-Fe(1 0 0)/$Fe_nGe_sFe_n$/Fe by inspecting the properties of $r(\mathscr{C};t;\delta)$, $t = 2n + s$, for a given value of s. From this figure one can see that for $n \geqslant 12$ a linear regime with respect to n is entered, i.e., in the limit of $\delta \to 0$ for all $n \geqslant 12$ the very same sheet resistance is obtained. Fig. 23—the corresponding plot to Fig. 20—shows the variation of the sheet resistance of bcc-Fe(1 0 0)/$Fe_nGe_sFe_n$/Fe at a given value of s and δ with respect to the number of lead layers (n) for the parallel and the antiparallel magnetic configuration. For a given value of δ (2 mry) the GMR is varied in Fig. 24 with respect to the number of spacer layers (fixed number of lead layers) and with respect to the number of lead layers at a fixed number of spacer layers. As can be seen in the first case the GMR varies only little in the regime of $6 \leqslant s \leqslant 21$, in the second case for $n \geqslant 8$ the GMR stays almost constant. In fact in the limit of $\delta \to 0$ and for $n \geqslant 8$ the GMR at a given spacer thickness would be exactly constant.

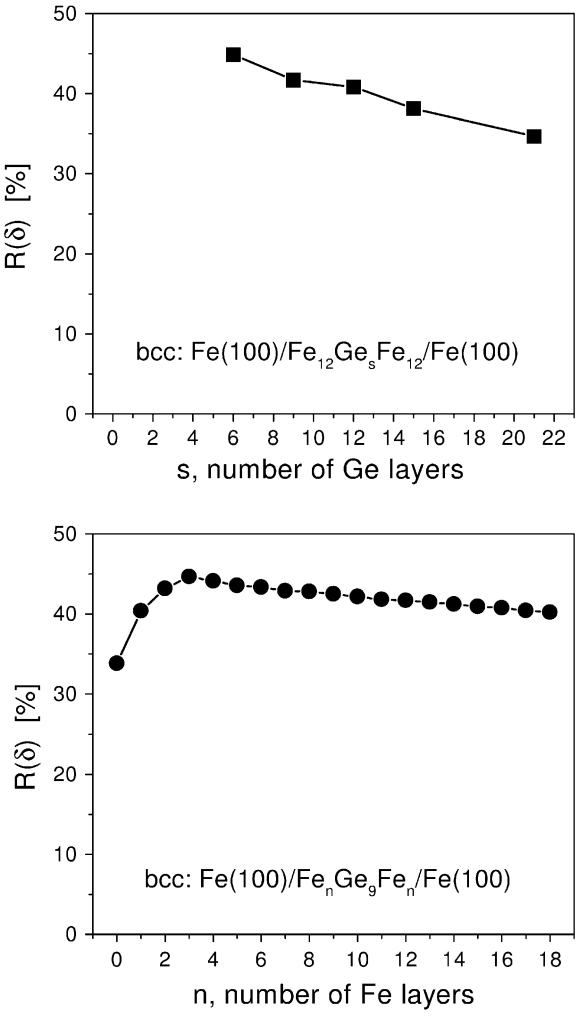

Fig. 24. Top: Variation of the magnetoresistance in bcc Fe(1 0 0)/$Fe_{12}Ge_sFe_2$/Fe with respect to the number of Ge layers s. Bottom: variation of the magnetoresistance in bcc Fe(1 0 0)/$Fe_nGe_9Fe_n$/Fe, with respect to n. In both entries $\delta = 2$ mry. From Ref. [40].

7.7.2. *Different terminations of the spacer*

In Fig. 25 the sheet resistances (extrapolated to $\delta \to 0$) are displayed as the product of t and $r(\mathscr{C}; t)$ when the number of spacer layers in bcc-Fe(1 0 0)/$Fe_n(ZnSe)_sFe_n$/Fe is varied. This product is approximately linear in $t = 2n + s$; a linear fit can therefore be used to extend the curve of the GMR versus spacer thickness to very large spacer thicknesses. In Fig. 26 the magnetoresistance ratio ("pessimistic value") is plotted versus the spacer thickness (the curve corresponding to the linear fit is shown as dashed line); as can be seen it is different for different terminations and becomes constant for large spacer thicknesses.

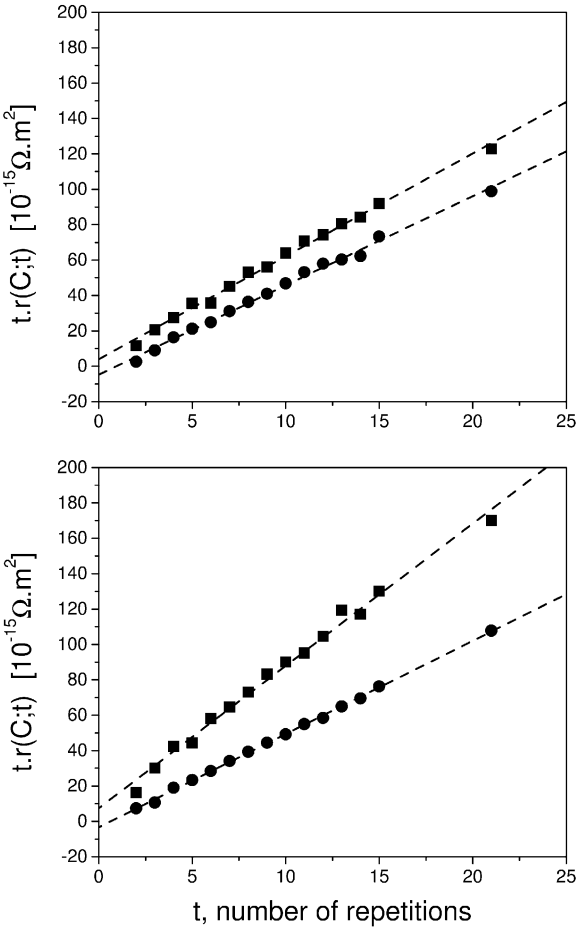

Fig. 25. Product of sheet resistances in Fe(1 0 0)/Fe$_n$(ZnSe)$_s$Fe$_n$/Fe (continued to the real energy axis) $r(\mathscr{C};t)$ and $t=(2n+s)$ versus t. Top: Zn-termination, bottom: Se-termination. Circles and squares refer to the parallel and antiparallel configuration, respectively. From Ref. [41].

By partitioning the difference of the sheet resistances

$$\Delta r(t) = r(\mathscr{A}\mathscr{P};t) - r(\mathscr{P};t) \tag{193}$$

with respect to the magnetic configurations into contributions arising from different parts of the heterostructure, namely the left and right electrodes (leads), L_{left} and L_{right}, the interface regions between electrodes and spacer, I_{left} and I_{right}, and the remaining spacer part S,

$$\Delta r(t;\delta) = \Delta r_{L_{\text{left}}}(t;\delta) + \Delta r_{L_{\text{right}}}(t;\delta) + \Delta r_{I_{\text{left}}}(t;\delta) + \Delta r_{I_{\text{right}}}(t;\delta) + \Delta r_S(t;\delta)\ , \tag{194}$$

a very informative "picture" of where the magnetoresistance comes from can be given. In the case of bcc-Fe(1 0 0)/Fe$_n$(ZnSe)$_s$Fe$_n$/Fe the GMR effect is almost entirely caused by the interface contributions, see Fig. 27.

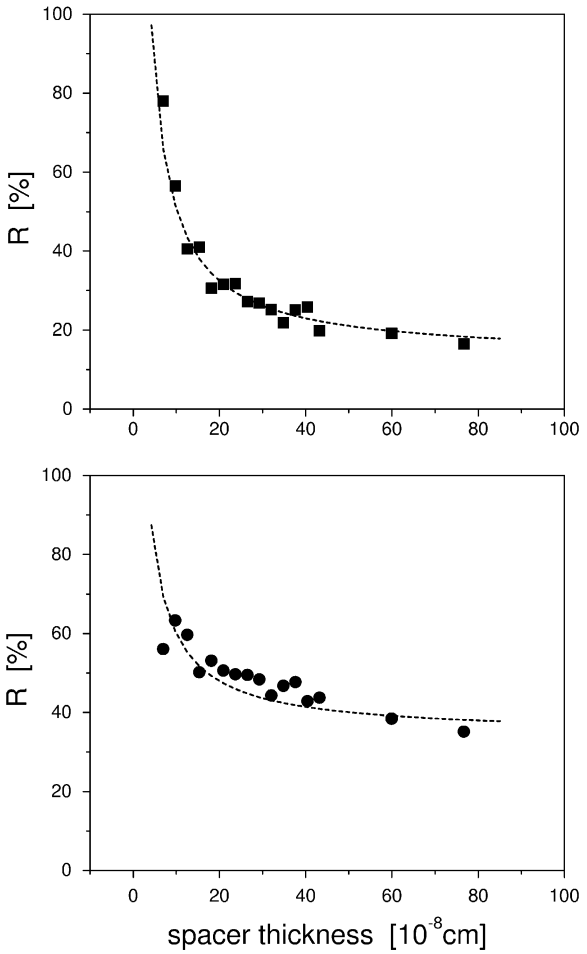

Fig. 26. Magnetoresistance $R(t)$ in Fe(1 0 0)/ZnSe/Fe(1 0 0) heterostructures as a function of the spacer thickness. Top: Zn-termination, bottom: Se-termination. The squares refer to the continued $\delta = 0$ values, the dashed lines to the magnetoresistance using the fitted sheet resistances. From Ref. [41].

7.7.3. Interdiffusion at the interfaces

Clearly enough the larger the regime of antiferromagnetic coupling, the more technically applicable a certain system appears to be. However, this is not necessarily implies that the GMR follows the same trends as the IEC. In Fig. 28 the IEC is shown for the system bcc-Fe(1 0 0)/$Fe_{12}Si_nFe_{12}$/Fe(1 0 0) as a function of the number of lead layers considering a two layer interdiffusion at the interfaces. Note that 12 Fe layers serve again as a buffer to the semi-infinite leads in order to reach a regime of Fe layers with no oscillations in the layer-resolved Madelung potentials. From this figure it is evident that with increasing interdiffusion the regime of antiferromagnetic coupling grows. For the GMR, however, interdiffusion is disastrous: as can be seen from Fig. 30 even a small interdiffusion reduces the GMR effect drastically. As in this figure three different spacer thicknesses are shown,

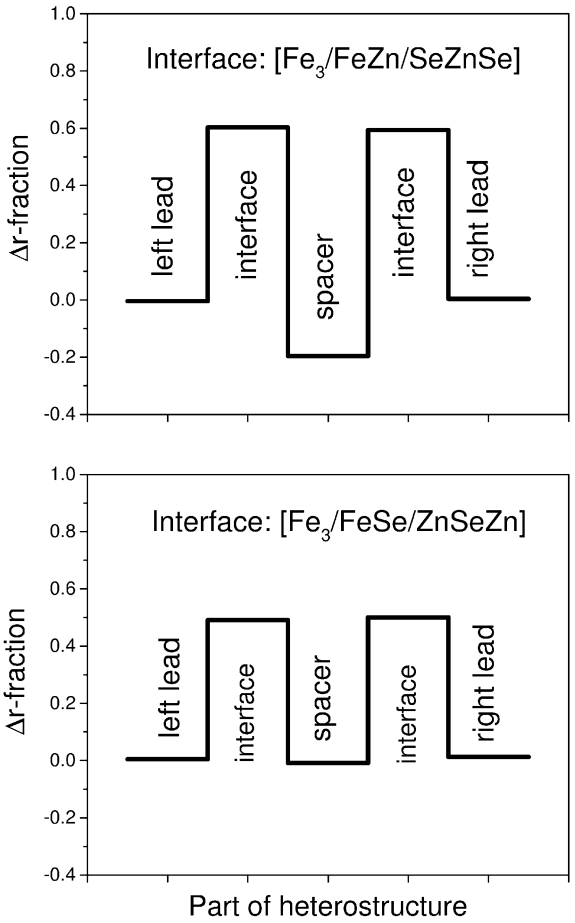

Fig. 27. Normalized fractions of the difference in the sheet resistance between the antiferromagnetic and the ferromagnetic configuration in Fe(1 0 0)/$(ZnSe)_{21}$/Fe(1 0 0). The various regions of the heterostructure are given explicitly. From Ref. [41].

all of them characterized by the same functional behavior, the effect of interdiffusion on the GMR seems to be independent of the number of spacer layers. If one could produce a Fe/Si/Fe trilayer with very little or even no interdiffusion, which is difficult because of the formation of silicides at the interfaces, the corresponding GMR would be reasonably large even for rather thick spacers, see Figs. 29–31.

7.7.4. The role of the spacer: structural effects

Experimentally very little is known about the actual structure in the spacer parts of heterostructures. Although it was already shown that most of the GMR effect in such structures is due to the interfaces, it nevertheless is worthwhile to consider also structural aspects in the spacer. It should be recalled that the use of two-dimensional lattice Fourier transformations, see e.g. Eq. (151),

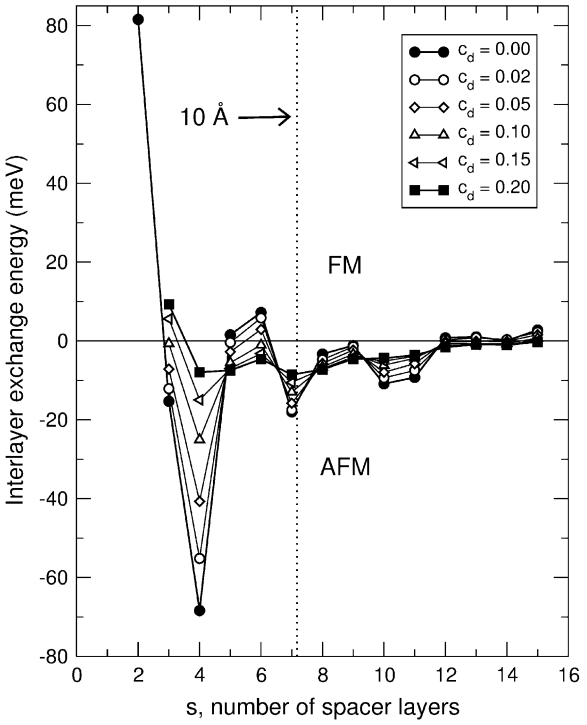

Fig. 28. Changes of the IEC in bcc-Fe(1 0 0)/Si$_s$/Fe with respect to the number of spacer layers for different interdiffusion concentrations c_d. From Ref. [42].

implies that in all layers considered (including the leads) one and the same two-dimensional translational invariance has to apply. If therefore the spacer material would correspond to a complex two-dimensional lattice (lattice with sublattices) then the same complex two-dimensional lattice has to apply for the leads. Unfortunately this restriction leaves only two options open, namely either to assume a particular structure for the spacer which then has to serve for the whole system including the leads, or, to assume that the structure of the leads applies also for the rest of the system. The examples shown up-to-now refer to the last case. Quite clearly in reality the structure of the leads and the spacer material is important. Structural rearrangements can occur; lattice distortions, interface interdiffusion, growth conditions (macroscopical roughness), etc., matter.

One can, however, simulate the effect of the structure of the spacer. In Table 6 the actual composition of three different types of Fe/Ge$_s$/Fe systems are shown, the corresponding GMR ($\delta = 2$ mry) values are displayed in Fig. 24. For the present purpose only system C ($s = 15$) with $c = 1$ is of interest, for which the corresponding GMR value amounts to about 30%. Comparing this values with the corresponding entry for $s = 15$ in Fig. 24, which amounts to about 37%, it is evident that by leaving out every second plane in the spacer the GMR is changed only moderately. This proves indirectly that the structure of the spacer seems to be of little importance for the size of the GMR effect.

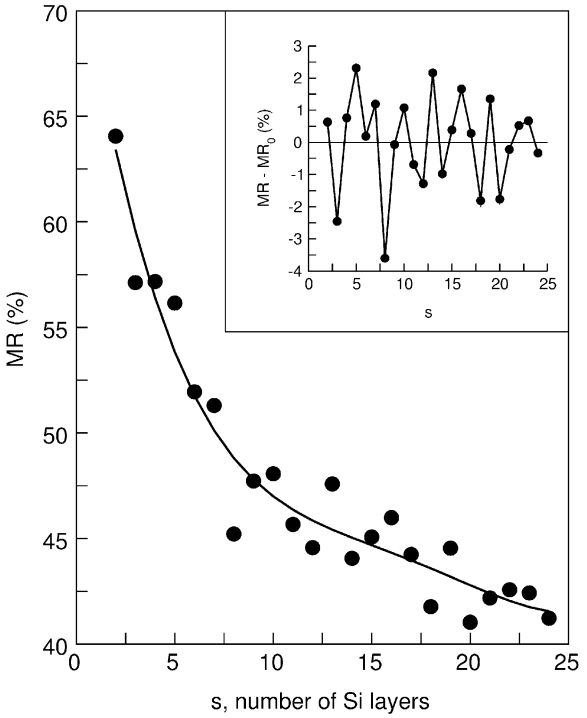

Fig. 29. Magnetoresistance for Fe/Si_s/Fe trilayers versus the number of Si spacer layers s. The full line is a 4th order fit of the magnetoresistance to the data points. Inset: Difference between the calculated points and the fit depending on the number of Si layers. From Ref. [42].

7.7.5. *Conducting properties of the spacer material*

Another question frequently posed is that of the "semi-conductor" properties of the spacer material in systems such as e.g. Fe/Ge_s/Fe. This question leads back to the problem of the characteristic volume and the definition of the so-called bulk properties. Optical gaps in semi-conductors are bulk properties (same value in all unit cells), which are not necessarily preserved in thin films of the same material sandwiched by metallic leads. Even if the density-of-states in the interior of rather thick "non-metallic" spacers vanishes this local gap can be of different size as in the bulk material and surely is not uniformly characteristic for the whole system, leads included.

7.8. *References to fully relativistic ab initio CPP calculations*

The previous sections were meant to illustrate the formal and numerical procedures applied when using the Kubo–Greenwood equation for CPP-transport. Table 7 provides an overview of papers in this direction.

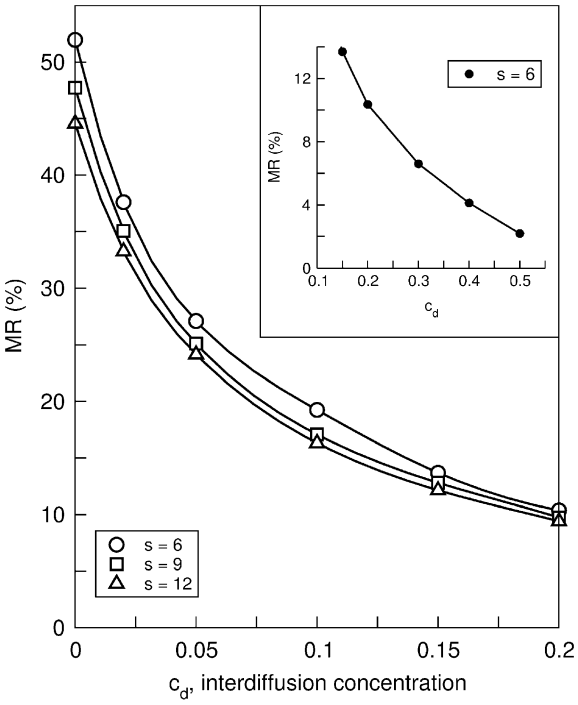

Fig. 30. Dependence of the magnetoresistance on the interdiffusion concentration for Fe/Si_s/Fe systems. From Ref. [42].

8. Tunneling magnetoresistance and the relation to a Landauer-type description of CPP-transport

In this section the question is addressed of when one ought to speak of "metallic" CPP and when of "tunneling". For this purpose the system bcc-Fe(1 0 0)/$Fe_n Vac_s Fe_n$/Fe(1 0 0) is considered, i.e., a system in which two semi-infinite pieces of Fe are separated by s vacuum layers. Clearly enough considering vacuum as spacer no questions about the structure or other properties of the spacer arise. In Fig. 32 the changes of the layer-resolved Madelung potentials with respect to the growing thickness of the separating vacuum are shown; in Fig. 33 for the layer-resolved sheet resistances,

$$r_i(\mathscr{C};\delta) = \sum_j \rho_{ij}(\mathscr{C};\delta), \quad r(\mathscr{C};\delta) = \sum_i r_i(\mathscr{C};\delta)\ , \tag{195}$$

corresponding to the parallel and the antiparallel magnetic configuration. Although one easily can see from Fig. 33 that for $s \geqslant 3$ the sheet resistances start to grow considerably in the center of the vacuum part, this is yet no indication that actually "tunneling" occurs. Considering the density of states (DOS) in the central vacuum layer, when the total number of vacuum layers is varied, it turns out that only for $s \geqslant 9$ the corresponding DOS at the Fermi energy (of the leads) has vanished, see Fig. 34.

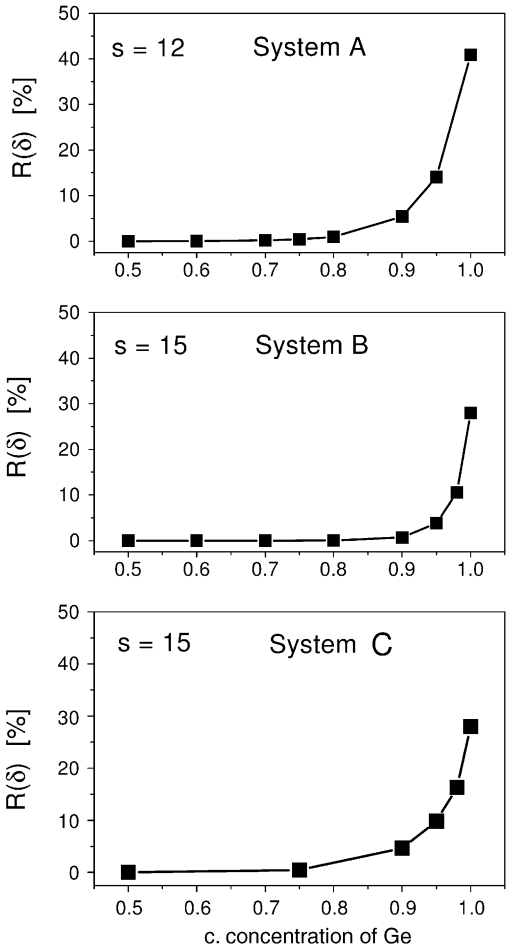

Fig. 31. Calculated magnetoresistance for the three types of spacer considered, see Table 6. The number of spacer layers is indicated, $\delta = 2$ mry. From [40].

8.1. Exponential growth

Let us define for illustrative purposes the following auxiliary quantities for perpendicular electric transport by restricting the summation in Eq. (145) to $p = 1$ and $q = n$:

$$\bar{\sigma}_{zz}(\mathscr{C}; n) = \frac{1}{4}\sum_{k,l=1}^{2}(-1)^{k+l}\left\{\sum_{i,j=1}^{n}\sigma_{zz}(\mathscr{C}; \varepsilon_k, \varepsilon_l; n)\delta_{i1}\delta_{jn}\right\}$$

$$= \frac{1}{4}\sum_{k,l=1}^{2}(-1)^{k+l}\sigma_{zz}^{1n}(\mathscr{C}; \varepsilon_k, \varepsilon_l; n)\ , \tag{196}$$

Table 6
Investigated Fe/Ge/Fe systems

System A	System B	System C
Homogeneous alloying	Interdiffusion and ordering	Alloying and ordering
bcc bulk Fe	bcc bulk Fe	bcc bulk Fe
Fe_{12}	Fe_{12}	Fe_{12}
Ge_cVac_{1-c}	$Ge_{1-c}Vac_c$	Vac
Ge_cVac_{1-c}	Ge_cVac_{1-c}	Ge_cVac_{1-c}
Ge_cVac_{1-c}	$Ge_{1-c}Vac_c$	Vac
Ge_cVac_{1-c}	Ge_cVac_{1-c}	Ge_cVac_{1-c}
⋮	⋮	⋮
⋮	⋮	⋮
Ge_cVac_{1-c}	Ge_cVac_{1-c}	Ge_cVac_{1-c}
Ge_cVac_{1-c}	$Ge_{1-c}Vac_c$	Vac
Ge_cVac_{1-c}	Ge_cVac_{1-c}	Ge_cVac_{1-c}
Ge_cVac_{1-c}	$Ge_{1-c}Vac_c$	Vac
Fe_{12}	Fe_{12}	Fe_{12}
bcc bulk Fe	bcc bulk Fe	bcc bulk Fe

Table 7
References to CPP calculations using the fully relativistic versions of the SKKR-method and the Kubo–Greenwood equation

System	Reference
Fe/Ge/Fe	[40,43]
Fe/ZnSe/Fe	[41,43]
Fe/Si/Fe	[42,45]
Fe/InP/Fe	[43,44]

i.e., by considering a very simplified realization of a Landauer-type approach in terms of a two-end-point conductivity, where the two end-points are situated well inside the leads.

In terms of this quantity now the question of the so-called exponential increase of the sheet resistances can be addressed. From Fig. 35 it is evident that only $\bar{\sigma}_{zz}(\mathscr{C};n)$ increases linearly with the number of vacuum layers, while the quantity corresponding to the Kubo–Greenwood equation (summation over all two-point conductivities) shows an asymptotic behavior of approximately proportional to $\ln(s)$ for $s \geqslant 6$. This is also reflected in the corresponding MR ratios, see Fig. 36: for strict exponential growth the MR ratio becomes a constant with increasing number of vacuum layers, whereas in the Kubo–Greenwood approach this ratio rapidly approaches zero for $s \geqslant 6$. Therefore, the question of exponential growth has to be reviewed in a more analytical way. Abbreviating $r(C;2n+s;\delta)$ simply by $r_{\mathscr{C}}(s)$ and assuming that the growth of $r_{\mathscr{C}}(s)$ with s is of an

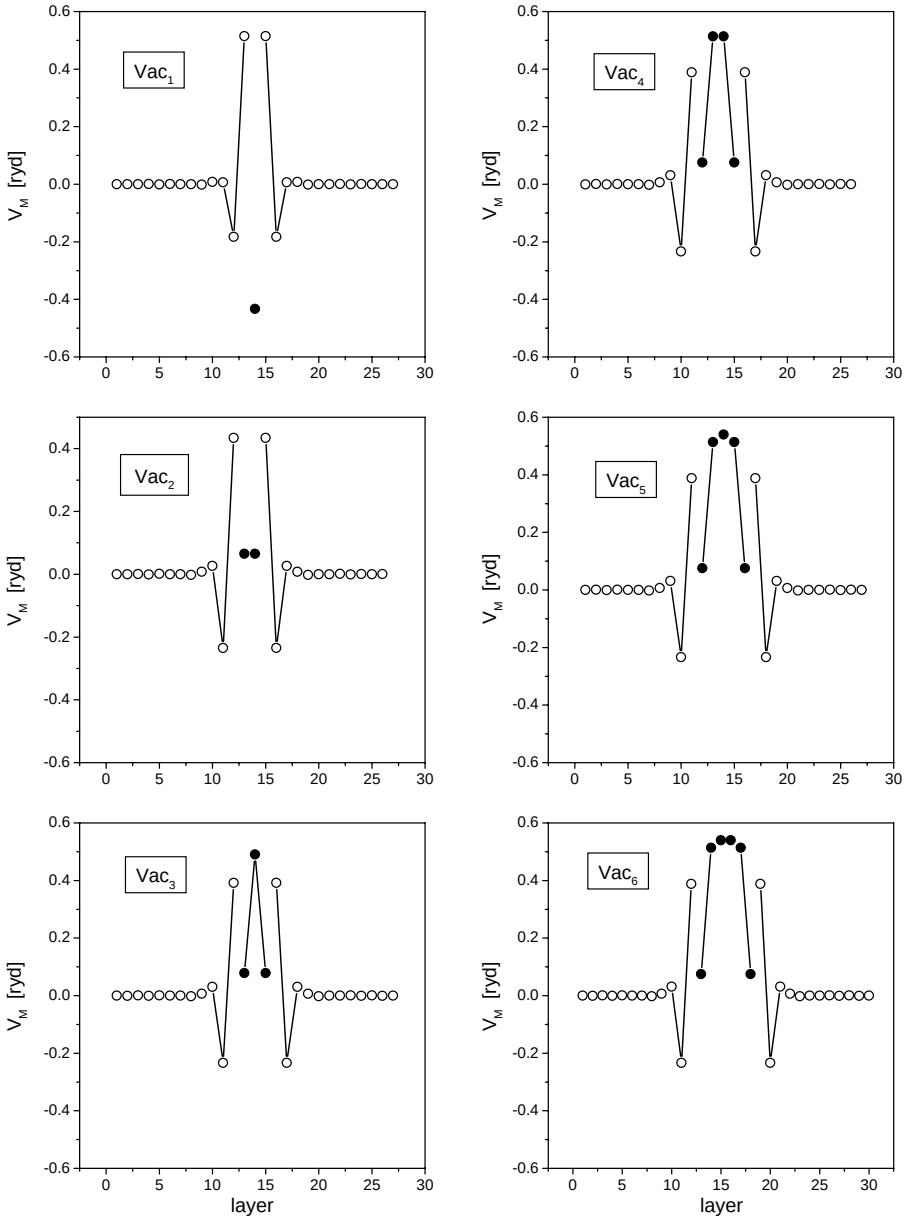

Fig. 32. Layer-resolved Madelung potentials in bcc-Fe(1 0 0)/Fe$_n$Vac$_s$Fe$_n$/Fe(1 0 0), $n \geqslant 11$. Open circles refer to Fe-like contributions, full circles to contributions from the vacuum layers. The number of vacuum layers s is marked explicitly. From Ref. [46].

exponential form,

$$r_P(s) = A_P \exp(K_P s) \quad \text{and} \quad r_{AP}(s) = A_{AP} \exp(K_{AP} s) \ , \tag{197}$$

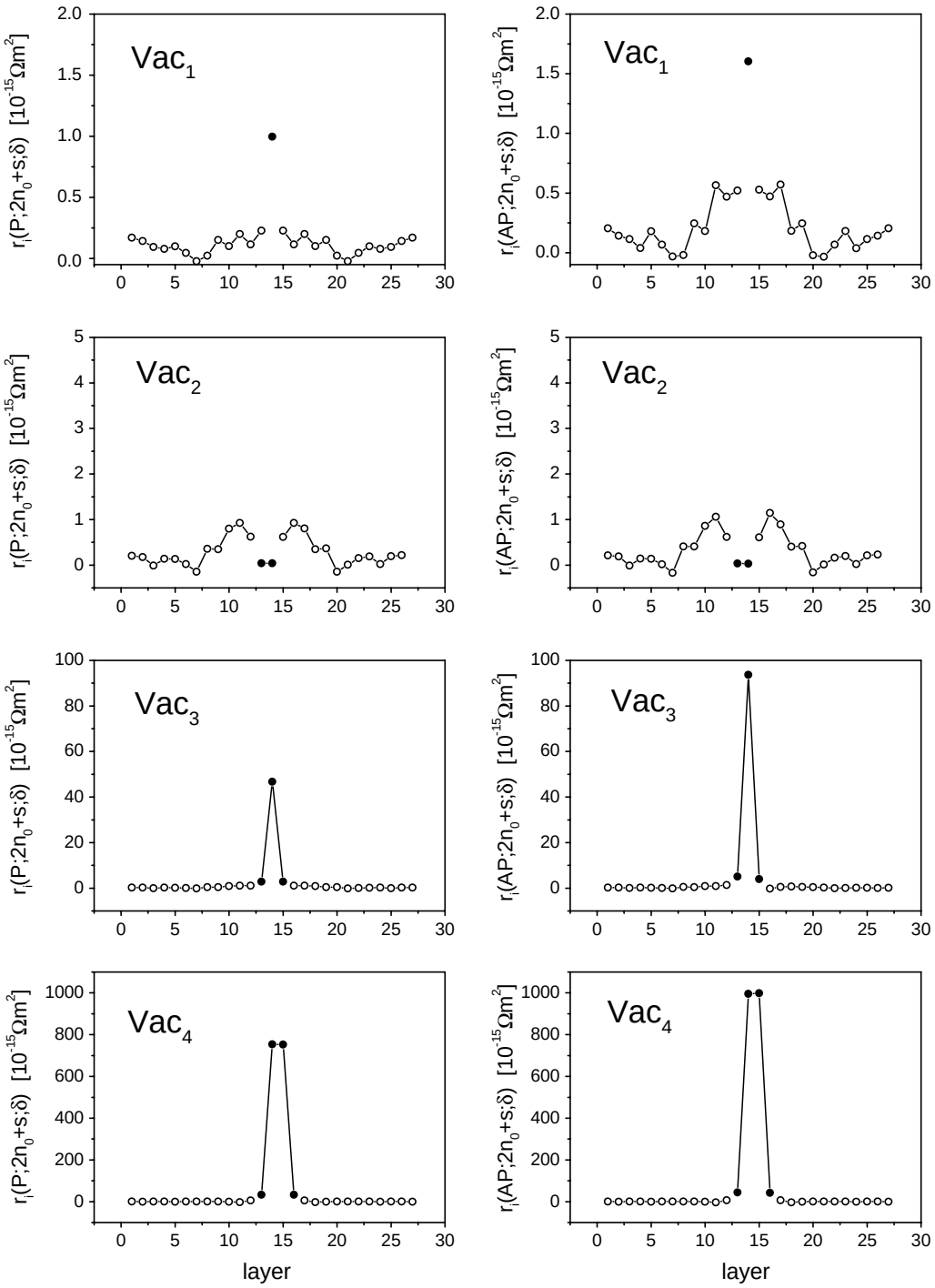

Fig. 33. Layer-resolved sheet resistances in bcc-Fe(1 0 0)/Fe$_n$Vac$_s$Fe$_n$/Fe(1 0 0) $r_i(\mathscr{C}; 2n+s; \delta)$, $n \geqslant 11, \delta = 2$ mry, for the parallel (left) and the antiparallel (right) magnetic configuration. Open circles refer to Fe-like contributions, full circles to contributions from the vacuum layers. The number of vacuum layers s is marked explicitly. From Ref. [46].

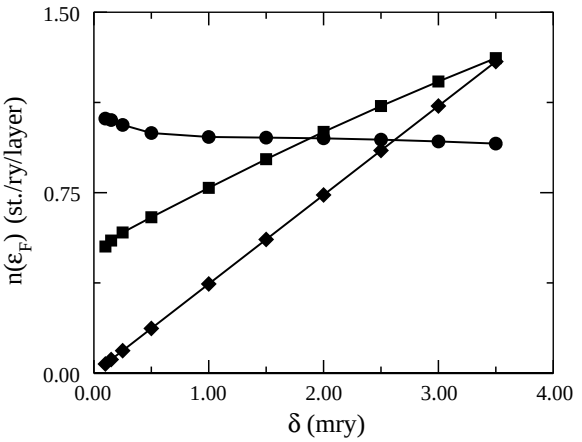

Fig. 34. Density of states of the center vacuum layer at the complex Fermi energy $\varepsilon_F + i\delta$ as a function of δ in bcc-Fe(1 0 0)/$Fe_{12}Vac_sFe_{12}$/Fe(1 0 0) for $s=3$ (circles), $s=6$ (squares; multiplied by 100), and $s=9$ (diamonds; multiplied by 250). From Ref. [46].

then quite clearly the corresponding magnetoresistance $R(s)$ is given by

$$R(s) = 1 - C\exp[(K_P - K_{AP})s] \ , \tag{198}$$

where $C = A_P/A_{AP}$. This now implies that the following cases have to be distinguished

$$K_{AP} < K_P \rightarrow \lim_{s\to\infty} R(s) = -\infty \ , \tag{199}$$

$$K_{AP} = K_P \rightarrow \lim_{s\to\infty} R(s) = 1 - C \in [0,1) \ , \tag{200}$$

$$K_{AP} > K_P \rightarrow \lim_{s\to\infty} R(s) = 1 \ , \tag{201}$$

leaving the conclusion that with "strict" exponential growth of the sheet resistances in the limit of infinitely separated magnetic leads $R(s)$ tends to zero only in the particular case of $A_P = A_{AP}$ ($C = 1$) and $K_P = K_{AP}$, i.e., $r_P(s) = r_{AP}(s)$; $R(s)$ tends to a constant, if $K_P = K_{AP}$ and $A_P \neq A_{AP}$ (the logarithmic dependencies correspond to two parallel lines). It seems therefore that only a description of electric properties in terms of Eq. (196) leads to strict exponential growth of the sheet resistances and consequently to a finite magnetoresistance even in the case of infinitely separated Fe leads.

8.2. Metallic conductivity versus tunneling

Changing the barrier in the middle of a large enough vacuum spacer, see top of Fig. 37 causes interesting effects, namely (1) for an increasing (large enough) barrier the sheet resistances become constant (as to be expected, bottom of Fig. 37), while (2) for barrier values close to

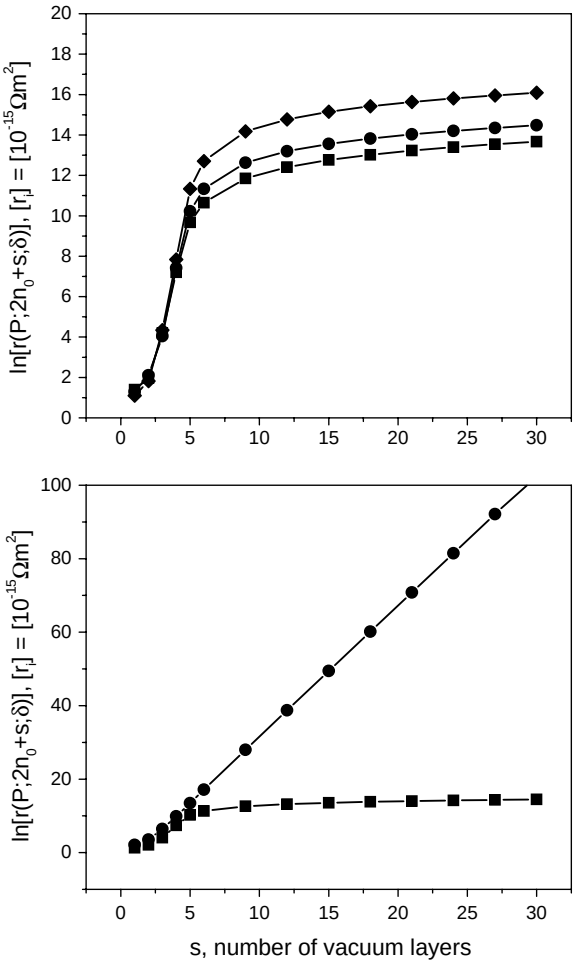

Fig. 35. Top: $\ln[r(\mathscr{P};2n+s;\delta)]$, $n \geqslant 11$, in bcc-Fe(1 0 0)/Fe$_n$Vac$_s$Fe$_n$/Fe(1 0 0) as calculated in terms of the Kubo–Greenwood approach and displayed versus the number of vacuum layers s. Diamonds, circles and squares refer in turn to $\delta = 0, 2.0$ and 3.0 mry. Bottom: Comparison between Eq. (196) (Landauer-type, circles) and the Kubo–Greenwood equation (squares). Displayed is $\ln[r(\mathscr{P};2n+s;\delta)], n \geqslant 11, \delta = 2$ mry, as a function of the number of vacuum layers s. From Ref. [46].

the selfconsistently determined one a sharp increase occurs. In using this particular regime of barriers, where the sheet resistances vary rapidly, a first kind of distinction between metallic conductance and tunneling can be given. From Fig. 38 it is obvious that there is a cusp when this barrier is reduced to the Madelung potential of the leads (vertical line): below this value the barrier is of attractive character (metallic behavior of electric transport), above (repulsive barrier) tunneling seems to be the case. However, in terms of the MR ratio this is perhaps too qualitative, since inspecting the dependency of the sheet resistances for $s = 3$ with respect to the imaginary part of the Fermi energy, two different types of behavior can be traced. If for matter of simplicity k denotes the slope of a particular sheet resistance with increasing δ then one can distinguish the

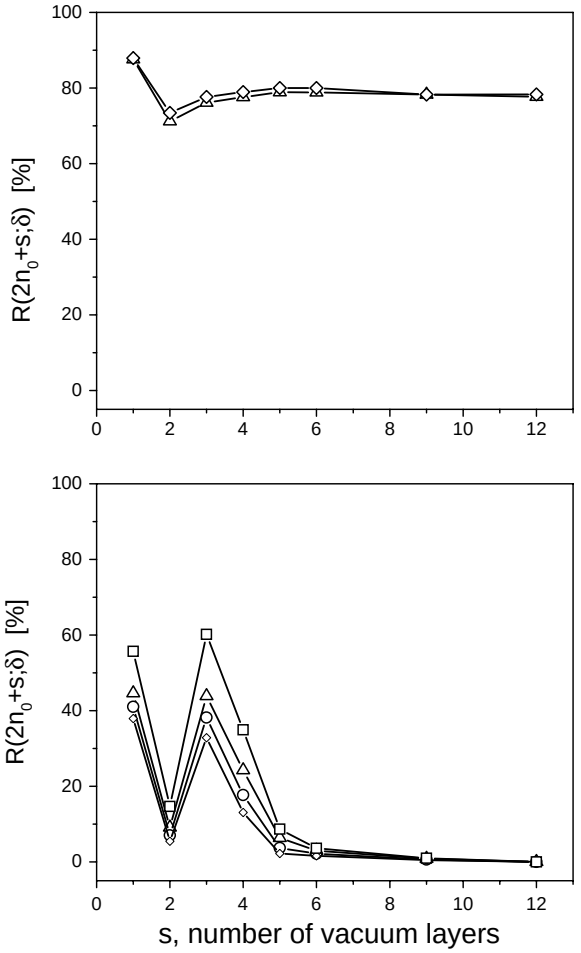

Fig. 36. Magnetoresistance $R(2n+s;\delta)$, $n \geqslant 11$, in bcc-Fe(1 0 0)/$Fe_n Vac_s Fe_n$/Fe(1 0 0) as described in terms of Eq. (196) (Landauer-type, top) and a Kubo–Greenwood approach (bottom) versus the number of vacuum layers s. Squares, triangles, circles and diamonds refer to $\delta = 0, 2, 2.5$ and 3 mry. From Ref. [46].

following case

I.	$k > 0$:	metallic behavior,	increase of selfenergy ("disorder")
II.	$k < 0$:	tunneling,	increasing DOS at the Fermi level

In Fig. 39 the parallel and the antiparallel sheet resistance are depicted for $s = 3$. As can be seen the parallel sheet resistance belongs to type I, the antiparallel to type II. This is the very reason for the peak of the MR ratio in the lower half of Fig. 36. For all other values of s the sheet resistances

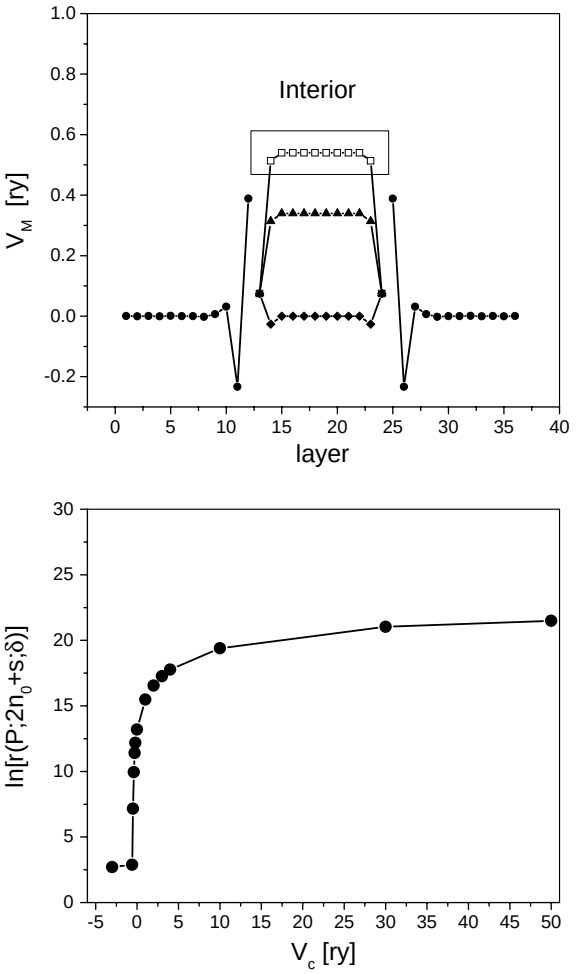

Fig. 37. Top: Layer-resolved Madelung potentials and shifted potential barriers in the vacuum region of bcc-Fe(1 0 0)/$Fe_{12}Vac_{12}Fe_{12}$/Fe(1 0 0). Circles: Fe; squares, triangles and diamonds refer to the vacuum region with $V_C = 0, -0.2$ ry and $-V_M$, respectively. Bottom: $\ln[r(\mathscr{P}; 2n + s; \delta)], n \geqslant 11, \delta = 2$ mry, of bcc-Fe(1 0 0)/$Fe_{12}Vac_{12}Fe_{12}$/Fe(1 0 0) as a function of V_C. From Ref. [46].

in both magnetic configurations belong to one and the same type such as type II for $s > 3$. For an interesting experimentalist's view of tunneling see Ref. [47].

9. Exchange bias in the GMR of spin valves

Exchange bias occurs when systems with F-AFM interfaces are cooled through the Néel temperature (T_N) of the AFM part, whereby the Curie temperature (T_C) of the FM part has to be larger than T_N. After the field cool procedure, at a temperature $T < T_N$, the hysteresis loop of the FM–AFM system is shifted along the field axis generally in the opposite direction of the cooling

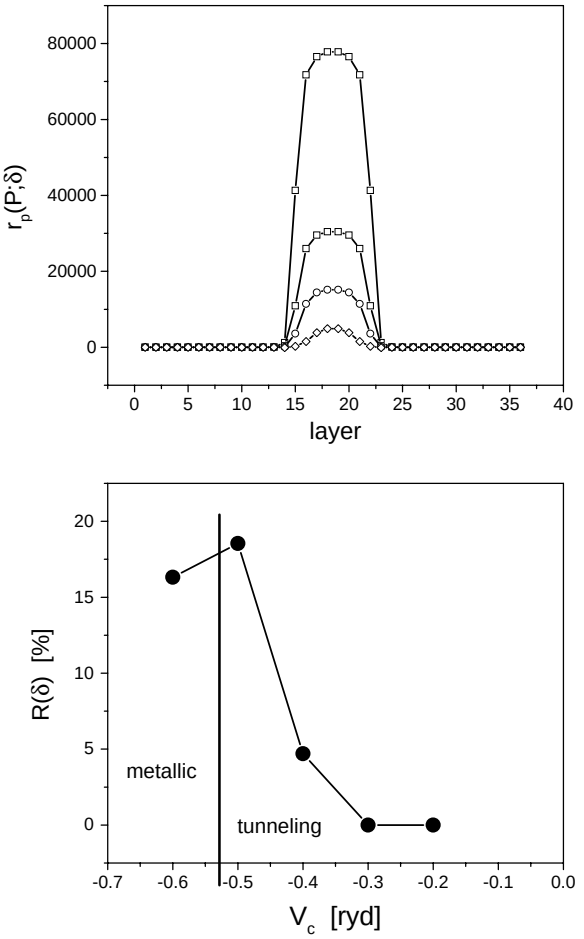

Fig. 38. Top: Sheet resistance $r(\mathscr{P}; 2n_0 + s; \delta)$ (top) and magnetoresistance $R(2n_0 + s; \delta)$ (bottom), $\delta = 2$ mry, in bcc-Fe(1 0 0)/$Fe_{12}Vac_{12}Fe_{12}$/Fe(1 0 0) as a function of the constant shift V_C. In the top part squares, triangles, circles and diamonds refer to $V_C = 0, -0.2, -0.3$ and -0.4 ryd, respectively, in the lower part the regimes of metallic and tunneling behavior of electric transport are separated by the condition $V_M^i = -V_C$ (vertical line). From Ref. [46].

field, i.e., the absolute value of the coercive field for decreasing and increasing field is different. This loop shift is usually termed exchange bias and was found and investigated in quite a few different experiments such as magnetization and magnetic torque measurements, ferromagnetic resonance, neutron diffraction, magnetoresistance, etc., see Fig. 40. For an excellent review on this topic the reader is referred to Nogués and Schuller [48]. Up to now, however, only phenomenological or semi-classical models are in use in order to explain exchange bias effects.

In principle Fig. 40 has to be taken literally and both the abscissa and the ordinate in this figure have to be defined in quantum mechanical terms. In the following exclusively GMR experiments are dealt with, other properties will need other descriptions or even other theoretical tools like statistical mechanics in the case of magnetization measurements.

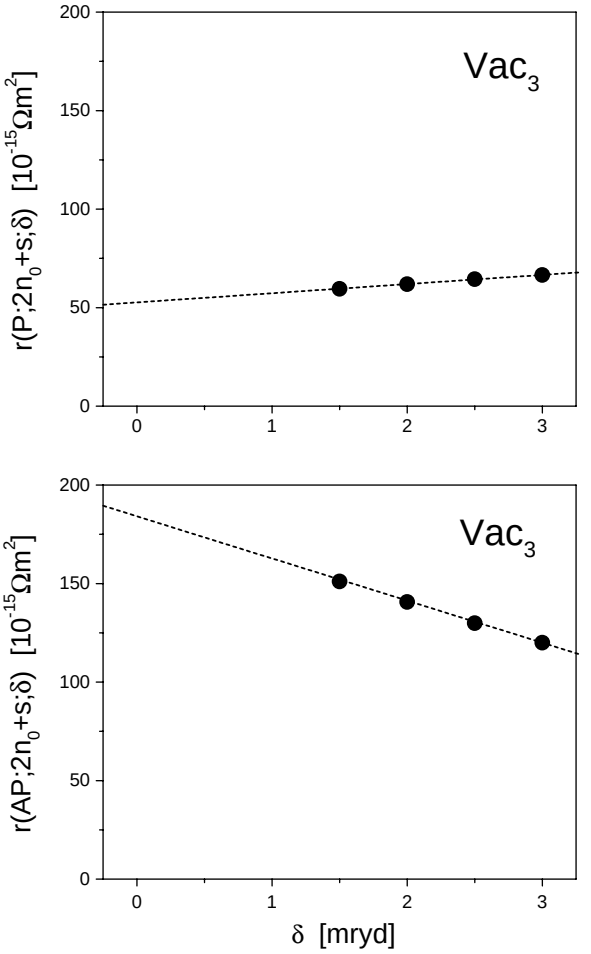

Fig. 39. Analytical continuation of the sheet resistances $r(\mathscr{C};2n+s;\delta), n \geqslant 11, s=3$ in bcc-Fe(1 0 0)/Fe$_n$Vac$_s$Fe$_n$/Fe(1 0 0) to the real energy axis. Top: parallel configuration, bottom: antiparallel configuration. Full circles refer to calculated values, dotted lines to the corresponding linear fit. From Ref. [46].

9.1. Mappings

9.1.1. Collinear configurations

Let $\mathscr{C}_0$ be the collinear ground state magnetic configuration of total energy $E(\mathscr{C}_0)$ and C_i some collinear magnetic configuration of total energy $E(\mathscr{C}_i)$, then

$$\Delta E(\mathscr{C}_i) = E(\mathscr{C}_i) - E(\mathscr{C}_0) \geqslant 0 \ , \tag{202}$$

which trivially implies that

$$\Delta E(\mathscr{C}_i) = 0 \rightarrow E(\mathscr{C}_i) = E(\mathscr{C}_0) \rightarrow \mathscr{C}_i \equiv \mathscr{C}_0 \ . \tag{203}$$

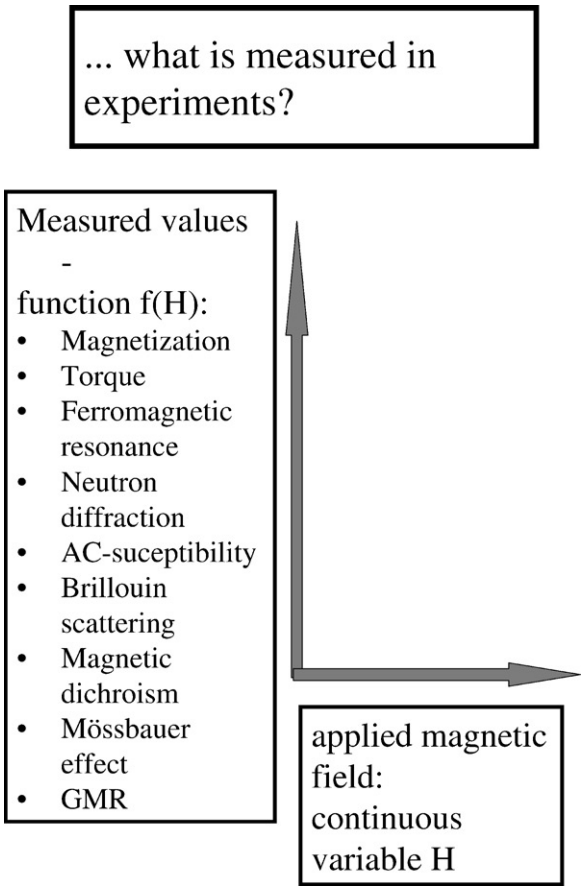

Fig. 40. Scheme of measurement.

The set of collinear configurations $\{\mathscr{C}_i\}$ can therefore be mapped onto these (discrete) energy differences,

$$f : \{\mathscr{C}_i\} \rightarrow \{\Delta E(\mathscr{C}_i)\}, \tag{204}$$

such that because of Eq. (203) there exits an inverse mapping,

$$f^{-1} f = I \ , \tag{205}$$

with I denoting the identity.

Since, because of Eqs. (204) and (205),

$$f(\mathscr{C}_i) = \Delta E(\mathscr{C}_i), \quad \mathscr{C}_i = f^{-1}(\Delta E(\mathscr{C}_i)) \ , \tag{206}$$

the magnetoresistance $R(\mathscr{C}_i)$ can formally be written as an implicit function of $\Delta E(\mathscr{C}_i)$,

$$R(\mathscr{C}_i) = \frac{r[\mathscr{C}_i] - r[\mathscr{C}_0]}{r[\mathscr{C}_i]} = \frac{r[f^{-1}(\Delta E(\mathscr{C}_i))] - r[f^{-1}(\Delta E(\mathscr{C}_0))]}{r[f^{-1}(\Delta E(\mathscr{C}_i))]} \ . \tag{207}$$

Table 8
Expansion coefficients

Case	Relation	Mapping onto configurations
I	$a_1 \gg a_2$	Isomorphic
II	$\|a_1\| \sim \|a_2\|$	Iso- or homomorphic
III	$\|a_1\| \ll \|a_2\|$	Homomorphic

9.1.2. Non-collinear configurations

Suppose now that according to Eqs. (43) and (45) $\mathscr{C}_0$ is characterized by a set of collinear unit vectors n_k

$$\mathscr{C}_0 = \{\ldots, n_{k-1}, n_k, n_{k+1}, \ldots\} \ , \tag{208}$$

where k numbers atomic layers, and $\mathscr{C}_i(\Theta)$ by

$$\mathscr{C}_i(\Theta) = \{\ldots, n_{k-1}, U(\Theta)n_k, n_{k+1}, \ldots\} \ . \tag{209}$$

where $U(\Theta)$ is a rotation of $n_k, 0 \leqslant \Theta \leqslant 2\pi$, around an axis perpendicular to n_k. Just as in the case of the GMR (Section 6.6.4), the energy difference

$$\Delta E(\mathscr{C}_i(\Theta)) = E(\mathscr{C}_i(\Theta)) - E(\mathscr{C}_0) \tag{210}$$

can now be fitted in terms of the following expansion, see also Eq. (165):

$$\Delta E(\mathscr{C}_i(\Theta)) = \sum_{m=1}^{\infty} a_m(1 - \cos^m\Theta) \ . \tag{211}$$

Using the coefficients a_m for a classification of the proposed mapping in the case of continuous magnetic configurations, one arrives at the conclusion summarized in Table 8. An example for the most likely case, namely case I, is shown in Fig. 16. For case I in Table 8 Eq. (206) remains valid even for non-collinear configurations.

9.1.3. Relations to the interlayer exchange coupling in terms of grand potentials

In the same manner as total energies also grand potentials and the concept of the IEC, see Section 4, can be used. Suppose $\mathscr{C}_k$ is an arbitrary assumed (collinear) magnetic configuration, then the IEC of configuration $\mathscr{C}_i$ with respect to $\mathscr{C}_k$ is given by

$$\Delta E_b(\mathscr{C}_i) = E_b(\mathscr{C}_i) - E_b(\mathscr{C}_k) \ . \tag{212}$$

According to Eq. (128) the condition

$$\Delta E_b(\mathscr{C}_0) = \min_{\mathfrak{v}}\{\Delta E_b(\mathscr{C}_i)\} \ , \tag{213}$$

where $\mathfrak{v} = \{\mathscr{C}_i\}$ denotes the set of all collinear magnetic configurations, provides then an identification of the energetically lowest state of magnetic configuration $\mathscr{C}_0$ (ground state). Since

$$\varepsilon(\mathscr{C}_i) \equiv \Delta E_b(\mathscr{C}_i) - \Delta E_b(\mathscr{C}_0) \geqslant 0 \ , \tag{214}$$

the magnetoresistance can again be viewed as an implicit function of $\varepsilon(\mathscr{C}_i)$. Allowing for continuous configurations, $\varepsilon(\mathscr{C}_i)$, $\mathscr{C}_i \notin \boldsymbol{v}$, this quantity becomes a continuous variable ε. Furthermore, assuming that usually case I in Table 8 applies, ε becomes a continuously growing variable. All $\varepsilon(\mathscr{C}_i), \mathscr{C}_i \in \boldsymbol{v}$, then simply refer to certain (discrete) values of ε.

9.2. Definition of the exchange bias

It should be noted that in terms of the IEC, redefined in Eqs. (213) and (214), the magnetoresistance can be viewed as an implicit function of ε,

$$R(\varepsilon) = \frac{r(\mathscr{C}_0) - r(\varepsilon)}{r(\mathscr{C}_0)} \ , \tag{215}$$

where in CPP $r(\varepsilon)$ is that sheet resistance (resistivity in the case of CIP) which (with respect to $\mathscr{C}_0$) corresponds to a magnetic configuration of interlayer exchange energy ε. Clearly enough for certain regimes of ε the magnetoresistance $R(\varepsilon)$ remains constant while in other regimes rapid changes with ε occur: the interlayer exchange energy ε acts like a magnetic field (external energy) that is switched on continuously. Increasing ε "forces" the system to gradually assume the magnetic configuration with the next highest energy, etc. Consequently one can define the exchange bias E_{bias} in terms of $R(\varepsilon)$ in the following manner:

$$0 \leqslant \varepsilon \leqslant E_{\text{bias}} : R(\varepsilon) = 0; \ \ \varepsilon > E_{\text{bias}} : R(\varepsilon) \neq 0 \ . \tag{216}$$

Obviously for all $\varepsilon \leqslant E_{\text{bias}}$ it is sufficient to consider only collinear configurations, while for $\varepsilon > E_{\text{bias}}$ also particular non-collinear configurations have to be taken into account. It should be noted that of course this definition applies only to systems for which a recordable change in the MR can be observed, e.g., in spin-valve systems with an AF part.

9.3. Exchange bias in the GMR of a spin valve with CoO as antiferromagnetic part

As an example for the above discussed approach a spin valve system with CoO as antiferromagnetic part of the system, namely $\text{Co}(1\,1\,1)/\text{Co}_6/(\text{CoO})_n/\text{Co}_6/\text{Cu}_6/\text{Co}_6/\text{Co}(1\,1\,1)$, $n = 6, 12$, is considered [49]. In Table 9 the first 10 collinear magnetic configurations lowest in energy are listed. Note that in this table each row refers to an atomic layer, an entry zero (one) means that in this plane the orientation of magnetization is parallel (antiparallel) to the surface normal. The corresponding interlayer exchange energies and magnetoresistances are displayed in Fig. 41. As one can see from this figure in going from configuration 7 to configuration 8, there is a jump in the IEC as well as in the magnetoresistance. However, one can also see that from configuration 1 to configuration 7 the IEC slightly increases, whereas the magnetoresistance remains zero. In Fig. 42 the IEC and the magnetoresistance is plotted for the case that one goes continuously from configuration 7 to configuration 10 in terms of the non-collinear configuration headed by Θ in Table 9. As easily can be guessed from this figure the functional behavior of the IEC and the MR with respect to Θ strictly follows case I in Table 8. Fig. 43 shows the magnetoresistance as function of the IEC and is therefore the equivalent representation of what was demanded in Fig. 40, namely a plot of the measured quantity—the magnetoresistance—as a function of a continuous variable. In the top part of Fig. 44 the IEC of configurations 1–7 is shown on an enlarged scale, i.e., for those configurations

Table 9
Magnetic configurations in Co(1 1 1)/Co_6/$(CoO)_6$/Co_6/Cu_6/Co_6/Co(1 1 1)

Layers		**Discrete**			**Cont.**	**Discrete**						
Co(111)	**i**	**10**	**9**	**8**	Θ	**7**	**6**	**5**	**4**	**3**	**2**	**1**
Co	1	0	0	0	0	0	0	0	0	0	0	0
⋮	⋮	⋮	⋮	⋮	⋮	⋮	⋮	⋮	⋮	⋮	⋮	⋮
Co	6	0	0	0	0	0	0	0	0	0	0	0
O	1	1	1	1	1	1	1	1	1	1	1	1
Co	1	1	1	1	1	1	1	1	1	1	1	1
O	2	0	0	0	0	0	0	0	0	0	0	0
Co	2	0	0	0	0	0	0	0	0	0	0	0
O	3	1	1	0	1	1	1	1	1	1	1	0
Co	3	1	1	1	1	1	1	1	1	1	1	1
O	4	0	0	0	0	0	0	0	0	0	0	0
Co	4	0	0	0	0	0	0	0	0	0	0	0
O	5	1	0	0	1	1	1	1	1	1	0	0
Co	5	1	1	1	1	1	1	1	1	1	1	1
O	6	0	0	0	0	0	0	0	0	0	0	0
Co	6	0	0	0	0	0	0	0	0	0	0	0
Co	1	0	0	0	0	0	0	0	0	0	0	0
Co	2	0	0	0	0	0	0	0	0	0	0	0
Co	3	0	0	0	0	0	0	0	0	0	0	0
Co	4	0	0	0	0	0	0	0	0	0	0	0
Co	5	0	0	0	0	0	0	0	0	0	0	0
Co	6	0	0	0	0	0	0	0	0	0	0	0
Cu	1	0	0	0	0	0	0	0	0	0	0	0
Cu	2	0	0	0	Θ	1	0	0	0	0	0	0
Cu	3	0	0	0	Θ	1	0	1	0	0	0	0
Cu	4	0	0	0	Θ	1	0	1	0	1	1	1
Cu	5	0	0	0	Θ	1	0	1	1	1	1	1
Cu	6	0	0	0	Θ	1	1	1	1	1	1	1
Co	1	0	0	0	Θ	1	1	1	1	1	1	1
Co	2	0	0	0	Θ	1	1	1	1	1	1	1
Co	3	0	0	0	Θ	1	1	1	1	1	1	1
Co	4	0	0	0	Θ	1	1	1	1	1	1	1
Co	5	0	0	0	Θ	1	1	1	1	1	1	1
Co	6	0	0	0	Θ	1	1	1	1	1	1	1

for which the magnetoresistance remains zero. According to the definition given in Eq. (216) the exchange bias in this system corresponds therefore to the IEC of configuration 7, $E_{\text{bias}} = \varepsilon(\mathscr{C}_7)$. The spin-flip energy, i.e., the energy to flip the orientation of the magnetization in one of the Co-slab, is then defined by $\varepsilon(\mathscr{C}_8) - \varepsilon(\mathscr{C}_7)$ and refers to the Co-slab farest away from the CoO part of the system (pinning effect!). Finally in the lower part of Fig. 44 the variation of E_{bias} with respect to the number of CoO double layers is displayed. In order to give a rough estimate in kOe, by using the relation $\Delta E = \mu_B B$ (1 meV = 172.76 kOe), E_{bias} amounts to about 6 kOe, which compares reasonably well with experimental data ($E_{\text{bias}} \leqslant 9.5$ kOe) for Co/CoO type systems, see, e.g., Ref. [48].

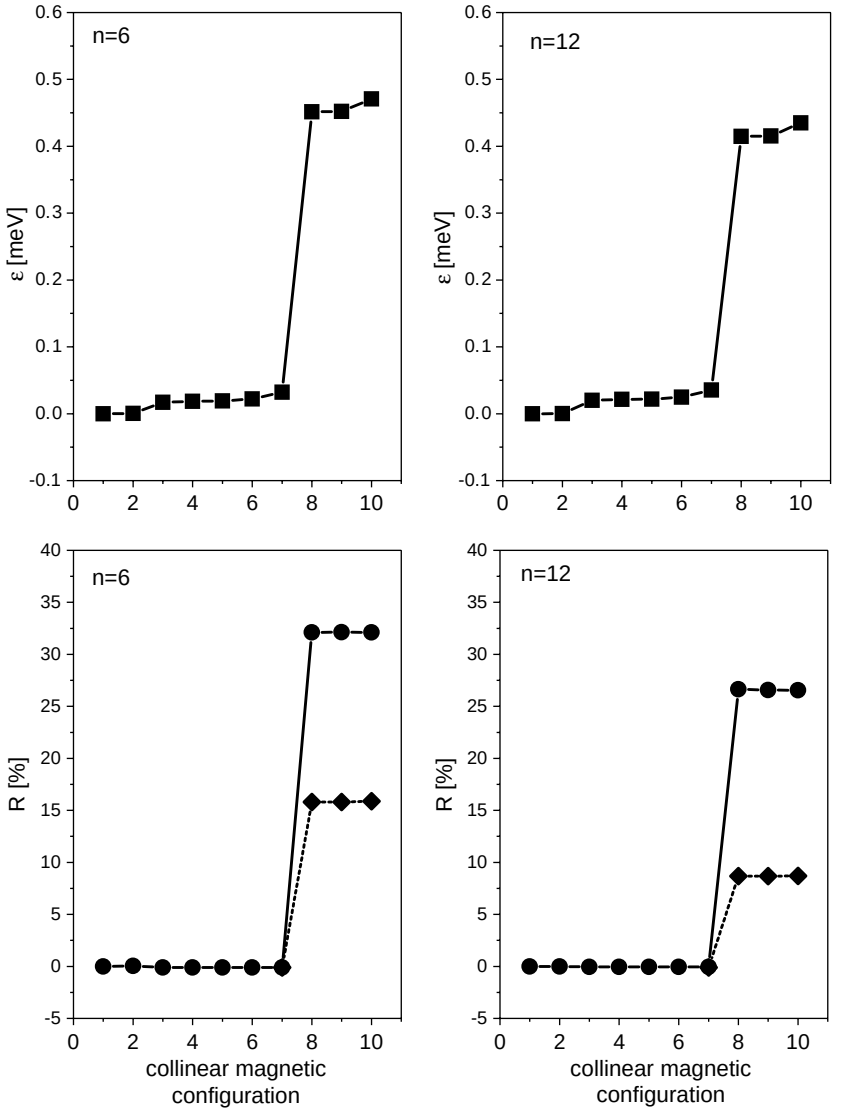

Fig. 41. The 10 lowest interlayer exchange energies and corresponding magnetoresistances in Co(1 1 1)/Co_6/$(CoO)_n$/Co_6/Cu_6/Co_6/Co(1 1 1). CPP and CIP are denoted by circles and diamonds, respectively. The number of repetitions of a CoO double layer is marked explicitly. From [49].

10. Electric properties of nanostructures

10.1. Magnetic nanostructures–an upcoming field of research

Because of their extraordinary magnetic properties (very large magnetic moments and magnetic anisotropies) magnetic nanostructures on metallic substrates seem to become *the* major field of research, both experimental and theoretical, in the coming years. The controlled production of

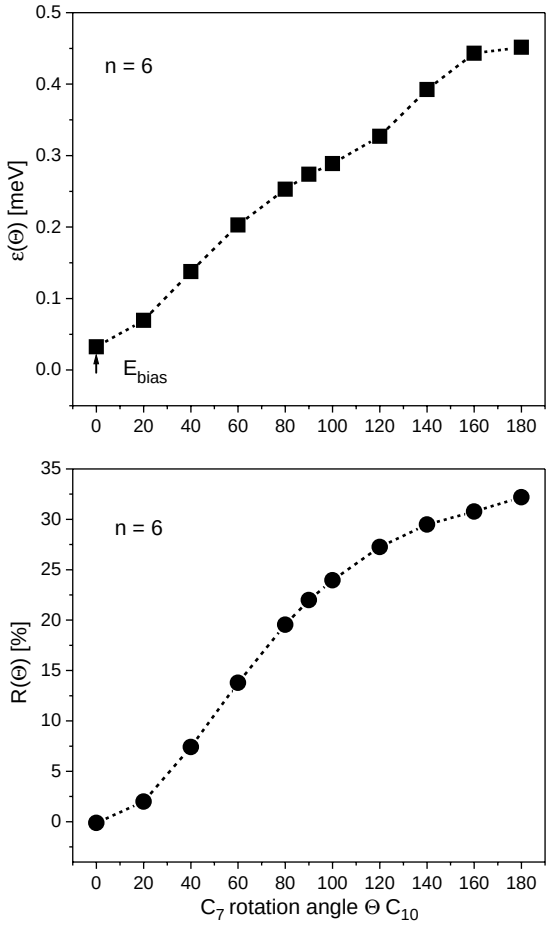

Fig. 42. Interlayer exchange energy and CPP magnetoresistance Co(1 1 1)/Co_6/$(CoO)_n$/Co_6/Cu_6/Co_6/Co(1 1 1) as a function of the rotation angle Θ for a rotation around the y-axis. The two collinear magnetic configurations that correspond to the endpoints are marked explicitly. From [49].

magnetic nanowires or regular arrays of magnetic "islands" on metallic substrates, however, is at present still a tough experimental challenge; so is the theoretical description of such systems. In Fig. 45 a schematic view of such nanostructures is shown. Clearly enough in order to describe theoretically the electric properties of such a system, no longer two-dimensional translational invariance can be assumed in the Kubo–Greenwood equation, see Eq. (133), i.e., one has to use the corresponding real space description, Eqs. (140)–(144). This in turn implies to go back to the convergence properties of such an approach for "bulk-like" properties, which really means to check out how well pure metals or statistically disordered binary alloys can be described in terms of a Kubo–Greenwood equation in real space. It should be noted that this also implies to make use of the embedded cluster method discussed in Section 3.9 in order to evaluate properly the Green's functions (scattering path operators) to be used in the Kubo–Greenwood equation.

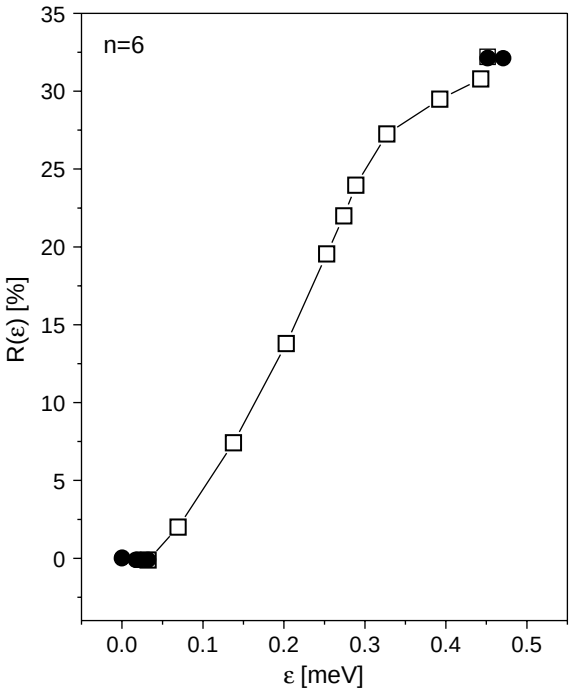

Fig. 43. CPP magnetoresistance Co(1 1 1)/Co_6/$(CoO)_n$/Co_6/Cu_6/Co_6/Co(1 1 1) for $n = 6$ as a function of the interlayer exchange energy. Collinear magnetic configurations are shown in terms of full symbols. From [49].

10.2. Size-dependence of clusters in real space

In Fig. 46 the site resolved contributions to the conductivity tensor elements $\sigma^{0i}_{\mu\mu}(\mathscr{C}; n; \delta)$,

$$\sigma^{0i}_{\mu\mu}(\mathscr{C}; n; \delta) = \frac{1}{4}\sum_{k,l=1}^{2}(-1)^{k+l}\sigma^{0i}_{\mu\mu}(\mathscr{C}; \varepsilon_k, \varepsilon_l; n) \ , \tag{217}$$

$$\varepsilon_k, \varepsilon_l = \varepsilon_F \pm \mathrm{i}\delta \ , \tag{218}$$

$\delta = 2$ mry, are displayed for fcc-Ag. Although these contributions appear to be quite local, Fig. 47 proves that indeed respective clusters of Ag atoms,

$$\mathbb{C}(r) = \{\mathbf{R}_{oi} \,|\, |\mathbf{R}_{oi}| \leqslant r\} \ , \tag{219}$$

where r is the cluster radius (size of the cluster) and the index 0 refers to an arbitrary origin in $\mathscr{L}^{(3)}$, have to be quite big in fcc-Ag such that $r\rho_{\mu\mu}(\mathscr{C}; r; \delta)$,

$$\rho_{\mu\mu}(\mathscr{C}; r; \delta) = \frac{1}{\sigma^{0j}_{\mu\mu}(\mathscr{C}; r; \delta)} \ , \tag{220}$$

$$\sigma_{\mu\mu}(\mathscr{C}; r; \delta) = \sum_{\mathbf{R}_{oi}\in\mathbb{C}(r)} \sigma^{0j}_{\mu\mu}(\mathscr{C}; r; \delta) \ , \tag{221}$$

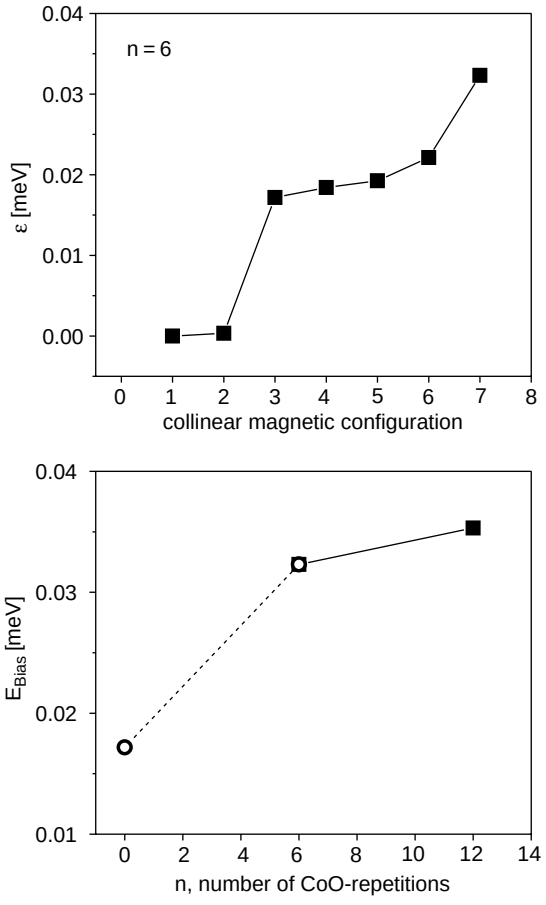

Fig. 44. Top: Interlayer exchange energy $\varepsilon \leqslant E_{\text{bias}}$ Co(1 1 1)/Co$_6$/(CoO)$_n$/Co$_6$/Cu$_6$/Co$_6$/Co(1 1 1) for $n = 6$. Bottom: Exchange bias as a function of the number of repetitions of a CoO double layer. The value at $n = 0$ (open symbol) is an extrapolation, see text. From [49].

grows linearly with r. As in all previously discussed cases this linear form can then be used to extrapolate $\rho_{\mu\mu}(\mathscr{C}; r; \delta)$ to infinitely large clusters,

$$\rho_{\mu\mu}(\mathscr{C}; \delta) = \lim_{r\to\infty} \rho_{\mu\mu}(\mathscr{C}; r; \delta) \ . \tag{222}$$

10.3. Dependence on the imaginary part of the Fermi energy

In Fig. 48 the numerical continuation of $\rho_{\mu\nu}(\mathscr{C}; \delta)$,

$$\rho_{\mu\mu}(\mathscr{C}) = \lim_{\delta\to 0} \rho_{\mu\mu}(\mathscr{C}; \delta) \ , \tag{223}$$

to the real axis is illustrated for fcc-Ag and two examples of Cu_cPt_{1-c} bulk alloys. As can be seen the resistivity for fcc-Ag is indeed zero as it has to be, the obtained residual resistivities for Cu_cPt_{1-c} are rather good agreement with previous theoretical calculations using three-dimensional

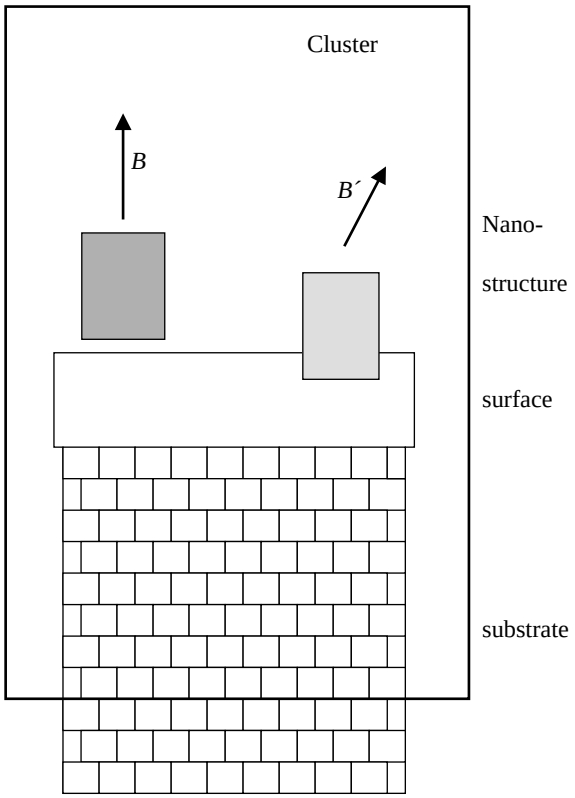

Fig. 45. Schematic view of magnetic nanostructures on a metal substrate. B and B' indicate the orientation of the magnetization.

periodic boundary conditions and with existing experimental data. Since in (non-magnetic) cubic systems the conductivity tensor is of the following form,

$$\rho = \begin{pmatrix} \rho_{xx} & 0 & 0 \\ 0 & \rho_{yy} & 0 \\ 0 & 0 & \rho_{zz} \end{pmatrix} = \begin{pmatrix} \rho_0 & 0 & 0 \\ 0 & \rho_0 & 0 \\ 0 & 0 & \rho_0 \end{pmatrix} , \tag{224}$$

i.e., all diagonal elements have to be of the same value, this can be used to determine the inherent errors involved in calculating (bulk residual) resistivities by evaluating the following quantity,

$$\Delta\rho = \lim_{\delta\to 0} \lim_{r\to\infty} |\rho_{\mu\mu}(\mathscr{C}; r; \delta) - \rho_{\nu\nu}(\mathscr{C}; r; \delta)|, \quad \mu \neq \nu , \tag{225}$$

which by definition should be zero. Fig. 49 shows that by using the real space Kubo–Greenwood equation properly the inherent errors are rather very small and seem to be nearly independent of the imaginary part of the Fermi energy.

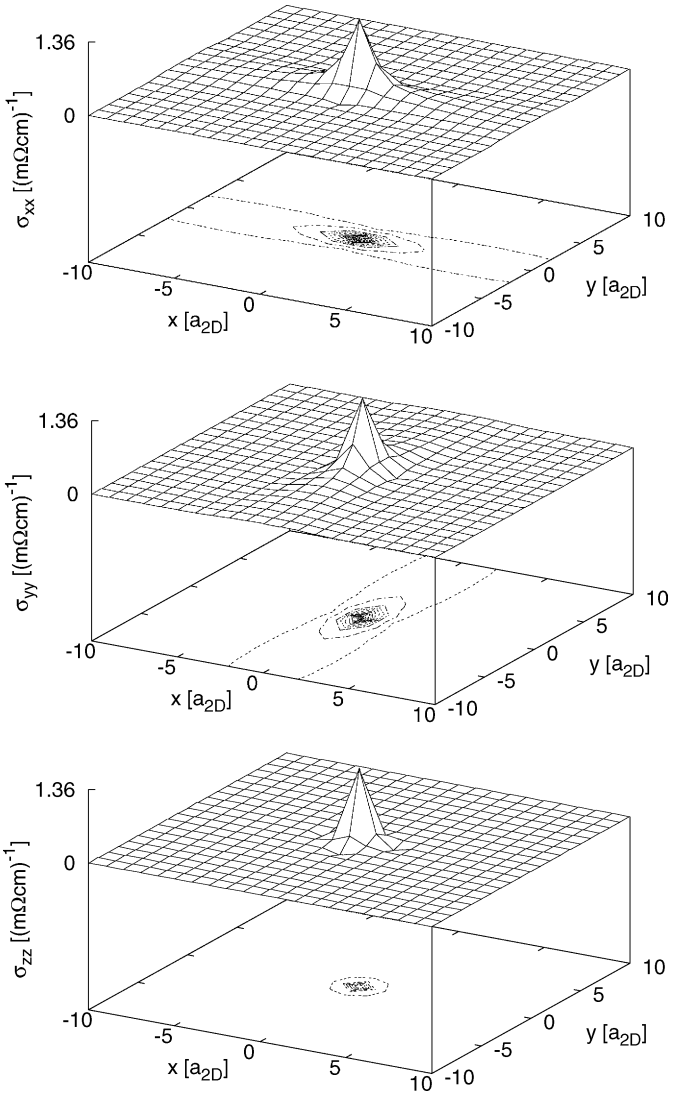

Fig. 46. Site-resolved conductivity tensor elements in fcc-Ag. From Ref. [26].

10.4. Applications to nanostructures

Although at present only very preliminary theoretical (and experimental) results for nanostructures (small magnetic clusters on metal surfaces, "quantum wires") exist, the theoretical approach to describe (future) experimental data seems to be reasonably settled. Provided that for a particular magnetic arrangement $\mathscr{C}$ the following convergence properties are fulfilled:

$$|\rho_{\mu\mu}(\mathscr{C}; r + d) - \rho_{\mu\mu}(\mathscr{C}; r)| \leqslant \Delta \ , \tag{226}$$

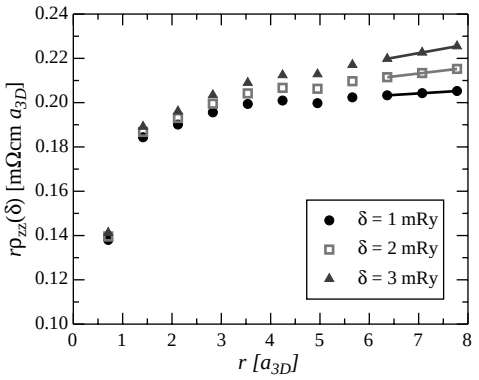

Fig. 47. Three-dimensional cluster of Ag embedded in fcc-Ag ($a_0 = 7.7849$ a.u.). The size of the cluster r times the zz-component of the resistivity is shown for three different values of δ versus r. From Ref. [26].

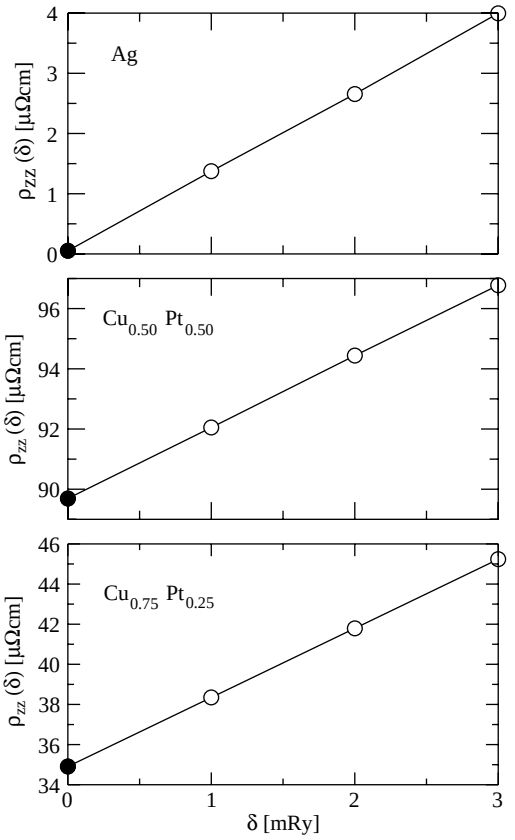

Fig. 48. Extrapolation of the zz-component of the resistivity ρ_{zz} in the limit of $r \to r_0$ for three-dimensional clusters of Ag in fcc-Ag and Cu_cPt_{1-c} in fcc-Cu_cPt_{1-c} with respect to the imaginary part of the Fermi energy δ. The lattice constant for fcc-Ag is 7.7895 a.u.; for fcc-Cu_cPt_{1-c} 7.140 and 6.995 a.u. for $c = 0.5$ and 0.75, respectively. From Ref. [26].

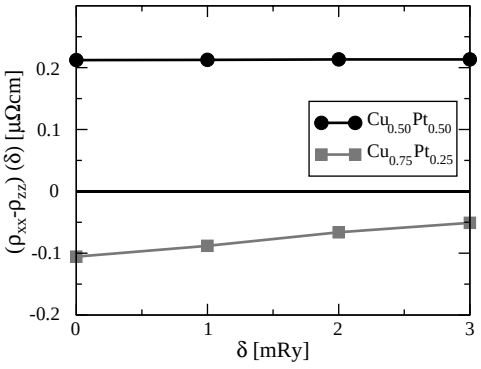

Fig. 49. Difference between $\rho_{xx}(r = r_0; \delta)$ and $\rho_{xx}(r = r_0; \delta)$ for Cu_cPt_{1-c} versus δ. This difference defines the remaining numerical error. From Ref. [26].

where Δ is a sufficiently small number and r is defined in Eq. (143), then $\rho_{\mu\mu}(\mathscr{C}; r)$ refers to the resistivity of a cluster that not only includes a nanostructure but also a sufficient number of substrate atoms, see Fig. 45. Furthermore, suppose that for the system without the nanostructure(s), i.e., for the substrate only the corresponding resistivity is given by $\rho^0_{\mu\mu}(\mathscr{C}; r)$, then the following difference:

$$\Delta\rho_{\mu\mu}(\mathscr{C}; r) = \rho_{\mu\mu}(\mathscr{C}; r) - \rho^0_{\mu\mu}(\mathscr{C}; r) \ , \tag{227}$$

can be regarded as a kind of "residual resistivity" caused by the nanostructure(s). If as indicated in Fig. 45 nanostructures with different orientations of the magnetization are present then again magnetoresistances (MR) of the type

$$\mathrm{MR} = \frac{\Delta\rho_{\mu\mu}(\mathscr{C}; r) - \Delta\rho_{\mu\mu}(\mathscr{C}'; r)}{\Delta\rho_{\mu\mu}(\mathscr{C}; r)} \tag{228}$$

exist which can be exploited for technological purposes.

11. The TB-LMTO method and the "Kubo–Landauer" equation

11.1. The (orthogonal) TB-LMTO Hamiltonian

The non-relativistic (orthogonal) TB-LMTO Hamiltonian [52,53] is given by

$$\mathbf{H}^{\gamma,\sigma} = \mathbf{C}^{\sigma} + (\boldsymbol{\Delta}^{\sigma})^{1/2}\{\mathbf{S}^{\beta}(1 - (\boldsymbol{\gamma}^{\sigma} - \boldsymbol{\beta})\mathbf{S}^{\beta})^{-1}\}(\boldsymbol{\Delta}^{\sigma})^{1/2} \ , \tag{229}$$

$$\mathbf{H}^{\gamma,\sigma} = \{H^{\gamma,\sigma}_{\mathbf{R}L,\mathbf{R}'L'}\}, \quad \mathbf{C}^{\sigma} = \{C^{\sigma}_{\mathbf{R}L}\delta_{\mathbf{R},\mathbf{R}'}\delta_{L,L'}\}, \quad \mathbf{S}^{\beta} = \{S^{\beta}_{\mathbf{R}L,\mathbf{R}'L'}\} \ , \tag{230}$$

$$\boldsymbol{\Delta}^{\sigma} = \{\Delta^{\sigma}_{\mathbf{R}L}\delta_{\mathbf{R},\mathbf{R}'}\delta_{L,L'}\}, \quad \boldsymbol{\gamma}^{\sigma} = \{\gamma^{\sigma}_{\mathbf{R}L}\delta_{\mathbf{R},\mathbf{R}'}\delta_{L,L'}\} \ , \tag{231}$$

$$\boldsymbol{\beta}^{\sigma} = \{\beta_L \delta_{\mathbf{R},\mathbf{R}'} \delta_{L,L'} \delta_{\sigma\sigma'}\} \ , \tag{232}$$

$$\sigma = \uparrow, \downarrow, \quad L = (\ell m) \ , \tag{233}$$

where $\mathbf{R}$ denotes sites, $X^{\beta}_{\mathbf{R}L,\mathbf{R}'L'}$ a site and angular momentum dependent matrix, and σ is the spin index ($\sigma = \uparrow, \downarrow$). The parameters $C^{\sigma}_{\mathbf{R}L}$, $\Delta^{\sigma}_{\mathbf{R}L}$, and $\gamma^{\sigma}_{\mathbf{R}L}$ are usually called potential parameters, $\mathbf{S}^{\beta}$ (non-random) screened structure constants, and $\boldsymbol{\beta}$ is the "screening" matrix. Note that for matters of consistency with the literature in this section the "standard" notation used in TB-LMTO papers is adopted.

If one and the same two-dimensional translational symmetry applies in each atomic layer p, $\mathbf{k}_{\parallel}$-projections can be defined with $\mathbf{k}_{\parallel} \in \mathrm{SBZ}$. Assuming additionally a (three-dimensional) parent lattice [18], i.e., excluding layer relaxations, the screened structure constants $S^{\beta}_{p,q}$ are simply given by [52]

$$S^{\beta}_{p,q}(\mathbf{k}_{\parallel}) = \begin{cases} S^{\beta}_{0,0}(\mathbf{k}_{\parallel}), & q = p \ , \\ S^{\beta}_{0,1}(\mathbf{k}_{\parallel}), & q = p+1 \ , \\ S^{\beta}_{1,0}(\mathbf{k}_{\parallel}), & q = p-1 \ , \\ 0, & \text{otherwise} \ , \end{cases} \tag{234}$$

where the index 0 refers to an arbitrarily chosen layer in the parent lattice serving as origin of counting. The potential parameters in Eq. (231) are related to the so-called potential function

$$\mathbf{P}^{\sigma}(z) = \{P^{\sigma}_{\mathbf{R}L}(z) \delta_{L,L'}\} \tag{235}$$

by

$$P^{\sigma}_{\mathbf{R}L}(z) = \frac{z - C^{\sigma}_{\mathbf{R}L}}{\Delta^{\sigma}_{\mathbf{R}L} + \gamma^{\sigma}_{\mathbf{R}L}(z - C^{\sigma}_{\mathbf{R}L})}, \quad z = \varepsilon + \mathrm{i}\delta \ . \tag{236}$$

11.1.1. Simplification at the Fermi energy

At a given (linearization) energy such as the Fermi energy ε_F an even simpler Hamiltonian applies, namely

$$\mathbf{H}^{\beta,\sigma} = \mathbf{C}^{\beta,\sigma} + (\Delta^{\beta,\sigma})^{1/2} \mathbf{S}^{\beta} (\Delta^{\beta,\sigma})^{1/2} \tag{237}$$

with

$$P^{\beta,\sigma}_{\mathbf{R}L}(z) = \frac{z - C^{\beta,\sigma}_{\mathbf{R}L}}{\Delta^{\beta,\sigma}_{\mathbf{R}L}}, \quad z = \varepsilon_F + \mathrm{i}\delta \ . \tag{238}$$

11.1.2. Surface Green's function

The Green's function matrix G^{σ} can be formulated in terms of an auxiliary Green's function matrix $g^{\beta,\sigma}$

$$G^{\sigma}(\mathbf{k}_{\parallel}, z) = (\Delta^{\beta,\sigma})^{-1/2} g^{\beta,\sigma}(\mathbf{k}_{\parallel}, z)(\Delta^{\beta,\sigma})^{-1/2} \ ,$$

$$g^{\beta,\sigma}(\mathbf{k}_{\parallel}, z) = (P^{\beta,\sigma}(z) - S^{\beta}(\mathbf{k}_{\parallel}))^{-1} \ . \tag{239}$$

In using now the same partitioning of configuration space as before in Eq. (92), with p numbering the atomic layers,

$$\begin{aligned}
&\mathscr{L}: -\infty < p \leqslant 0; \quad \text{left lead} ,\\
&\mathscr{I}: 1 \leqslant p \leqslant n; \quad \text{intermediate region} ,\\
&\mathscr{R}: n+1 \leqslant p < \infty; \quad \text{right lead} ,
\end{aligned} \tag{240}$$

the so-called embedding potentials $\Gamma_p^{\beta,\sigma}$ [52] can be defined,

$$\Gamma_p^{\beta,\sigma}(\mathbf{k}_\parallel, z) = \begin{cases} S_{1,0}^{\beta}(\mathbf{k}_\parallel)\mathscr{G}_{\mathscr{L}}^{\beta,\sigma}(\mathbf{k}_\parallel, z)S_{0,1}^{\beta}(\mathbf{k}_\parallel), & p = 1 ,\\ S_{0,1}^{\beta}(\mathbf{k}_\parallel)\mathscr{G}_{\mathscr{R}}^{\beta,\sigma}(\mathbf{k}_\parallel, z)S_{1,0}^{\beta}(\mathbf{k}_\parallel), & p = n ,\\ 0, & \text{otherwise} , \end{cases} \tag{241}$$

where $\mathscr{G}_{\mathscr{L}}^{\beta,\sigma}$ and $\mathscr{G}_{\mathscr{R}}^{\beta,\sigma}$ are the surface Green's functions of the (ideal) left and right semi-infinite system (leads). The layer-diagonal blocks of the inverse of the auxiliary Green's function matrix can then be written as

$$(g^{\beta,\sigma}(\mathbf{k}_\parallel, z))_{p,p}^{-1} = \begin{cases} P_1^{\beta}(z) - S_{0,0}^{\beta,\sigma}(\mathbf{k}_\parallel) - \Gamma_1^{\beta,\sigma}(\mathbf{k}_\parallel, z), & p = 1 ,\\ P_p^{\beta}(z) - S_{0,0}^{\beta,\sigma}(\mathbf{k}_\parallel), & 1 < p < n ,\\ P_N^{\beta}(z) - S_{0,0}^{\beta,\sigma}(\mathbf{k}_\parallel) - \Gamma_N^{\beta,\sigma}(\mathbf{k}_\parallel, z), & p = n , \end{cases} \tag{242}$$

while its off-diagonal blocks ($1 \leqslant p, q \leqslant n$) are given by

$$(g^{\beta,\sigma}(\mathbf{k}_\parallel, z))_{p,q}^{-1} = \begin{cases} -S_{0,1}^{\beta}(\mathbf{k}_\parallel), & q = p+1 ,\\ -S_{1,0}^{\beta}(\mathbf{k}_\parallel), & q = p-1 ,\\ 0, & \text{otherwise} . \end{cases} \tag{243}$$

11.2. The "Kubo–Landauer" equation

The Hamiltonian corresponding to Eq. (237) can be viewed [54] as a direct sum of the following terms:

$$\hat{H} = \sum_p [\hat{H}_{p,p} + \hat{H}_{p,p+1} + \hat{H}_{p,p-1}] , \tag{244}$$

namely in terms of interactions only between "principal layers", see in particular Eq. (243), i.e., the blocks $\hat{H}_{p,q}$ are given by

$$\hat{H}_{p,q} = \hat{\Pi}_p \hat{H} \hat{\Pi}_q , \tag{245}$$

with $\hat{\Pi}_p$ denoting a projection operator onto layer p.

Let d be the distance between two neighboring layers, then (the operator of) the plane position, $\hat{Z}_\perp$, can be expressed as

$$\hat{Z}_\perp = d \sum_p p \hat{\Pi}_p \ , \tag{246}$$

and consequently the velocity perpendicular to the planes of atoms, $\hat{v}_\perp$, as

$$\hat{v}_\perp = \frac{1}{\mathrm{i}\hbar}[\hat{Z}_\perp, \hat{H}] = \frac{d}{\mathrm{i}\hbar} \sum_p [\hat{H}_{p+1,p} - \hat{H}_{p,p+1}] \ . \tag{247}$$

Because of this construction the properly normalized operator $\hat{J}$ of the electric current perpendicular to the atomic layers corresponds to a sum of current operators $\hat{J}_{p,p+1}$ between layers p and $p+1$,

$$\hat{J} = \frac{1}{n} \sum_p \hat{J}_{p,p+1}, \quad \hat{J}_{p,p+1} = \frac{e}{\mathrm{i}\hbar}[\hat{H}_{p+1,p} - \hat{H}_{p,p+1}] \ , \tag{248}$$

where n is the number of layers which in principle tends to ∞. Note that the interlayer distance d disappears due to the normalization.

Using the above described approximations the Kubo–Greenwood equation (linear response regime), see also Eq. (133) for the conductance $C(\varepsilon_F)$,

$$C(\varepsilon_F) = \pi\hbar \sum_{i,j} \langle i|\hat{J}|j\rangle\langle j|\hat{J}|i\rangle \delta(\varepsilon_F - \varepsilon_i)\delta(\varepsilon_F - \varepsilon_j) \ , \tag{249}$$

reduces to

$$C(\varepsilon_F) = \frac{\pi\hbar}{n^2} \sum_{i,j} \sum_{p,q} \langle i|J_{p,p+1}|j\rangle\langle j|J_{q,q+1}|i\rangle \delta(\varepsilon_F - \varepsilon_i)\delta(\varepsilon_F - \varepsilon_j) \ , \tag{250}$$

where the $|i\rangle$ and $|j\rangle$ are (orthonormalized) eigenstates of the Hamiltonian in Eq. (237). For comparison, see also Ref. [55].

Furthermore, *assuming current conservation* the double sum over p and q (layer indices) in Eq. (250) can be eliminated, i.e., can then be chosen arbitrarily, e.g., can refer to atomic planes in the left lead ($p = 1$) and in the right lead ($q = n$). The resulting equation,

$$C(\varepsilon_F) = \pi\hbar \sum_{i,j} \langle i|\hat{J}_{p,p+1}|j\rangle\langle j|\hat{J}_{q,q+1}|i\rangle \delta(\varepsilon_F - \varepsilon_i)\delta(\varepsilon_F - \varepsilon_j) \ , \tag{251}$$

very often is called "Kubo–Landauer" equation. It should be noted that the δ-functions in Eq. (251) can again be expressed in terms of the resolvent of the Hamiltonian, see Eqs. (50)–(52).

11.3. Transmission and reflection matrices

11.3.1. The collinear case

As is shown in Appendix A of Ref. [54], see also Ref. [56], in using Eq. (251) the conductance per interface atom can be expressed as

$$C_M = \sum_\sigma C_M^\sigma, \quad C_M^\sigma = \frac{e^2}{h} \frac{1}{N_\parallel} \sum_{\mathbf{k}_\parallel} T_M^\sigma(\mathbf{k}_\parallel, \varepsilon_F) \ , \tag{252}$$

where $N_{\|}$ is the order of the applied translational group (number of $\mathbf{k}_{\|}$-points in the SBZ), e is the electron charge, h is the Planck constant (the quantity $2e^2/h$ is usually called the conductance quantum), and $M = F$ (AF) denotes the ferromagnetic (antiferromagnetic) configuration of the magnetizations in the magnetic slabs, see also the section on magnetic configurations. Note that Eq. (234) is now formulated in a "Landauer-type language" [7,57–59].

According to Eq. (251) the transmission coefficients $T^{\sigma}(\mathbf{k}_{\|}, \varepsilon_F)$ for a particular magnetic configuration can be replaced by [54]

$$T^{\sigma}(\mathbf{k}_{\|}, \varepsilon_F) = \lim_{\delta \to 0+} \frac{1}{2} \mathrm{tr}\{B_1^{\beta,\sigma}(\mathbf{k}_{\|}, \varepsilon_F) g_{1,n}^{\beta,\sigma}(\mathbf{k}_{\|}, z_+) B_n^{\beta,\sigma}(\mathbf{k}_{\|}, \varepsilon_F) g_{n,1}^{\beta,\sigma}(\mathbf{k}_{\|}, z_-) + B_1^{\beta,\sigma}(\mathbf{k}_{\|}, \varepsilon_F) g_{1,n}^{\beta,\sigma}(\mathbf{k}_{\|}, z_-) B_n^{\beta,\sigma}(\mathbf{k}_{\|}, \varepsilon_F) g_{n,1}^{\beta,\sigma}(\mathbf{k}_{\|}, z_+)\} \ , \tag{253}$$

where tr denotes the trace over angular momenta and sites per unit cell in a "principal layer",

$$B_1^{\sigma}(\mathbf{k}_{\|}, \varepsilon_F) = \mathrm{i}(\Gamma_1^{\beta,\sigma}(\mathbf{k}_{\|}, z_+) - \Gamma_1^{\beta,\sigma}(\mathbf{k}_{\|}, z_-)) \ , \tag{254}$$

$$B_n^{\sigma}(\mathbf{k}_{\|}, \varepsilon_F) = \mathrm{i}(\Gamma_n^{\beta,\sigma}(\mathbf{k}_{\|}, z_+) - \Gamma_n^{\beta,\sigma}(\mathbf{k}_{\|}, z_-)) \ , \tag{255}$$

and $z_{\pm} = \varepsilon_F \pm \mathrm{i}\delta$. The magnetoresistance ratio is then defined as

$$\begin{aligned} \mathrm{GMR} &= (R_{AF}^{\uparrow} + R_{AF}^{\downarrow})/(R_F^{\uparrow} + R_F^{\downarrow}) - 1 \\ &= (C_F^{\uparrow} + C_F^{\downarrow})/(C_{AF}^{\uparrow} + C_{AF}^{\downarrow}) - 1 \ , \end{aligned} \tag{256}$$

where $R_M^{\sigma} = 1/C_M^{\sigma}$ is the resistance per interface atom. Note that this definition corresponds to the so-called "optimistic" value, see previous sections.

The reflection and transmission coefficients are related by

$$R^{\sigma}(\mathbf{k}_{\|}, \varepsilon_F) = \mathrm{tr}\{I - T^{\sigma}(\mathbf{k}_{\|}, \varepsilon_F)\} \ , \tag{257}$$

where I is the unit matrix, and can be expressed as

$$R^{\sigma}(\mathbf{k}_{\|}, \varepsilon_F) = \lim_{\delta \to 0+} \mathrm{tr}\{[B_n^{\sigma}(\mathbf{k}_{\|}, \varepsilon_F) g_{n,n}^{\beta,\sigma}(\mathbf{k}_{\|}, z_+) + \mathrm{i}I][B_n^{\sigma}(\mathbf{k}_{\|}, \varepsilon_F) g_{n,n}^{\beta,\sigma}(\mathbf{k}_{\|}, z_-) - \mathrm{i}I]\} \ , \tag{258}$$

such that conductances can be evaluated using layer-diagonal blocks of the Green's function matrix $g^{\beta,\sigma}(z)$ only rather than the layer off-diagonal blocks as in the case of the transmission coefficients (for details, see Appendix B of Ref. [54]).

There exists, however, a direct way of expressing the transmission coefficients $T^{\sigma}(\mathbf{k}_{\|}, \varepsilon_F)$ in terms of layer-diagonal blocks of $g^{\beta,\sigma}(z)$, namely by viewing the left (semi-infinite) system to consist of the left lead and $n-1$ layers in the 'intermediate' part of the system, see Eq. (240), i.e., by using a different partitioning of the inverse of the Green's function matrix in Eq. (243) (see Appendix A

of Ref. [54]). In this case one arrives at

$$T^{\sigma}(\mathbf{k}_{\parallel},\varepsilon_F)=\lim_{\delta\to 0+}\frac{1}{2}\,\mathrm{tr}\{\tilde{B}^{\sigma}_{n}(\mathbf{k}_{\parallel},\varepsilon_F)g^{\beta,\sigma}_{n,n}(\mathbf{k}_{\parallel},z_+)B^{\sigma}_{n}(\mathbf{k}_{\parallel},\varepsilon_F)g^{\beta,\sigma}_{n,n}(\mathbf{k}_{\parallel},z_-) + \tilde{B}^{\sigma}_{n}(\mathbf{k}_{\parallel},\varepsilon_F)g^{\beta,\sigma}_{n,n}(\mathbf{k}_{\parallel},z_-)B^{\sigma}_{n}(\mathbf{k}_{\parallel},\varepsilon_F)g^{\beta,\sigma}_{n,n}(\mathbf{k}_{\parallel},z_+)\}\ , \tag{259}$$

where the B^{σ}_{n} are defined in Eqs. (254) and (255), and the $\tilde{B}^{\sigma}_{N}$,

$$\tilde{B}^{\sigma}_{n}(\mathbf{k}_{\parallel},\varepsilon_F)=\mathrm{i}(\tilde{\Gamma}^{\beta,\sigma}_{n}(\mathbf{k}_{\parallel},z_+)-\tilde{\Gamma}^{\beta,\sigma}_{n}(\mathbf{k}_{\parallel},z_-))\ , \tag{260}$$

refer to the embedding potential $\tilde{\Gamma}^{\beta,\sigma}_{n}$ of this semi-infinite system.

11.3.2. The non-collinear case

Non-collinearly aligned magnetizations of the magnetic slabs require to view the potential functions and the screened structure constants as 2×2 supermatrices in spin space. A rotation of the orientation of the magnetization in one particular layer p by an angle θ_p is then assumed to be with respect to the one along the z-axis predefined by the local density approximation. The potential function in the original frame of reference (coordinate system),

$$P^{\beta}_{p}(z)=\begin{pmatrix} P^{\beta,\uparrow}_{p}(z) & 0\\ 0 & P^{\beta,\downarrow}_{p}(z)\end{pmatrix}\ , \tag{261}$$

is then transformed as follows:

$$P^{\beta}_{p}(z,\theta_p)=U(\theta_p)P^{\beta}_{p}(z)U^{\dagger}(\theta_p),\quad U(\theta)\in SU2\ , \tag{262}$$

$$U(\theta)=\begin{pmatrix} c & s\\ -s & c\end{pmatrix}\ , \tag{263}$$

with $c=\cos(\theta/2)$, $s=\sin(\theta/2)$. Clearly enough the spin-independent structure constants in the original frame of reference are also block-diagonal in spin space

$$S^{\beta}_{pq}(\mathbf{k}_{\parallel})=\begin{pmatrix} S^{\beta,\uparrow}_{pq}(\mathbf{k}_{\parallel}) & 0\\ 0 & S^{\beta,\downarrow}_{pq}(\mathbf{k}_{\parallel})\end{pmatrix},\quad S^{\beta,\uparrow}_{pq}(\mathbf{k}_{\parallel})=S^{\beta,\downarrow}_{pq}(\mathbf{k}_{\parallel})\ . \tag{264}$$

11.3.3. Restrictions

It should be noted that because of the special approximation for the current matrices made in Eqs. (246)–(248), the use of the Kubo–Landauer equation is restricted to perpendicular electric transport only!

12. Applications of the "Kubo–Landauer" equation within the TB-LMTO method

The examples shown in the following refer to the use of the so-called Kubo–Landauer equation, see Eq. (251), expressed in terms of transmission matrices, Eq. (252), as evaluated by means of

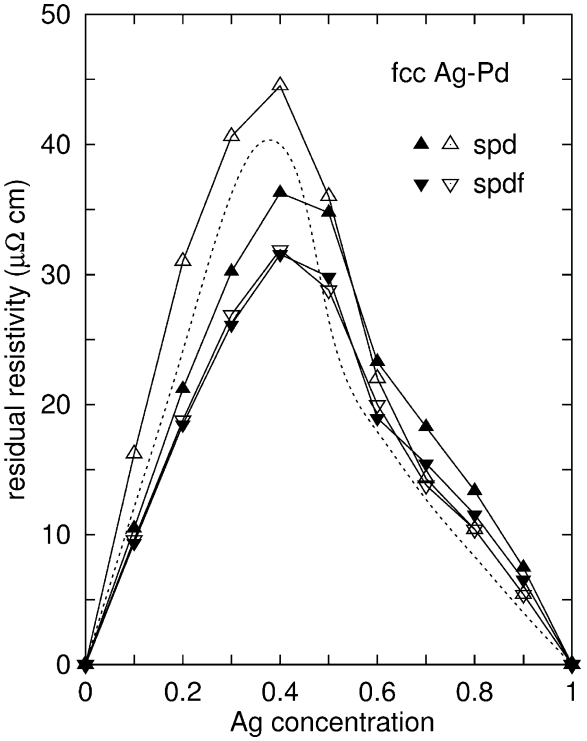

Fig. 50. The residual resistivity of the disordered fcc Ag-Pd alloys calculated by the present TB-LMTO approach (full symbols) and by the standard KKR method. Results for angular momentum cut-off $\ell_{\max} = 2$ (*spd*-basis, triangles-up) and $\ell_{\max} = 3$ (*spdf*-basis, triangles-down) are given. The dotted curve refers to experimental results. From Ref. [56].

the (non-relativistic) TB-LMTO method. It should be recalled that the Kubo–Landauer equation applies only for CPP electric transport in layered systems. It is not applicable to CIP! However, assuming three-dimensional periodicity it can be used in order to evaluate bulk residual resistivities for substitutionally disordered alloys [56].

12.1. Binary substitutional bulk alloys

In Fig. 50 the residual resistivity of fcc-Ag_cPd_{1-c} is shown as a function of the Ag concentration. The comparison displayed there with respect to a previous calculation using the (classical) Korringa–Kohn–Rostoker method and to available experimental data indicates that the approximation made for the current operator, see Eq. (248), as modified for three-dimensional periodicity [56], reproduces the experimental data quite well. Since this calculation is based on the coherent potential approximation neglecting vertex correction, it is also evident that—at least in the case of three-dimensional periodicity—these vertex corrections are rather small.

12.2. Spin valve systems

12.2.1. Redefinition of the CPP-GMR

Since in the non-relativistic case the conductance (or resistance) in the individual spin channels of the antiferromagnetic configurations are identical,

$$C_{AF}^{\uparrow} \equiv C_{AF}^{\downarrow}, \quad R_{AF}^{\uparrow} \equiv R_{AF}^{\downarrow} \ , \tag{265}$$

$$C_F = C_F^{\uparrow} + C_F^{\downarrow}, \quad C_{AF} = C_{AF}^{\uparrow} + C_{AF}^{\downarrow} \ , \tag{266}$$

the GMR as defined in Eq. (256) using the "optimistic view",

$$\mathrm{GMR} = \frac{R_{AF}^{\uparrow} + R_{AF}^{\downarrow}}{R_F^{\uparrow} + R_F^{\downarrow}} - 1 = \frac{C_F^{\uparrow} + C_F^{\downarrow}}{C_{AF}^{\uparrow} + C_{AF}^{\downarrow}} - 1 \ , \tag{267}$$

reduces to

$$\mathrm{GMR} = \frac{C_F^{\uparrow} + C_F^{\downarrow}}{2C_{AF}^{\uparrow}} - 1 \ , \tag{268}$$

an easy scheme for the GMR applies

$$\begin{aligned}
&\mathrm{GMR} = \tfrac{1}{2} : 3C_{AF}^{\uparrow} = C_F^{\uparrow} + C_F^{\downarrow}, \quad \tfrac{3}{2}\, C_{AF} = C_F, \quad \tfrac{2}{3}\, R_{AF} = R_F \ , \\
&\mathrm{GMR} = 1 : 4C_{AF}^{\uparrow} = C_F^{\uparrow} + C_F^{\downarrow}, \quad 2C_{AF} = C_F, \quad \tfrac{1}{2}\, R_{AF} = R_F \ , \\
&\mathrm{GMR} = \tfrac{3}{2} : 5C_{AF}^{\uparrow} = C_F^{\uparrow} + C_F^{\downarrow}, \quad \tfrac{5}{2}\, C_{AF} = C_F, \quad \tfrac{2}{5}\, R_{AF} = R_F \ .
\end{aligned} \tag{269}$$

12.2.2. Thickness variation of the spacer and the magnetic slabs

In Figs. 51 and 52 the conductances and the GMR in fcc-Cu(1 0 0)/Co_m/Cu_s/Co_m/Cu(1 0 0) are shown for a given spacer thickness varying the thickness of the magnetic slabs (Fig. 51), and varying the thickness of the spacer (Fig. 52) at a given thickness of the magnetic slabs. As easily can be seen from Fig. 51 at a Cu spacer thickness of 5 ML (monolayers) the GMR approaches a constant value of about 100% as the thickness of the magnetic slabs increases. Particular attention should be given to the "asymptotic" value of semi-infinite Co leads, i.e., to the case of the system fcc-Co/Cu_s/Co(1 0 0), since this value drastically shows the importance of including the correct structure of the leads. Clearly enough in the system fcc-Co/Cu_s/Co(1 0 0) the Fermi energy refers to bulk fcc-Co, which of course is quite different from that of fcc-Cu. In Fig. 52 the opposite case is displayed, namely variation of the thickness of the spacer at a given thickness of the magnetic slabs. In this case the GMR oscillates around a value of 115%. This remarkably high value is caused by a rather high conductance in the spin down channel of the ferromagnetic configuration, see also Eq. (269).

12.2.3. Alloying in the spacer and in the magnetic slabs

In Fig. 53 the conductances and the GMR are shown with respect to the thickness of a homogeneously alloyed spacer. In here the system fcc-Cu(1 0 0)/Co_5/$(\mathrm{Cu}_{1-x}\mathrm{Pd}_x)_s$/$\mathrm{Co}_5$/Cu(1 0 0),

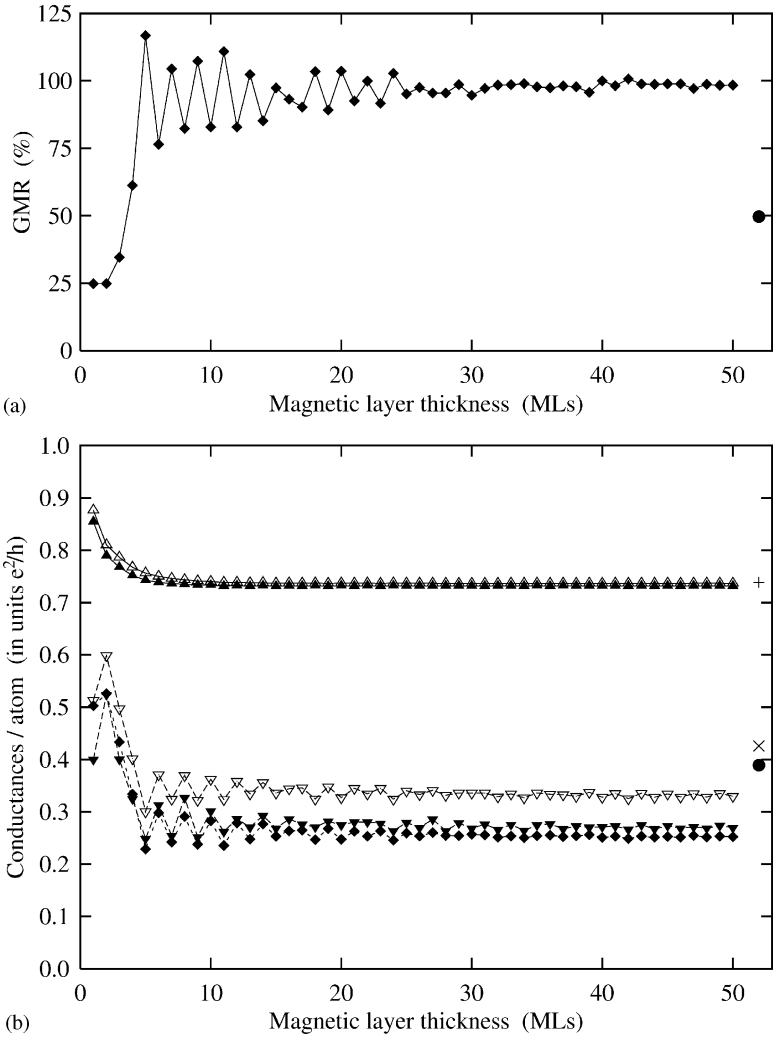

Fig. 51. Ideal $Co_m/Cu_5/Co_m$ trilayers sandwiched by semi-infinite Cu leads with varying thickness m of the magnetic slabs: (a) magnetoresistance ratio (diamonds) and the limit of semi-infinite Co slabs (bullet); (b) conductances per atom for the ferromagnetic ↑-spin (up-triangles), ferromagnetic ↓-spin (down-triangles), and antiferromagnetic configuration (diamonds). Empty symbols (up- and down-triangles) refer to the ferromagnetic ↑- and ↓-spin conductances of a single Co slab of varying thickness embedded into a Cu host. For semi-infinite Co slabs the ferromagnetic ↑- (+), ↓- (×), and antiferromagnetic (bullet) conductances are shown, respectively. From Ref. [54].

$x = 0.15, 0.5$, is considered to show that the GMR is drastically reduced with increasing Pd concentration. Alloying the magnetic slabs can lead to a similar reduction of the GMR. In the system fcc-Cu(1 0 0)/$(Co_{85}Ni_{15})_5/Cu_s/(Co_{85}Ni_{15})_5$/Cu(1 0 0) the GMR is about halfed as compared to the use of pure Co magnetic slabs, i.e., as compared to the system fcc-Cu(1 0 0)/$Co_5/Cu_s/Co_5$/Cu(1 0 0) (Fig. 54).

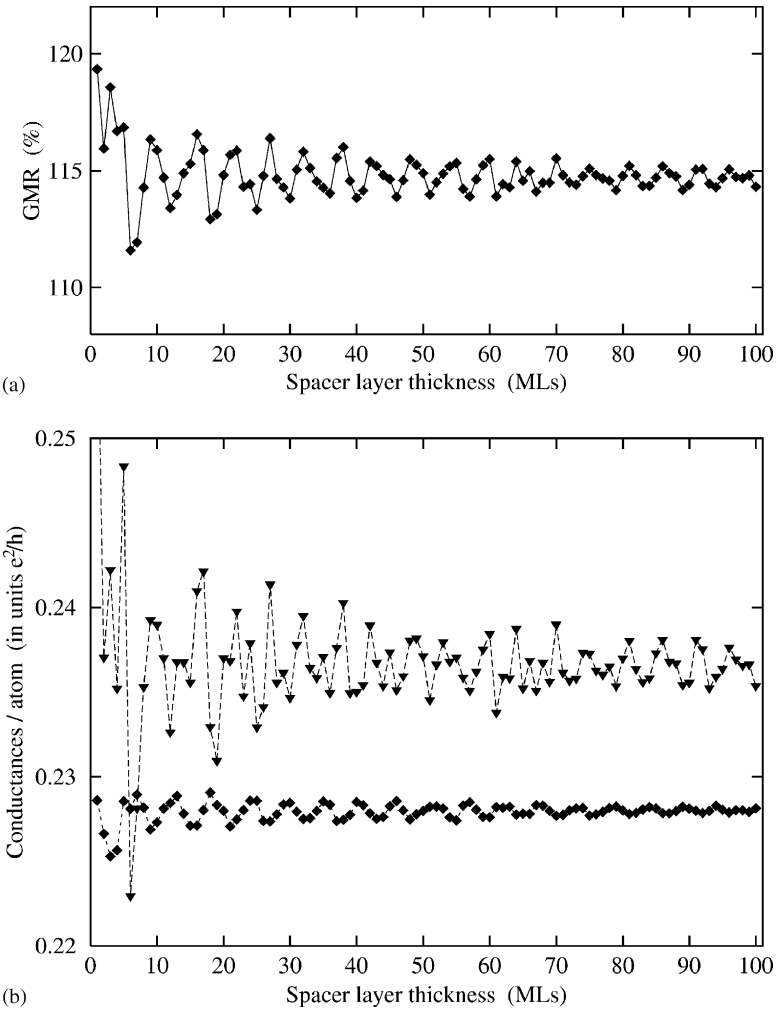

Fig. 52. Ideal $Co_5/Cu_s/Co_5$ trilayers sandwiched by semi-infinite Cu leads with varying spacer thickness s: (a) magnetoresistance ratio (diamonds); (b) conductances per atom for the ferromagnetic $\downarrow$-spin (down-triangles) and antiferromagnetic configuration (diamonds). Note the reduced scale on the vertical axis compared to Fig. 51. From Ref. [54].

12.3. Tunneling junctions

In Fig. 55 the resistance for a fcc-Co(0 0 1)/Vac_s/Co(0 0 1) heterojunction as evaluated using Eqs. (251)–(252) is shown versus the number of vacuum layers for the parallel as well as the antiparallel magnetic configuration; in Fig. 56 the corresponding magnetoresistance is displayed. As easily can be seen from Fig. 56 the magnetoresistance has a minimum at $s=2$, a maximum at $s=4$ and falls off for $s \geqslant 4$, indicating a vanishing magnetoresistance for s becoming large. The shape of the magnetoresistance with respect to the number of vacuum layers is indeed very similar to the results obtained in terms of the Kubo–Greenwood approach for bcc-Fe(0 0 1)/Vac_s/Fe(0 0 1) shown

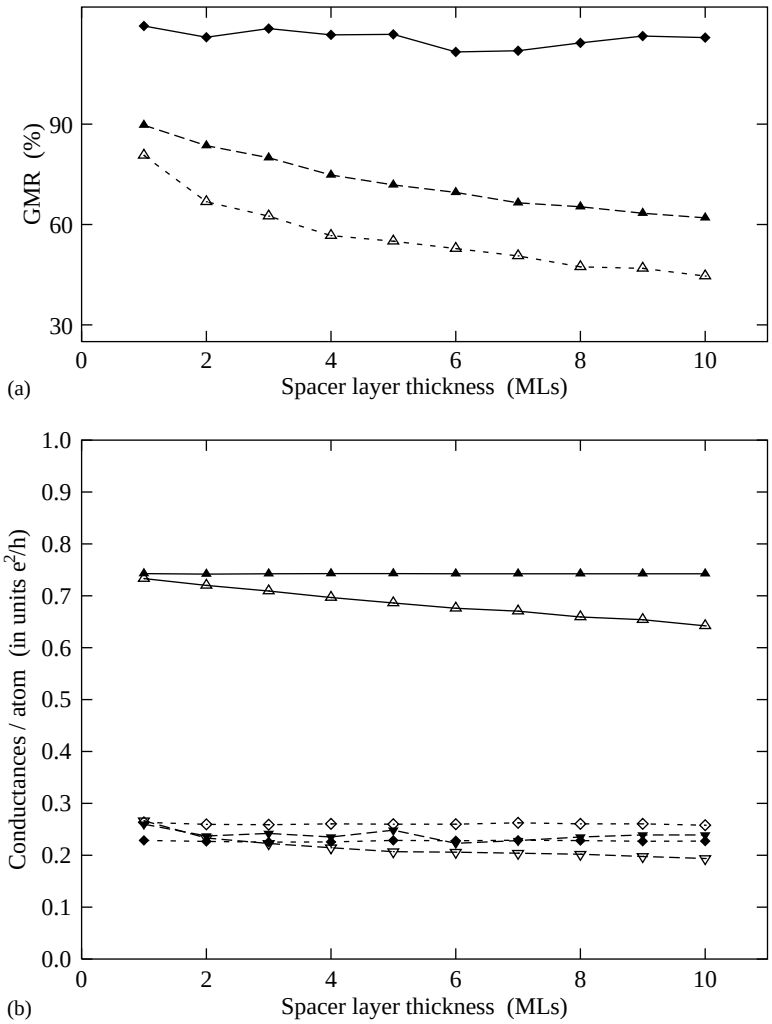

Fig. 53. Comparison of $Co_5/(Cu_{100-x}Pd_x)_s/Co_5$ trilayers ($x = 15$ and 50) with ideal $Co_5/Cu_s/Co_5$ trilayers sandwiched by semi-infinite Cu leads as a function of the spacer thickness s: (a) magnetoresistance ratio (diamonds, ideal trilayer; full triangles, alloyed spacer with $x = 15$; empty triangles, alloyed spacer with $x = 50$); (b) conductances per atom for the ferromagnetic ↑-spin (up-triangles), ferromagnetic ↓-spin (down-triangles), and antiferromagnetic configuration (diamonds). Full symbols refer to an ideal trilayer, empty symbols to a trilayer with an alloyed spacer corresponding to $x = 15$. From Ref. [54].

in Fig. 56. This in turn implies that the "visually obvious" exponential growth of the resistances in Fig. 55, see in particular Eqs. (198)–(201), is only approximate and that an asymptotic behavior of the form

$$\lim_{s\to\infty} (r_{AP}(s) - r_P(s)) = 0 \ , \tag{270}$$

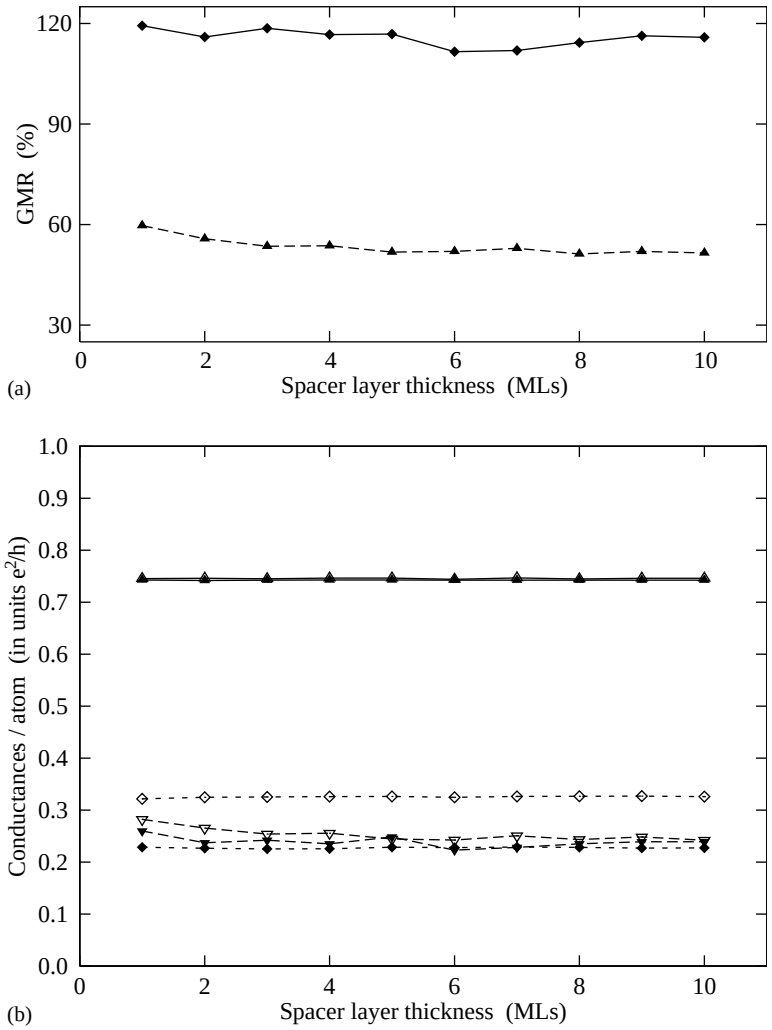

Fig. 54. Comparison of $(Co_{85}Ni_{15})_5/Cu_s/(Co_{85}Ni_{15})_5$ trilayers with ideal $Co_5/Cu_s/Co_5$ trilayers sandwiched by semi-infinite Cu leads as a function of the spacer thickness s: (a) magnetoresistance ratio (diamonds, ideal trilayer; triangles, alloyed magnetic slabs); (b) conductances per atom for the ferromagnetic ↑-spin (up-triangles), ferromagnetic ↓-spin (down-triangles), and antiferromagnetic configuration (diamonds). Full symbols refer to an ideal trilayer, empty symbols to a trilayer with alloyed magnetic layers. From Ref. [54].

has to apply, which of course is the behavior one intuitively would expect as it appears unphysical to assume that two pieces of a magnetic metal separated by a "macroscopic" distance would show a finite magnetoresistance. Since the TB-LMTO calculations correspond to non-selfconsistent potentials, the similarity between Figs. 37 and 56 is the most important aspect of this comparison: there is a peak at about 4 ML beyond which the magnetoresistance continuously falls off. It should be noted in comparing Fig. 37 with Fig. 56 that (1) the position of this peak and (2) the actual fall off of the magnetoresistance with respect to s depends slightly on the types of potentials

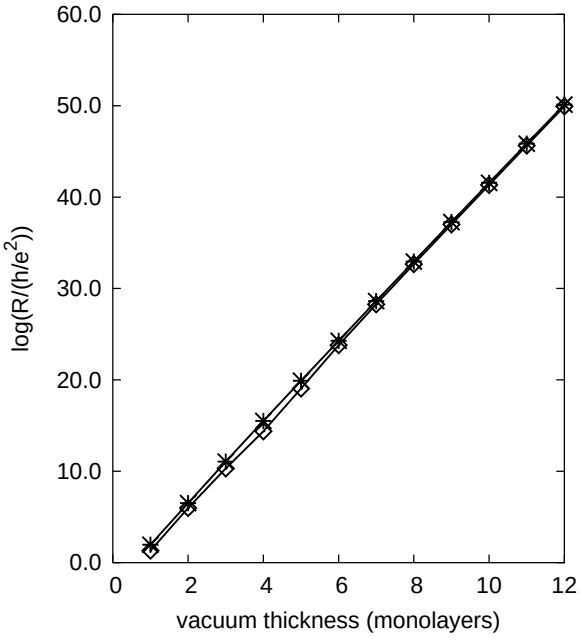

Fig. 55. Parallel (open squares) and antiparallel (stars) resistance of Co(1 0 0)/Vac$_s$/Co(1 0 0) as calculated in terms of the transition matrix formalism versus the number of vacuum layers s. From Ref. [46].

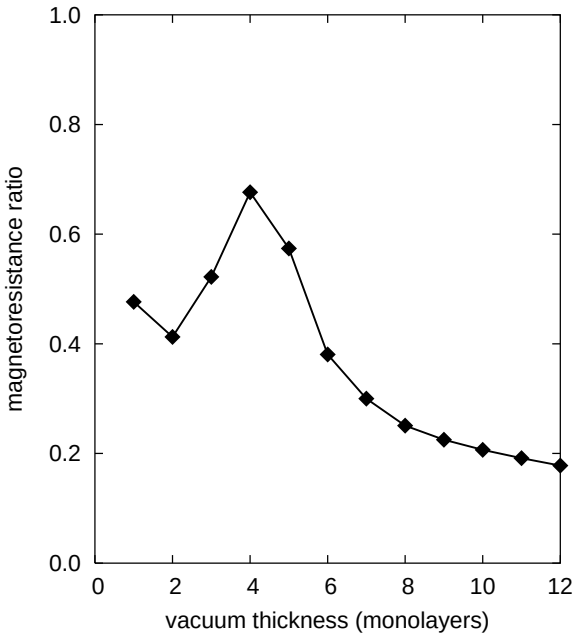

Fig. 56. Magnetoresistance ratio Co(1 0 0)/Vac$_s$/Co(1 0 0) as calculated in terms of the transition matrix formalism versus the number of vacuum layers s. From Ref. [46].

Table 10
References to CPP calculations using the TB-LMTO version of the Kubo-Landauer equation

System	Reference
fcc-Cu(1 0 0)/Co_m/Cu_s/Co_m/Cu(1 0 0)	[54,62]
fcc-Co/Cu_s/Co(1 0 0)	[54,62–64]
fcc-Co/X/Cu_s/X/Co(1 0 0), X = Fe, Ni	[63]
fcc-Cu(1 0 0)/Co_5/$(Cu_{1-x}Pd_x)_s$/Co_5/Cu(1 0 0)	[54,62]
fcc-Co/$(Cu_{0.85}Ni_{0.15})_s$/Co(1 0 0)	[62,63]
fcc-Cu(1 0 0)/$(Co_{85}Ni_{15})_5$/Cu_s/$(Co_{85}Ni_{15})_5$/Cu(1 0 0)	[54,62,64]
fcc-Cu(1 0 0)/Co_5/$(Cu_{0.84}Ni_{0.16})_s$/Co_5/Cu(1 0 0)	[60,61]
CsCl-Rh(Fe_cPd_{1-c})	[65,66]
CsCl-Fe(Rh_cPd_{1-c})	[65,66]
fcc-Co(1 0 0)/Vac_s/Co(1 0 0)	[46]
fcc-Ag_cPd_{1-c} (bulk)	[56]

applied (type of magnetic metal, charge selfconsistency, etc.). Most likely also spin–orbit effects apply.

12.4. References to ab initio TB-LMTO CPP calculations

In Table 10 references are listed referring to ab initio calculations of CPP electric transport using the Kubo–Landauer equation in the context of the TB-LMTO method.

13. Alternative approaches

In Tables 11–16 a short survey of alternative ab initio to electrical properties of solid systems mainly with reduced dimensions is given including a characterization of applied methods. For an introduction to the so-called layer KKR method see either the original formulation in Ref. [67] or a short description in [17]. With a very few exceptions all cited references have to be termed ab initio, i.e., are based on the use of the (local spin) density function.

14. Conclusion

It was the main purpose of this review to show that in dealing with electric properties of magnetic solid systems with reduced dimensions a very clear concept of magnetic configurations has to be used. In the case of ab initio type descriptions—virtually all of them are based on the Density Functional—this concept follows from the approximations made in the local (spin) Density Functional (LSDF). The following important issues have to be recalled:

1. *collinearity and non-collinearity* is a geometrical concept which has to be cast into an algebraic form in terms of rotations. Only in the case of a relativistic description (at least inclusion of a spin–orbit interaction term) such rotations are tight to the lattice. The rotations themselves have

Table 11
Abbreviations

Abbreviation	Full name
K	Kubo equation
KL	Kubo-Landauer equation
TM	Transmission matrix (Landauer) method
LB	Linearized Boltzmann equation
KKR	(classical) Korringa-Kohn-Rostoker method
LKKR	Layer Korringa-Kohn-Rostoker method
SKKR	Screened Korringa-Kohn-Rostoker method
LCAO	Linear combination of atomic orbitals
C/R	conductance or resistance given
σ/ρ	conductivity or resistivity given
GMR	giant magneto resistance given
σ_{ij}, σ_{ii}	layer-resolved or -diagonal conductivity tensor given
bulk-2d	bulk: two-dimensional periodicity used
bulk-3d	bulk: three-dimensional periodicity used
bulk-1d	bulk: real space scattering
CIP	current-in-plane
CPP	current perpendicular to the planes of atoms

Table 12
Table of references to alternative approaches

	[68]	[69]	[70]	[71]	[72]	[73]	[74]	[75]	[76]	[77]	[78]	[79]
K	√		√				√		√		√	√
KL								√				
TM					√			√				
LB		√				√						
KKR												
LKKR	√			√	√		√		√	√	√	√
SKKR												
LCAO												
C/R										√	√	
σ/ρ	√											
GMR												√
σ_{ij}, σ_{ii}	√						√		√		√	
bulk-2d									√			
bulk-3d												
bulk-1d		√										
CIP							√				√	√
CPP			√				√			√		

Table 13
Table of references to alternative approaches, Continuation I

	[80]	[81]	[82]	[83]	[84]	[85]	[86]	[87]	[88]	[89]	[90]	[91]
K				√								
KL												
TM	√	√	√							√		
LB					√	√	√	√	√			
KKR				√								
LKKR	√	√	√	√								
SKKR							√	√	√	√		√
LCAO					√	√						
C/R	√	√										
σ/ρ												√
GMR	√				√		√	√	√		√	
σ_{ij}, σ_{ii}				√								
bulk-2d										√		
bulk-3d					√	√	√	√	√	√		√
bulk-1d												
CIP					√	√	√	√	√			
CPP	√	√	√		√	√	√	√	√			

Table 14
Table of references to alternative approaches, Continuation II

	[92]	[93]	[94]	[95]
K				
KL				
TM	√	√	√	
LB				
KKR				
LKKR				
SKKR	√	√	√	√
LCAO				
C/R	√	√		
σ/ρ				
GMR	√			
σ_{ij}, σ_{ii}				
bulk-2d	√	√	√	√
bulk-3d	√	√		√
bulk-1d				
CIP	√	√		
CPP	√	√		

Table 15
Investigated systems in terms of alternative approaches

System	Reference
Co/Cu/Co	[68,73,74,78,79,83,88]
$(Co_9Cu_7)_r$	[86,89,91]
$((Ni_{81}Fe_{19})_nCu_m)_r$	[90]
$(Fe_nCr_m)_r$	[84,87]
$U_2Pd_2X,\ X = In, Sn$	[85]
Fe/Ge/Fe	[71]
Fe/GaAs/Fe	[71,92,93,95]
Fe/ZnSe/Fe	[72,80,92,93,95]
Fe/Si/Fe	[95]
Fe/Ge/Fe	[95]
Fe/MgO/Fe	[81]
Fe/Vac/Fe	[82]
Co/Vac/Co	[94]
Fe/Barrier/Fe	[77]

Table 16
References to some three-dimensional periodic bulk calculations

System	Reference
Bulk-Ni_cFe_{1-c}	[69,98]
Bulk (fcc)-CO	[76]
Bulk-Cu_cZn_{1-c}	[96]
Bulk-Cu_cGa_{1-c}	[96]
Bulk-Cu_cGe_{1-c}	[96]
Bulk-Cu_cGe_{1-c}	[96]
Bulk-Ag_cPd_{1-c}	[97]
Bulk-Cu_cPt_{1-c}	[97,101]
Bulk-Mo_cNi_{1-c}	[97]
Bulk-Au_cPd_{1-c}	[100]
Bulk-Co_cPd_{1-c}	[99]
Bulk-Co_cPt_{1-c}	[99]
Single impurities in bulk	[100,102,103]

to be defined with respect to a particular axis centred in a chosen site serving as origin. Since the particle density ("charge density") and magnetization density are measured with respect to a—in general—radial vector, the origin of rotation *must* to coincide with the origin of this vector. It *cannot* be moved around ad libidum.

2. *collinearity and non-collinearity* as visualized in terms of a classical spin model (classical vectors) have little in common with a quantum mechanical description: spinors are *not* classical vectors!
3. once *collinearity and non-collinearity* are quantum mechanically well-defined definitions of the interlayer exchange coupling (IEC), magnetic anisotropy energy and of course of the

magnetoresistance follow en suite. This applies to bulk systems (e.g., anisotropic magnetoresistance in ferromagnetic binary alloys) as well as for layered systems or nanostructures supported by substrates.

In speaking of solid *systems of reduced dimensions* this implies that

1. three-dimensional periodic boundary conditions *do not* apply
2. *at best* such a systems shows *two-dimensional translational invariance* ("layered system")
3. each experimentally observed effect has to be analyzed with respect to *appropriate boundary conditions*. Such boundary conditions can be e.g. the existence of a surface, of interfaces or the use of leads.

Each ab initio type approach has to be viewed with a clear understanding of the approximations made. This includes in the case of electric properties concepts like "current conservation" (*relativistic level*) and "spin current conservation" (*non-relativistic level*). Furthermore, since all implementations of such approaches are based on numerical procedures, attempts have to be made to estimate inherent numerical errors.

All above mentioned issues were amply discussed in the various sections of this review. It remains to be recalled that over the last decade remarkable progress has been made in describing quantitatively in terms of ab initio approaches electric properties of solid systems with reduced dimensions even for such complicated systems such as (industrial) spin valves. This includes not only the GMR but also the individual resistances or resistivities, which of course have to be given in absolute numbers.

Appendix A. the Kohn–Sham–Dirac Hamiltonian

In principle within the (non-relativistic) density functional theory (DFT) the Kohn–Sham–Dirac Hamiltonian is given by

$$\mathscr{H} = \boldsymbol{\alpha}\cdot\mathbf{p} + \beta mc^2 + V^{\mathrm{eff}}[n,\mathbf{m}] + \beta\boldsymbol{\Sigma}\cdot\mathbf{B}^{\mathrm{eff}}[n,\mathbf{m}]\ , \tag{271}$$

$$\alpha_i = \begin{pmatrix} 0 & \sigma_i \\ \sigma_i & 0 \end{pmatrix}, \quad \beta = \begin{pmatrix} I_2 & 0 \\ 0 & -I_2 \end{pmatrix}\ , \tag{272}$$

$$\Sigma_i = \begin{pmatrix} \sigma_i & 0 \\ 0 & \sigma_i \end{pmatrix}, \quad I_2 = \begin{pmatrix} 1 & 0 \\ 0 & 1 \end{pmatrix}\ , \tag{273}$$

$$V(\mathbf{r}) \equiv V^{\mathrm{eff}}[n,\mathbf{m}] = V^{\mathrm{ext}} + V^{\mathrm{Hartree}} + \frac{\delta E_{xc}[n,\mathbf{m}]}{\delta n}\ , \tag{274}$$

$$\mathbf{B}(\mathbf{r}) \equiv \mathbf{B}^{\mathrm{eff}}[n,\mathbf{m}] = \mathbf{B}^{\mathrm{ext}} + \frac{e\hbar}{2mc}\,\frac{\delta E_{xc}[n,\mathbf{m}]}{\delta \mathbf{m}}\ , \tag{275}$$

where n is the particle density, $\mathbf{m}$ the magnetization density, $V^{\mathrm{eff}}[n,\mathbf{m}]$ the effective potential, $\mathbf{B}^{\mathrm{eff}}[n,\mathbf{m}]$ the effective (exchange) magnetic field, V^{ext} and $\mathbf{B}^{\mathrm{ext}}$ the corresponding external fields,

and the α_i are Dirac- and the σ_i Pauli (spin) matrices,

$$\sigma_x = \begin{pmatrix} 0 & 1 \\ 1 & 0 \end{pmatrix}, \quad \sigma_y = \begin{pmatrix} 0 & -i \\ i & 0 \end{pmatrix}, \quad \sigma_z = \begin{pmatrix} 1 & 0 \\ 0 & -1 \end{pmatrix} , \tag{276}$$

$$\boldsymbol{\alpha} = (\alpha_1, \alpha_2, \alpha_3), \quad \boldsymbol{\sigma} = (\sigma_x, \sigma_y, \sigma_z) . \tag{277}$$

For non-relativistic Kohn–Sham Hamiltonians the same formal definitions for $V(\mathbf{r})$ and $\mathbf{B}(\mathbf{r})$ apply.

In the various local approximations to the (spin) density functional (LSDF) the occurring functional derivatives are replaced (approximated) by

$$\frac{\delta E_{xc}[n, \mathbf{m}]}{\delta n(\mathbf{r})} = V_{xc}([n, m], \mathbf{r}) \sim f(r_s) , \tag{278}$$

$$\frac{\delta E_{xc}[n, \mathbf{m}]}{\delta \mathbf{m}} = W_{xc}([n, m], \mathbf{r}) \sim g(r_s, \xi) , \tag{279}$$

$$r_s = \left(\frac{3}{4\pi}\right) n^{-1}(r), \quad \xi = \frac{|m(r)|}{n(r)} , \tag{280}$$

namely by functions of r_s and ξ, with $n(r)$ and $m(r)$ being usually the spherical averages of the (single) particle and the magnetization density.

Appendix B. Current conservation

B.1. Relativistic case

In writing the Kubo equation for perpendicular electric transport in the following way,

$$j_i(n) = \sum_{j=1}^{n} \sigma_{ij}(n) E_j(n) , \tag{281}$$

where the indices refer to atomic layers, and $j_i(n)$ and $E_i(n)$ are the current and the electric field in a particular layer, *current conservation* means that the local electric fields $E_i(n)$ over the length of measurement, nd, with d being the interlayer distance, has to be viewed as an averaged (uniform) quantity, see also Refs. [36,104,105],

$$E_i(n) = \langle E(n) \rangle, \quad \forall i . \tag{282}$$

Eq. (281) reduces therefore to

$$j_i(n) = \langle E(n) \rangle \sum_{j=1}^{n} \sigma_{ij}(n) , \tag{283}$$

which multiplied from the left with $\rho_{ki}(n)$,

$$\rho_{ki}(n)j_i(n) = \langle E(n)\rangle \sum_{j=1}^{n} \rho_{ki}(n)\sigma_{ij}(n) \ , \tag{284}$$

summed over and taking into account Eq. (170) yields

$$\sum_{i=1}^{n} \rho_{ki}(n)j_i(n) = \langle E(n)\rangle \sum_{i=1}^{n}\sum_{j=1}^{n} \rho_{ki}(n)\sigma_{ij}(n) = \langle E(n)\rangle \ . \tag{285}$$

In the limit of n becoming very large (N_0),

$$\lim_{n\to N_0}\left(\sum_{i=1}^{n} \rho_{ki}(n)j_i(n)\right) = \lim_{n\to N_0}\langle E(n)\rangle = E_0 \ , \tag{286}$$

E_0 has to be a constant. This, however, is just another way of expressing the Cauchy series in Eq. (173),

$$\lim(\langle E(n+m)\rangle - \langle E(n)\rangle) < \Delta; \quad n,m \in \mathbb{N}^+ \ , \tag{287}$$

where Δ is an infinitesimal small number.

B.2. Non-relativistic case: spin-current conservation

In the non-relativistic case one has to assume that the formally spin-dependent (s), layer-resolved electric fields fulfill the following spin-resolved Kubo equation,

$$j_i^s(n) = \sum_{j=1}^{n} \sigma_{ij}^s(n)E_j^s(n) \ , \tag{288}$$

such that by the same arguments as before a condition of uniform $E_j^s(n)$ leads to *spin current conservation*,

$$\sum_{i=1}^{n} \rho_{ki}^s(n)j_i^s(n) = \langle E^s(n)\rangle \sum_{i=1}^{n}\sum_{j=1}^{n} \rho_{ki}^s(n)\sigma_{ij}^s(n) = \langle E^s(n)\rangle \ . \tag{289}$$

Since the total current in the layers is the sum over both spin channels,

$$j_i(n) = \sum_s j_i^s(n) \ , \tag{290}$$

this finally leads back to Eq. (286)

$$\sum_s \lim_{n\to N_0}\left(\sum_{i=1}^{n} \rho_{ki}^s(n)j_i^s(n)\right) = \sum_s \lim_{n\to N_0}\langle E^s(n)\rangle = E_0 \ . \tag{291}$$

It should be noted therefore that in a non-relativistic approach simultaneous conservation of the current in both spin channels has to be required.

References

[1] J.M. Luttinger, W. Kohn, Motion of electronics and holes in perturbed periodic fields, Phys. Rev. 97 (1955) 689.
[2] R. Kubo, Statistical-mechanical theory of irreversible processes. I. General theory and simple application to magnetic and conduction problems, J. Phys. Soc. Japan 12 (1957) 570.
[3] R. Kubo, S.J. Miyake, Quantum theory of galvanomagnetic effect at extremely strong magnetic fields, Solid State Phys. 17 (1965) 269.
[4] R. Kubo, M. Toda, N. Hashitsume, Statistical Physics II: Nonequilibrium Statistical Mechanics, Springer, Berlin, 1985.
[5] D.A. Greenwood, The Boltzmann equation in the theory of electrical conduction in metals, Proc. Phys. Soc. 71 (1958) 585.
[6] L. Smrčka, P. Středa, Transport coefficients in strong magnetic fields, J. Phys. C 10 (1977) 2153.
[7] R. Landauer, Philos. Mag. 21 (1970) 863.
[8] J.M. Luttinger, in: R.C. Clarke, G.H. Derrick (Eds.), Mathematical Methods in Solid State and Superfluid Theory, Oliver and Boyd, Edinburgh, 1967, pp. 15–193.
[9] D.S. Fisher, P.A. Lee, Relation between conductivity and transmission matrix, Phys. Rev. B 23 (1981) 6851.
[10] C.L. Kane, R.A. Serota, P.A. Lee, Long-range correlations in disordered metals, Phys. Rev. B 37 (1988) 6701.
[11] S. Datta, Electronic Transport in Mesoscopic Systems, Cambridge University Press, Cambridge, 1997.
[12] E.Y. Tsymbal, D.G. Pettifor, Perspectives of giant magnetoresistance, Solid State Phys. 56 (2001) 113–237.
[13] P. Hohenberg, W. Kohn, Inhomogeneous Electron Gas, Phys. Rev. 136 (1964) B864.
[14] W. Kohn, L.J. Sham, Self-consistent equations including exchange and correlations effects, Phys. Rev. 140 (1965) A1133.
[15] H. Eschrig, Fundamentals of Density Functional Theory, B. G. Teubner Verlagsgesellschaft, Stuttgart, Leipzig, 1996.
[16] P. Weinberger, L. Szunyogh, Perpendicular magnetism, Comput. Mater. Sci. 17 (2000) 414.
[17] P. Weinberger, Electron Scattering Theory for Ordered and Disordered Matter, Clarendon Press, Oxford University Press, 1990.
[18] P. Weinberger, Multilayers and symmetry, Philos. Mag. B 75 (1997) 509–533.
[19] P. Weinberger, P.M. Levy, J. Banhart, L. Szunyogh, B. Úfalussy, Band structure and electrical conductivity of disordered semi-infinite systems, J. Phys.: Condens. Matter 8 (1996) 7677.
[20] S.L. Altmann, P. Herzig, Point-Group Theory Tables, Clarendon Press, Oxford, 1994.
[21] B. Lazarovits, L. Szunyogh, P. Weinberger, Fully relativistic calculation of magnetic properties of Fe, Co and Ni adclusters on Ag(1 0 0), Phys. Rev. B 65 (2002) 104441/1-8.
[22] H.J.F. Jansen, Magnetic anisotropy in density-functional theory, Phys. Rev. B 59 (1999) 4699.
[23] A. Vernes, P. Weinberger, P. Mohn, C. Blaas, L. Szunyogh, C. Sommers, P.M. Levy, Magnetic properties, interface exchange coupling and electric transport in Fe/Cr/Fe trilayers, Philos. Mag. B 82 (2002) 85–104.
[24] W.H. Butler, Theory of electronic transport in random alloys: Korringa–Kohn–Rostoker coherent potential approximation, Phys. Rev. B 31 (1985) 3260.
[25] L. Szunyogh, P. Weinberger, Evaluation of the optical conductivity tensor: a Green's function approach, J. Phys.: Condens. Matter 11 (1999) 1045.
[26] K. Palotas, B. Lazarovits, L. Szunyogh, P. Weinberger, Ab initio studies of electric transport in terms of the real space Kubo-Greenwood equation, Phys. Rev. B, MS# BT8201, 2003, in press.
[27] K. Schroeder, CRC Handbook of Electrical Resistivities of Binary Metallic Alloys, CRC Press, Boca Raton, FL, 1983.
[28] C. Blaas, L. Szunyogh, P. Weinberger, C. Sommers, P.M. Levy, J. Shi, Theoretical evaluation of magnetotransport properties in Co/Cu/Co-based spin valves, Phys. Rev. B 65 (2002) 134427/1-8.
[29] C. Blaas, L. Szunyogh, P. Weinberger, C. Sommers, P.M. Levy, Electrical transport in bulk Ni_cFe_{1-c} alloys and related spin-valves, Phys. Rev. B 63 (2001) 224408.
[30] S. Jo, M. Seigler, Magnetoresistance and interlayer coupling in spin valves employing very thin Cu spacer, J. Appl. Phys. 91 (2002) 7110.
[31] P. Weinberger, L. Szunyogh, Theoretical characterization of the giant magnetoresistance in realistic spin valves, Phys. Rev. B 66 (2002) 144427.

[32] P. Weinberger, J. Zabloudil, R.H. Hammerling, L. Szunyogh, T.L. Monchesky, B. Heinrich, The role of interfaces in the magnetoresistance of Au/Fe/Au/Fe/Au spin valves, Phys. Rev. B, MS#BU8141, 2002, submitted for publication.
[33] C. Blaas, P. Weinberger, L. Szunyogh, P.M. Levy, C. Sommers, Ab-initio calculations of magnetotransport for magnetic multilayers, Phys. Rev. B 60 (1999) 492.
[34] C. Blaas, P. Weinberger, L. Szunyogh, J. Kudrnovsky, V. Drchal, P.M. Levy, C. Sommers, On the orientational dependence of the giant magneto-resistance and its relation to the interface exchange coupling, Eur. Phys. J. B 9 (1999) 245.
[35] C. Blaas, P. Weinberger, L. Szunyogh, P.M. Levy, C. Sommers, I. Mertig, Giant magneto-resistance of repeated multilayers of Cu_3Ni_3 on Cu(1 0 0), Philos. Mag. B 78 (1998) 549.
[36] B. Nikolić, Deconstructing Kubo formula usage: exact conductance of a mesoscopic system from weak to strong disorder limit, Phys. Rev. B 64 (2001) 165303.
[37] P.M. Levy, H. Ehrenreich, D. Turnbull (Eds.), Solid State Physics, Vol. 47, Academic Press, Cambridge, MA, 1994, pp. 367–462.
[38] H.E. Camblong, P.M. Levy, S. Zhang, Electron transport in magnetic inhomogeneous media, Phys. Rev. B 51 (1995) 16052.
[39] P.M. Levy, I. Mertig, Theory of giant magnetoresistance, in: D.D. Sarma, G. Kotliar, Y. Tokura (Eds.), Advances in Condensed Matter, Vol. 3 Science, Taylor & Francis, London, New York, 2002.
[40] P. Weinberger, L. Szunyogh, C. Blaas, C. Sommers, Perpendicular transport in Fe/Ge heterojunctions, Phys. Rev. B 64 (2001) 184429.
[41] H.C. Herper, P. Weinberger, A. Vernes, L. Szunyogh, C. Sommers, Electric transport in Fe/ZnSe/Fe heterostructures, Phys. Rev. B 64 (2001) 184442.
[42] H. Herper, P. Weinberger, L. Szunyogh, C. Sommers, Interlayer exchange coupling, magnetic anisotropy and perpendicular electric transport in Fe/Si/Fe trilayers, Phys. Rev. B 66 (2002) 064426.
[43] H. Herper, L. Szunyogh, C. Sommers, P. Weinberger, Perpendicular electric transport in Fe/Ge/Fe, Fe/ZnSe/Fe and Fe/InP/Fe heterostructures, J. Appl. Phys. 91 (2002) 8777.
[44] H.C. Herper, P. Weinberger, L. Szunyogh, C. Sommers, Perpendicular transport in Fe/InP/Fe heterostructures, J. Magn. Magn. Mater. 240 (2002) 180–182.
[45] H.C. Herper, P. Weinberger, L. Szunyogh, C. Sommers, P. Entel, Ab initio study of electric transport and interlayer exchange coupling in Fe/Si/Fe systems, Phase Transitions, 2003, in press.
[46] P. Weinberger, V. Drchal, J. Kudrnovsky, I. Turek, H. Herper, L. Szunyogh, C. Sommers, Aspects of magneto-tunnelöing drawn from ab-initio type calculations, Philos. Mag. B 82 (2002) 1027–1045.
[47] J.J. Akerman, I.K. Schuller, J.M. Slaughter, R.W. Dave, Tunneling criteria for magnetic-insulator magnetic structures, J. Appl. Phys. Lett. 79 (2001) 1.
[48] J. Nogués, I.K. Schuller, Exchange bias, J. Magn. Magn. Mater. 192 (1999) 203.
[49] P. Weinberger, Exchange bias due to configurational magnetic rearrangements, Phys. Rev. B 65 (2002) 014430.
[50] P. Weinberger, L. Szunyogh, Interlayer exchange coupling and giant magnetoresistance, J. Phys.: Condens. Matter, 2003, in press.
[51] P. Weinberger, Towards an ab-initio description of the exchange bias in spin-valve systems, Phase Transitions, 2003, in press.
[52] I. Turek, V. Drchal, J. Kudrnovský, M. Šob, P. Weinberger, Electronic Structure of Disordered Alloys, Surfaces and Interfaces, Kluwer Academic Publishers, Dordrecht, 1997.
[53] P. Weinberger, I. Turek, L. Szunyogh, The TB-LMTO method and its relation to the screened KKR-method, Int. J. Quant. Chem. 63 (1997) 165–188.
[54] J. Kudrnovsky, V. Drchal, C. Blaas, P. Weinberger, Ab initio theory of the perpendicular magneto-conductance in metallic multilayers, Phys. Rev. B 62 (2000) 15084.
[55] H.U. Baranger, A.D. Stone, Electrical linear-response theory in an arbitrary magnetic field: a new Fermi-surface formation, Phys. Rev. B 40 (1989) 8169.
[56] I. Turek, J. Kudrnovsky, V. Drchal, L. Szunyogh, P. Weinberger, Interatomic electron transport by semi-empirical and ab-initio tight-binding approaches, Phys. Rev. B 65 (2002) 125101/1-10.
[57] M. Büttiker, Small normal-metal loop coupled to an electron reservoir, Phys. Rev. B 32 (1985) 1846.
[58] M. Büttiker, Four-terminal phase-coherent conductance, Phys. Rev. Lett. 57 (1986) 1761.
[59] M. Büttiker, Role of quantum coherence in series resistors, Phys. Rev. B 33 (1986) 3020.

[60] V. Drchal, J. Kudrnovsky, P. Bruno, P.H. Dederichs, I. Turek, P. Weinberger, Electron transport in magnetic multilayers: effect of disorder, Phys. Rev. B 65 (2002) 214414/1-8.
[61] J. Kudrnovsky, V. Drchal, I. Turek, P.H. Dederichs, P. Weinberger, P. Bruno, Ab initio theory of perpendicular transport in layered magnetic systems, J. Magn. Magn. Mater. 240 (2002) 177–179.
[62] J. Kudrnovsky, V. Drchal, C. Blaas, P. Weinberger, I. Turek, P. Bruno, Ab initio theory of perpendicular transport in metallic magnetic multilayers, in: A. Meike, A. Gonis, P.E.A. Turchi, K. Rajan (Eds.), Properties of Complex Inorganic Solids, Kluwer Academic/Plenum Publishers, New York, 2000, pp. 343–365.
[63] J. Kudrnovsky, V. Drchal, I. Turek, C. Blaas, P. Weinberger, P. Bruno, The CPP transport in metallic magnetic multilayers, Surface Science 454–456 (2000) 918.
[64] J. Kudrnovsky, V. Drchal, I. Turek, C. Blaas, P. Weinberger, P. Bruno, Ab initio theory of the CPP-magnetoconductance, Czech. J. Phys. 40 (1999) 1583.
[65] I. Turek, J. Kudrnovsky, V. Drchal, P. Weinberger, P.H. Dederichs, Theory of electron transport in FeRh-based natural magnetic multilayers, Czech. J. Phys. 52 (2002) 203–208.
[66] I. Turek, J. Kudrnovsky, V. Drchal, P. Weinberger, P.H. Dederichs, Ab initio theory of transport in FeRh-based natural magnetic multilayers, J. Magn. Magn. Mater. 240 (2002) 162–164.
[67] J.B. Pendry, Low Energy Electron Diffraction—The Theory and Its Application to Determination of Surface Structure, Academic Press, London and New York, 1974.
[68] R.H. Brown, D.M.C. Nicholson, W.H. Butler, X.-G. Zhang, W.A. Shelton, Calculation of the canting angle dependence of the resistivity in Cu/Co spin valves, J. Appl. Phys. 81 (1997) 4008.
[69] D.M.C. Nicholson, W.H. Butler, W.A. Shelton, Yang Wang, X.-G. Zhang, G.M. Stocks, Magnetic structure and electric transport in permalloy, J. Appl. Phys. 81 (1997) 4023.
[70] X.-G. Zhang, W.H. Butler, Local field and quantum effects for current perpendicular to planes in multilayers, J. Appl. Phys. 81 (1997) 4576.
[71] W.H. Butler, X.-G. Zhang, Xindong Wang, Jan van Ek, J.M. MacLaren, Electronic structure of FM/semiconductor/FM spin tunneling structures, J. Appl. Phys. 81 (1997) 5518.
[72] J.M. MacLaren, W.H. Butler, X.-G. Zhang, Spin-dependent tunneling in epitaxial systems: band dependence of conductance, J. Appl. Phys. 83 (1998) 6521.
[73] W.H. Butler, X.-G. Zhang, J.M. MacLaren, Solution to the Boltzmann equation for layered systems for current perpendicular to the planes, J. Appl. Phys. 87 (2000) 5173.
[74] X.-G. Zhang, W.H. Butler, D.M.C. Nicholson, First-principles calculations of electrical conductivity and giant magnetoresistance of Co/Cu/Co spin valves, Phys. Rev. B 52 (1995) 13399.
[75] X.-G. Zhang, W.H. Butler, Landauer conductance in the diffusive regime, Phys. Rev. B 55 (1997) 10308.
[76] T.C. Schulthess, W.H. Butler, X.-G. Zhang, D.M.C. Nicholson, Calculation of conductivity in the presence of structural defects: application to spin dependence of conductivity in cobalt, Phys. Rev. B 56 (1997) 8970.
[77] J.M. MacLaren, X.-G. Zhang, W.H. Butler, Validity of the Julliere model of spin-dependent tunneling, Phys. Rev. B 56 (1997) 11827.
[78] W.H. Butler, X.-G. Zhang, T.C. Schulthess, D.M.C. Nicholson, J.M. MacLaren, V.S. Speriosu, B.A. Gurney, Conductance and giant magnetoconductance of Ci/Cu/Co spin valves: experiment and theory, Phys. Rev. B 56 (1997) 14574.
[79] R.H. Brown, D.M.C. Nicholson, W.H. Butler, X.-G. Zhang, W.A. Shelton, T.C. Schulthess, Giant magnetoresistance calculation for (1 1 1) Co/Cu/Co spin valves, Rev. B 58 (1998) 11146.
[80] J.M. MacLaren, X.-G. Zhang, W.H. Butler, Xingdong Wang, Layer KKR approach to Bloch-wave transmission and reflection: application to spin-dependent tunneling, Rev. B 59 (1999) 5470.
[81] W.H. Butler, X.-G. Zhang, T.C. Schulthess, J.M. MacLaren, Spin-dependent tunneling conductance of Fe/MgO/Fe sandwiches, Rev. B 63 (2001) 5470.
[82] W.H. Butler, X.-G. Zhang, T.C. Schulthess, J.M. MacLaren, Reduction of electron tunneling current due to lateral variation of the wave functions, Rev. B 63 (2001) 092492.
[83] W.H. Butler, X.-G. Zhang, D.M.C. Nicholson, T.C. Schulthess, J.M. MacLaren, Giant magnetoresistance from an electron waveguide effect in Cobalt–Copper multilayers, Phys. Rev. Lett. 76 (1996) 3216.
[84] P. Zahn, I. Mertig, M. Richter, H. Eschrig, Ab initio calculations of the giant magnetoresistance, Phys. Rev. Lett. 75 (1995) 2996.

[85] M. Richter, P. Zahn, M. Diviš, I. Mertig, Giant magnetoresistance in uranium intermetallics: ab initio calculations for U_2Pd_2In and U_2Pd_2Sn, Phys. Rev. B 54 (1996) 11985.
[86] P. Zahn, J. Binder, I. Mertig, R. Zeller, P.H. Dederichs, Origin of giant magnteoresistance: bulk or interface scattering, Phys. Rev. Lett. 80 (1998) 4309.
[87] B.Yu. Yavorsky, I. Mertig, A.Ya. Perlov, A.N. Yaresko, V.N. Antonov, Ab initio study of the angular dependence of giant magnetoresistance in Fe/Cr superlattices, Phys. Rev. B 62 (2000) 9586.
[88] P. Zahn, I. Mertig, $c(2 \times 2)$ interface alloys in Co/Cu multilayers: influence on interlayer exchange coupling and giant magnetoresistance, Phys. Rev. B 63 (2001) 104412.
[89] I. Riedel, P. Zahn, I. Mertig, Ab initio calculation of the transmission coefficients from a superlattice electronic structure, Phys. Rev. B 63 (2001) 195403.
[90] M.Ye. Zhuravlev, W. Schepper, S. Heitmann, H. Vinzelber, P. Zahn, I. Mertig, H.O. Lutz, A.V. Vedyayev, G. Reiss, A. Hütten, Reliable prediction of giant magnetoresistance characteristics, Phys. Rev. B 65 (2002) 144428.
[91] P. Zahn, N. Papanikolaou, F. Erler, I. Mertig, Evolution of Co/Cu multilayer conductivity during growth: an ab-initio study, Phys. Rev. B 65 (2002) 134432.
[92] P. Mavropoulos, O. Wunnicke, P.H. Dederichs, Ballistic spin injection and detection in Fe/semiconductor/Fe junctions, Phys. Rev. B 66 (2002) 024416.
[93] O. Wunnicke, P. Mavropouls, R. Zeller, P.H. Dederichs, Ballistic spin injection from Fe(0 0 1) into ZnSe and GaAs, Phys. Rev. B 65 (2002) 241306.
[94] O. Wunnicke, N. Papanikolaou, R. Zeller, P.H. Dederichs, Effects of resonant interface states on tunneling magnetoresistance, Phys. Rev. B 65 (2002) 064425.
[95] P. Mavropoulos, N. Papanikolaou, P.H. Dederichs, Complex band structure and tunneling through Ferromagnet/Insulator/Ferromagnet junctions, Phys. Rev. Lett. 85 (2000) 1088.
[96] J.C. Swihart, W.H. Butler, G.M. Stocks, D.M.C. Nicholson, R.C. Ward, First-principles calculation of the residual electrical resistivity of random alloys, Phys. Rev. Lett. 57 (1986) 1181.
[97] L. Dulca, J. Banhart, G. Czycholl, Electrical conductivity of finite metallic systems: disorder, Phys. Rev. B 61 (2000) 16502.
[98] J. Banhart, H. Ebert, A. Vernes, Applicability of the two-current model for systems with strongly spin-dependent disorder, Phys. Rev. B 56 (1997) 10165.
[99] H. Ebert, A. Vernes, J. Banhart, Anisotropic electrical resistivity of ferromagnetic Co-Pd and Co.Pt alloys, Phys. Rev. B 54 (1996) 8479.
[100] J. Banhart, Pressure dependence of the electrical residual resistivity of disordered alloys, Phys. Rev. B 53 (1996) 7128.
[101] J. Banhart, H. Ebert, P. Weinberger, J. Voitländer, Approximations made in evaluating the residual electrical DC resistivity of disordered alloys, Phys. Rev. B 50 (1994) 2104.
[102] T. Vojta, I. Mertig, R. Zeller, Calculation of the residual resistivity and the thermoelectric power of sp impurities in silver, Phys. Rev. B 46 (1992) 15761.
[103] I. Mertig, R. Zeller, P.H. Dederichs, Ab initio calculations of residual resistivities for dilute Ni alloys, Phys. Rev. B 47 (1993) 16178.
[104] B. Nikolic, P.B. Allen, Electron transport through a circular constriction, Phys. Rev. B 60 (1999) 3963.
[105] B. Nikolic, P.B. Allen, Resistivity of a metal between the Boltzmann transport regime and the Andersen transition, Phys. Rev. B 63 (2000) 020201.